NUTRIENT-SENSING GHS-R IN MACROPHAGE PROGRAMMING AND META-INFLAMMATION

A Dissertation

by

DA MI KIM

Submitted to the Office of Graduate and Professional Studies of
Texas A&M University
in partial fulfillment of the requirements for the degree of

DOCTOR OF PHILOSOPHY

Chair of Committee,	Yuxiang Sun
Committee Members,	Robert C. Alaniz
	Shaodong Guo
	Susanne Talcott
	Stephen B. Smith
Head of Department,	David Threadgill

May 2021

Major Subject: Nutrition

ABSTRACT

Metabolically triggered inflammation is termed “meta-inflammation,” which underlies the pathological processes of many metabolic dysfunctions. In both inflammatory processes of chronic inflammation and bacterial endotoxin-induced acute inflammation, macrophages have been shown to exhibit critical regulatory activity at all stages of inflammatory tissue responses. The ghrelin receptor, a.k.a. growth hormone secretagogue receptor (GHS-R), mediates the stimulatory effects of ghrelin on food intake and fat deposition. In this study, we investigated the roles of macrophage GHS-R in macrophage programming and meta-inflammation under physiological and pathological conditions.

We generated myeloid-specific GHS-R knockout mice (*LysM-Cre;Ghsr*$^{f/f}$) and tested the mice under different inflammatory conditions; normal physiological condition, lipopolysaccharide (LPS)-induced acute inflammatory condition, and high fat diet (HFD)-induced low grade chronic inflammatory condition. Under physiological conditions, myeloid-specific GHS-R did not alter body weight, tissue weight, or metabolic profile. Interestingly, systemic pro-inflammatory cytokines were down-regulated in RD-fed myeloid-specific GHS-R deleted mice. Therefore, we further studied the role of GHS-R under pathological conditions; LPS-induced acute inflammation and HFD-induced chronic inflammation. We found that myeloid-specific GHS-R deletion protects against LPS-induced lethal endotoxemia and pro-inflammation in serum and macrophages by reducing M1-macrophage polarization. In addition, myeloid-specific GHS-R deletion reduces hepatic inflammation in a paracrine manner. Under chronic inflammatory

conditions, fewer infiltrated macrophages were found in epididymal white adipose tissue (eWAT) and liver of HFD-fed *LysM-Cre;Ghsr*$^{f/f}$ mice, which suggests a down-regulated inflammatory state in these tissues. Reduced lipolysis in eWAT and serum-free fatty acid (FFA) was detected in HFD-fed *LysM-Cre;Ghsr*$^{f/f}$ mice, which indicates ameliorated liver steatosis in HFD-feeding. The regulatory effect of macrophage GHS-R on hepatic inflammation was in a paracrine manner by reducing M1-macrophage polarization, which is regulated by IRS2-PI3Kδ-AKT2 through PKA-CREB. Consistent with the macrophage phenotype change, elevated mitochondrial respiration, fatty acid oxidation (FAO), and reduced glycolysis were detected in GHS-R deleted macrophages.

These findings reveal that GHS-R is an important immune-metabolic regulator of macrophages. GHS-R governs macrophage infiltration, polarization, and cellular metabolic-programming, thus moderating tissue inflammation and systemic insulin sensitivity. Our findings suggest that GHS-R antagonists may present a novel therapeutic strategy for metabolic disorders such as endotoxemia and insulin resistance.

ACKNOWLEDGEMENTS

Foremost, I would like to express my thanks to my mentor, Dr. Yuxiang Sun for her continuous support of my Ph.D. study and research. The enthusiasm and dedication to research that she showed, meticulous attitude, and immense knowledge have inspired me throughout the period of my Ph.D. study.

I would like to thank my committee members: Drs. Robert C. Alaniz, Shaodong Guo, Susanne Talcott, and Stephen B. Smith for their contributions of time, insightful discussions, guidance, and scientific advice to my research and writing of this dissertation.

Also, I would like to thank to my dear friends and colleagues. They are Dr. Chia Shan (Jenny) Wu, Dr. Xiangcang Ye, Dr. Hongying Wang, Hye Won Han, Ji Yeon Noh, Pengfei Ji, Rece Norton, Dr. Gus A Wright, Dr. Sahar Eshghjoo, Dr. Quan Pan, Dr. Wanbao Yang, and James Shen; formal lab members- Daniel Villarreal, Dr. Yan Liu, Dr. Se-Young Cho; undergraduate mentees- Brooke Rebenschied, Ritika Gangarapu, and Gabrielle Woodcox for their kind help with the project and beyond; and the faculty and staff at the Department of Nutrition for making my time at Texas A&M University a wonderful journey.

Finally, I would like to thank my parents and my sister Da Young Kim, for their love, support, and encouragement for my study abroad.

CONTRIBUTORS AND FUNDING SOURCES

Contributors

This work was supervised by a dissertation committee consisting of Associate Professor Yuxiang Sun [advisor], Research Assistant Professor Robert C. Alaniz of the Department of Microbial Pathogenesis and Immunology [Outside Department], Associate Professor Shaodong Guo of the Department of Nutrition [Home Department], Associate Professor Susanne Talcott of the Department of Nutrition [Home Department], Regents Professor Stephen B. Smith of the Department of Meat Science [Outside Department].

The student independently conducted all the research for this dissertation. All the figures shown in this dissertation will be used for future publication.

Funding Sources

This work was supported by American Diabetes Association grant (#1-15-BS-177), National Institutes of Health grant (R01DK118334-A1 and RO1 AG064869), and Alzheimer's Research Foundation.

NOMENCLATURE

AMPK	AMP-activated Protein Kinase
BBB	Blood–Brain Barrier
BDNCF	Brain-Derived Neurotrophic Factor
BM	Bone Marrow
BSA	Bovine Serum Albumin
CCL2	CC-chemokine Ligand 2
CD	Cluster of Differentiation
CD62L	L-selectin
CEBP	CCAAT/enhancer-binding protein
CLP	Common Lymphoid Progenitor
CLS	Crown Like Structure
CM	Conditioned Media
CMP	Common Myeloid Progenitors
CPT1	Carnitine Palmitoyl Transferase I
CREB	cAMP-Response Element Binding Protein
CSF	Colony Stimulating Factor

CX3CL	C-X3-C Motif Chemokine Ligand
CX3CR1	Chemokine Receptor 1
DIO	Diet Induced Obese
ETC	Electron Transport Chain
eWAT	epididymal White Adipose Tissue
FAS	Fatty Acid Synthase
FFA	Free Fatty Acid
GAS	Gastrocnemius Muscles
G-CSF	Granulocyte Colony Stimulating Factor
GHS-R	Growth Hormone Secretagogue Receptor
GLUT1	Glucose Transporter1
GMPs	Granulocyte/Macrophage Progenitors
GOAT	Ghrelin O-Acyl Transferase
GPCRs	G Protein-Coupled Receptors
GTT	Glucose Tolerance Tests
HIF1α	Hypoxia-Inducible Factor-1α
HFD	High Fat Diet

HOMA-IR	Homeostatic Model Assessment for Insulin Resistance
HSCs	Hematopoietic Stem Cells
Hypo	Hypothalamus
ID2	Inhibitor of DNA Binding 2
IFN	Interferon
IGF1	Insulin-like Growth Facter 1
IL	Interleukin
ILC	Innate Lymphoid Cells
IM	Infiltrated Macrophages
iNOS	Inducible Nitric Oxide Synthase
IRS	Insulin Receptor Substrate
ITT	Insulin Tolerance Tests
JNK	c-Jun N-terminal Kinase
KC	Kupffer Cells
LFA1	lymphocyte Function-associated Antigen 1
LPS	Lipopolysaccharide
LXRα	Liver X Receptor-α

LY6C	Lymphocyte Antigen C6
MA	Mature Adipocyte
Mcp1	Monocyte Chemoattractant Protein-1
MEPs	Megakaryocyte/Erythrocyte Progenitors
MERTK	Tyrosine-protein Kinase MER
MFI	Mean Fluorescence Intensity
mTOR	Mammalian Target Of Rapamycin
NADPH	Nicotinamide Adenine Dinucleotide Phosphate Hydrogen
NAFLD	Nonalcoholic Fatty Liver Disease
NF-κB	Nuclear factor kappa B
NO	Nitric Oxide
NOD2	Nucleotide-binding Oligomerization Domain Protein 2
Notch1	Notch Homolog 1
NPCs	Non-Parenchymal Cells
PA	Palmitic Acid
PBS	Phosphate Buffered Saline
PECAM1	Platelet Endothelial Cell Adhesion Molecule

PI3K	Phosphatidylinositol-3-Kinase
PKA	Protein Kinase A
PMs	Peritoneal Macrophages
PPAR	Peroxisome Proliferator-Activated Receptor
PSGL1	P-selectin Glycoprotein Ligand 1
PTT	Pyruvate Tolerance Tests
RD	Regular Diet
RM	Resident Macrophages
ROS	Reactive Oxygen Species
Runx	Runt Related Transcription Factor
SVF	Stromal vascular fraction
TG	Triglyceride
TGF-β	Transforming Growth Factor-β
TLR4	Toll-like Receptor 4
TNFα	Tumor Necrosis Factor alpha
VCAM1	Vascular Cell Adhesion Molecule 1

TABLE OF CONTENTS

Page

LIST OF FIGURES

Page

CHAPTER I

INTRODUCTION

Inflammation and energy metabolism

Inflammation underlies a wide variety of inflammatory processes. The predominating historical concept of immunity and energy metabolism is considered to be different processes in different cells. However, current studies revealed that there is intersection between immunity and metabolism in the specific metabolic programs of distinct molecular, cellular, and organelle level. Meta-inflammation is a term describing metabolically triggered inflammation associated with many immune-related metabolic dysfunctions, tissue damage and chronic diseases such as obesity, diabetes, NAFLD, and autoimmune diseases (1-4). In both inflammatory processes, bacterial endotoxin (LPS)-induced inflammation and chronic inflammation increase circulating inflammatory mediators and induce the activation of various immune cells that together regulate the tissue damage and/or repair (5). Although many immune cells involved in the processes of tissue damage/repair (6), macrophages have been shown to involved in all stages of inflammatory and tissue reparative responses in different organ systems (7). Among many immune cells, macrophages are a crucial source of inflammatory mediators such as chemokines and cytokines that elicit their effects in an autocrine and/or paracrine manner and drive the initial cell response following tissue injury (7). Under metabolic stress, macrophages undergo extensive changes in glycolysis and oxidative phosphorylation, correlating inflammatory cytokine production (8).

From bone-marrow progenitor cells to tissue macrophages

Macrophages are one of the major professional phagocytic cells generated from committed HSCs located in the BM. In the BM where they are maintained before being released into the bloodstream, HSCs initially give rise to MPPs which then rise to the CLP and the CMP, which then advance into MEPs and GMPs (9-12). Further downstream, GMPs give rise to granulocytes and to macrophage and dendritic cell precursor (MDP), which generates the common dendritic cell precursors, as well as the monoblasts that are the precursors of pro-monocytes (13, 14). Next, monocytes are rised from pro-monocytes and released into the bloodstream (15). After circulating in the bloodstream for a few days after leaving the bone marrow environment, monocytes extravasate through the endothelium into tissues using adhesion molecules such as CD62L, PSGL1, LFA1, and PECAM1, together with chemotactic factors such as CSF1 and the chemokines CX3CL1 and CXCL12 (16-20). Once in tissues, monocytes differentiate into macrophages under control of CSF1 or under mediating inflammatory events in response to chemoattractant. All these stages of macrophage differentiation are manipulated by growth factors and transcription factors such as Notch1 and Runx1 (19, 21).

Resident and infiltrated macrophages in tissues

Subpopulations of tissue-resident macrophages are divided based on the anatomical location. Tissue-resident macrophages are derived in utero in the yolk sac and resided in tissues; the microglia (brain), Kupffer cells (liver), alveolar macrophage (lung),

osteoclasts (bone), and splenic, adipose, and cardiac macrophages (22-24). They are regarded as cells with limited mobility within the reside tissue, which plays a key role in tissue remodeling and homeostasis. While conventional approaches exam macrophage activation *in vitro* with the measurement of inflammatory stimuli-induced cytokine secretion and changes in gene expression, current studies highlight macrophage responsiveness *in vivo* with 6interaction between tissue-resident macrophages and innate immune cells (25-27). These tissue-resident macrophages engulf the foreign substance and recruit monocytes from circulation to the inflamed tissue (28). For example, tissue-specific macrophages dismantle dead cells into small particles and recruit peritoneal macrophages and neutrophils within an hour on the injured location (29). Publications various tissues, including liver, heart, and intestine, also report that tissue-resident macrophages become activated and release pro-inflammatory cytokines during the early phase of injury and inflammation, which in turn causes recruitment of circulating monocytes in the injury site (26, 28, 30). To be specific, in the liver, depletion of Kupffer cells results in reduced neutrophil recruitment, suggesting Kupffer cells potentially play an important role in healing liver injury by orchestrating neutrophile recruitment (29). Recruiting extra immune cells is through the process of generating large pools of neutrophils and monocytes in a process that is dependent on cytokines and chemokines (31). Several studies report that monocytes that exit bone marrow are diverse into two types, characterized by high expression of CX3CR1 and low expression of the LY6C which cannot respond to CCL2 (17, 32, 33). Under tissue injury, the NLR protein NOD2 in activated tissue-specific macrophages is accountable for the production of CCL2, which

induces the recruitment of monocytes to the injured site and differentiates to inflammatory macrophages (32). The described process shows that tissue-resident macrophages provide the first line of defense against invading pathogens via crosstalk between the damaged tissue and the bone marrow to increase the number and activation of tissue macrophages.

During embryonic development, tissue-resident macrophages are defined by expression of the cell surface marker (FcγRI (CD64) and MERTK) and the transcription factors (PU.1, CEB, MAF, and MAFB) (21). Interestingly, based on the location they engraft, macrophages become specialized by receiving specific signals that are produced in the local environment to regulate the expression of tissue-specific transcription factor according to the needs of their specific organ of residence (21, 34-36). In the **brain**, microglial cells are exposed to locally produced TGF-β, which drives SMAD transcription factor and generates genes specific to microglia, and IL-34, which is produced by neurons in several locations of the brain for microglia maintenance (25, 27). Microglia conversely interacts with surrounding environment by producing BDNCF and IGF1, which is crucial for the survival of layer V cortical neurons. In the **lung**, fetal monocytes are differentiated into alveolar macrophages by exposing them to epithelial cell-derived CSF2 which promotes the expression of PPARγ (37). Maturated alveolar macrophages are required to maintain lung homeostasis by clearing excess surfactant and regulating surfactant catabolism. In the **spleen**, SPIC transcription factor expression is regulated by heme which controls the maintenance of spleen red pulp macrophages and the expression of splenic red pulp macrophages-specific molecule, VCAM (38). Splenic macrophage maintenance depends on LXRα-mediated signals and trap circulating particulates and affects local B

cell maintenance in the marginal location of the spleen (39, 40). Microbial products in the **intestine** drive the production of IL-1β that stimulates ILC3s (41). CSF2 production mediated by ILC3 is necessary for the survival of intestinal immune cells (macrophages and DCs), and their production of IL-10 and retinoic acid are essential substrates for intestinal T (Treg) cell homeostasis. In the **skin**, IL-34 and TGF-β produced by keratinocytes drive the expression of the transcription factors in Langerhans cells which promotes skin tolerance and immunity (27, 42). In the **liver**, Kupffer cells are exposed to CSF1 and regulate LXRα to erythrocyte or clearance of antigen from portal circulation (43). Cardiac macrophages in the heart are exposed to CFS1 secreted locally (26) but the exact mechanism by which CFS1 drives cardiomyocyte homeostasis is unclear.

Macrophage infiltration in metabolic diseases

Tissue macrophages are important for maintaining the homeostasis of tissues (44, 45). Macrophages in tissues are classified into two categories: tissue-resident macrophages and infiltrated macrophages. Most resident macrophages of tissues are derived from progenitor cells generated from the yolk sac during development and control homeostasis in their reside tissue in the steady-state (46, 47). On the other hand, infiltrated macrophages are derived from monocytes (a.k.a. inflammatory monocytes) found in an inciting pathology, such as obesity and metabolic diseases (48, 49). It has been reported that blockade of macrophage infiltration inhibits activation of tissue-resident macrophages and leads to suppression of tissue injury (50). However, the role of macrophages in tissue injury is still controversial; both deleterious and protective functions of tissue macrophages have been

reported (51-53). This discrepancy could be a result of the heterogeneity of macrophages in tissues and difficulty in distinguishing between resident and infiltrated macrophages. Yet, the recent progress in multiparameter flow cytometry facilitated the ability to distinguish between macrophage subsets more accurately, which helps to unravel the high complexity of the macrophages in different organs (33, 54, 55). We propose to use flow cytometry and other cutting-edge techniques in this study to perform in-depth phenotypic and functional characterization of tissue macrophages at steady-state and pathological settings.

Macrophage polarization

Macrophages are a vital player in the immune system. They play a dynamic role in the maintenance of tissue homeostasis as well as innate immunity in various diseases (56). Their unique functions lead to corresponding feedbacks to environmental stimuli. Macrophage polarization is known to consist of classical M1- and alternative M2-subtypes according to their apparent phenotypes and functions. M1-like macrophages are stimulated by LPS and/or IFN-γ, associated with increased levels of glycolysis metabolism, decreased levels of OXPHOS, and production of pro-inflammatory cytokines involved in infectious and inflammatory diseases (57, 58). On the other hand, M2-like macrophages are activated by IL-4 and/or IL-13, associated with reduced pro-inflammatory response and wound healing, immunomodulation, as well as elevated OXPHOS (58-61). Polarized macrophages can reprogram their energy metabolism; glycolytic metabolism and mitochondrial OXPHOS (57, 61, 62). Metabolic activation of

macrophages in chronic or acute inflammatory diseases has been implied based on in vitro stimulation and was demonstrated to be related to classic M1 metabolism and the M1-to-M2 ratio (63-65).

Ghrelin/GHS-R actions and energy metabolism

Ghrelin, a 28-amino acid peptide mainly from the stomach duodenum, is a well-known orexigenic hormone that stimulates food intake. In the normal states, plasma ghrelin levels alternate based on the energy intake (66). When energy intake is low, circulating ghrelin levels increase. The ghrelin levels fall in response to a meal and decrease in diet-induced obesity (67). It is unexpected for an orexigenic hormone that over-nutritional status such as obesity induces ghrelin resistance and decreases ghrelin level (68). Several lines of evidence potentially explain this phenomenon in DIO. This downregulated secretion of ghrelin observed in obesity may be due to the elevation of insulin or leptin, which negatively correlated with levels of ghrelin as a physiological adaptation (69, 70). Research with gastric mucosal cells indicates that those from obese mice do not produce or reduce ghrelin upon physiological signals such as norepinephrine or glucose, which suggests obesity desensitizes ghrelin-promoting cells (71, 72). DIO increases duodenal somatostatin cells which is responsible for ghrelin secretion. Increased fatty acids and lactate in DIO also can decrease serum ghrelin level by directly engaging short- and long-chain fatty acid receptor, GPR43 and GPR120, respectively, which are located on the plasma membrane of gastric ghrelin cells (73). It is reported that amino acids increased during obesity also can directly interact with ghrelin cells by activating the calcium-

sensing receptor to decrease ghrelin release (74, 75). Moreover, circulating levels of ghrelin do not decrease after consumption of a meal in obese humans (76). These changes in ghrelin release may due to ghrelin cells from obese mice showing resistance to noradrenaline-mediated stimulatory action of the sympathoadrenal system on β1-adrenergic receptors in obesity (77). Furthermore, ghrelin resistance in the hypothalamus is observed in obese mice due to the impaired transport ability of ghrelin across the BBB (78). Consistently, ghrelin injection in obese mice fails to induce NPY/AgRP responsiveness, raising another aspect that reduced NPY/AgRP expressing neurons contribute to ghrelin resistance and suppressing the neuroendocrine ghrelin axis (79, 80).

Ghrelin/GHS-R actions in the macrophage

Ghrelin is ubiquitously expressed (81), whereas GHS-R expresses more locally; high expression of GHS-R is detected in the hypothalamus of the brain and low expression is detected in peripheral tissues such as adipose tissue and liver (82-84). Ghrelin and GHS-R are expressed highly in macrophages, and the expression increases during macrophage differentiation (85). Ghrelin signaling in macrophages regulates insulin pathways and inflammation both *in vitro* and *in vivo* (86, 87). The ghrelin/GHS-R signal has been reported to be involved in cholesterol release in human macrophages (86). Elevated cholesterol causes low-grade inflammation in humans (88), and the links between lipid metabolism and immune responses have been documented (86, 89). These observations

suggest that ghrelin signaling has important roles in immunity and inflammation, but the direct effects of ghrelin signaling need to be investigated.

Ghrelin/GHS-R reactive in inflammatory disease states

The effects of ghrelin on inflammation are controversial. Both pro- and anti-inflammatory effects have been reported under different metabolic/inflammation states (86, 90, 91). In early skin inflammation, ghrelin levels are reduced but then increase with tissue repair (92). Ghrelin shows protective effects during the early phase of sepsis but impairs immune responses during the latter phase, and its adverse effects are more detrimental in lean mice than obese mice (93). Also, pharmacological doses of ghrelin are shown to be anti-inflammatory (94-96), but the effects of physiological doses of ghrelin on inflammation remain unclear. Several studies have reported that ghrelin has anti-inflammatory effects (90, 94). In contrast, a recent study also showed that antagonism of GHS-R decreases pro-inflammatory gene expression in macrophages D. *et al.* showed ghrelin increases IL-8 production in GHS-R transgenic colonic epithelial cells (91). Our recent study showed that antagonism of GHS-R decreases pro-inflammatory gene expression in macrophages *in vitro* (97). It is known that GHS-R affects downstream signaling and physiological processes and causes high constitutive activity (98, 99). It has been suggested that there might be unknown or orphaned receptors binding ghrelin due to the observation that ghrelin induces the release of GH and food intake via GHS-R (100, 101) but stimulates osteoblast growth and liver glucose production by mechanisms independent of GHS-R (102-104). In addition, GHS-R signaling can be activated in the absence of ghrelin (105).

We reported that ghrelin null mice and GHS-R null mice have different thermogenic phenotypes and susceptibility for diet-induced adipose inflammation (102, 106, 107). Thus, the investigation is much needed to determine whether the effect of GHS-R is pro- or anti-inflammatory under a physiological and pathological condition in the early and late stages of inflammation.

Innovative aspects of the study

This study has the following innovative aspects: **1)** Research on ghrelin mostly focused on the roles of ghrelin signaling, primarily with its orexigenic function; very few studies have been done with its non-orexigenic roles. Studying the role of ghrelin in macrophages and different tissues directly challenges the established dogma. A large amount of work has been done with ghrelin or GHS-R, but accurate information for regulating their effects remains an enigma. This study is innovative because the effect of GHS-R in macrophages has been studied, which will help to fill the knowledge gap regarding the role of GHS-R in macrophages and may also help to explain the multifaceted roles of GHS-R. **2)** This study adopted a new technology that will provide an ideal way in determining the role of GHS-R in macrophage and underlying mechanisms by using newly generative tissue-specific knockout mice. We have generated a novel myeloid-specific GHS-R knockout model, which will allow us to study the role of macrophage GHS-R in inflammatory diseases in both chronic and acute conditions. **3)** It has been reported that blockade of macrophage infiltration inhibits activation of tissue-resident macrophages and leads to suppression of tissue injury (50). However, the role of macrophages in tissue injury is still

controversial with studies reporting on both sides; deleterious and protective functions of tissue macrophages (51-53). This discrepancy could be a result of the heterogeneity of macrophages in tissues and difficulty in distinguishing between resident and infiltrated macrophages. This study is innovative because multiparameter flow cytometry allowed to clearly distinguish between infiltrated macrophages and tissue-resident macrophages more accurately, which would help to unravel the high complexity of macrophage compartmentalization in different organs. **4)** Macrophage reprogramming has emerged as an exciting novel concept for the prevention/treatment of inflammation and metabolic diseases, but the regulatory mechanisms of macrophage polarization are largely unclear. This study is innovative because the investigation into the role and mechanism of GHS-R in macrophages will help to shed light on a novel paradigm regarding how nutrient-sensing signal metabolically reprograms macrophage polarization. Furthermore, it will provide "proof-of-concept" evidence as to whether targeting GHS-R in macrophages would be a unique strategy for combating meta-inflammation. **5)** Recent advance suggests that metabolism is crucial for macrophage activation (108, 109). Insulin signaling is one of the most fundamental metabolic regulatory mechanisms which alters inflammatory tissues, but the role of GHS-R in insulin signaling in macrophage is not clear. This study is innovative because it will provide novel insight into the role of GHS-R in reprograming macrophage polarization by activating insulin signaling. **6)** Further, this study is innovative because **of** a wide range of experimental approaches (e.g., *in vivo* integrative physiology, *ex vivo* primary cultures, GHS-R overexpressed macrophages, GHS-R antagonist, separating infiltrated macrophages with tissue-resident macrophages) will

allow us to test our hypothesis robustly. This project seeks to address this paucity in a comprehensive and physiologically relevant fashion, and therefore, it is both novel and innovative.

Overview of the dissertation

In this dissertation, I explored the role of macrophage GHS-R in driving metabolic dysfunction under different inflammatory states. In Chapter 2, I found that myeloid-specific GHS-R regulates systemic inflammation without altering phenotypic or metabolic characterization in normal physiological conditions (RD feeding). I used myeloid-specific GHS-R knockout mice (*LysM-Cre;Ghsr*$^{f/f}$) to show that myeloid-specific GHS-R is an essential immune regulator diminishing pro-inflammatory cytokines in macrophages which could lead to the reduction of circulating pro-inflammatory cytokine levels. However, macrophage infiltration to insulin target tissues such as eWAT and liver was not affected by ablation of GHS-R in myeloid-specific cells under physiological conditions. With our unique myeloid-specific GHS-R deleted model, I further explored the role of the macrophage GHS-R in endotoxemia in acute (Chapter 3) and chronic low-grade (Chapter 4) inflammatory conditions by regulating macrophage infiltration and meta-inflammation. In Chapter 3, I determined the role of macrophage GHS-R in the bacterial-induced endotoxemia model. First, myeloid-specific GHS-R deletion reduces the fatality rate by protesting tissue damage in the LPS-induced endotoxemia model. This protection resulted from the alleviation of systemic and macrophage pro-inflammatory cytokine levels by diminishing M1-like macrophage polarization. Furthermore, the regulatory role of GHS-R in macrophage in pro-inflammatory cytokine levels was

confirmed by gain (GHS-R overexpression)- and loss (GHS-R antagonist)-of-studies. In Chapter 4, I examined the role of macrophage GHS-R in the control of insulin resistance by macrophage infiltration and polarization under pathological conditions; the chronic low-grade inflammatory conditions induced by HFD feeding. While myeloid-specific GHS-R did not alter glucose homeostasis and insulin sensitivity in physiological conditions, myeloid-specific GHS-R played an essential role in maintaining glucose homeostasis and alleviating insulin resistance and liver steatosis via attenuating macrophage infiltration to insulin target tissues and maintaining tissue homeostasis under chronic inflammatory conditions. Using the DIO mouse model and PA-induced inflammation in macrophages, I found that macrophage GHS-R deletion could attenuate systemic inflammation, M1-macrophage polarization, and pro-inflammatory signaling. I demonstrated that GHS-R, a key regulator of macrophage infiltration and polarization, controlled chronic inflammation-induced metabolic disorders such as NAFLD and insulin resistance. In Chapter 5, I explored the mechanism by which GHS-R regulated macrophage polarization. I demonstrated that macrophage GHS-R deficiency decreased LPS-induced superoxide in macrophages. As a result of regulating the macrophage polarization, macrophage GHS-R deficiency protected mitochondrial function but reduced glycolysis in LPS-induced M1-like macrophages. FAO was promoted by macrophage GHS-R deficiency under PA-induced M1-like macrophages. With the GHS-R deficient macrophages from our *LysM-Cre;Ghsr*$^{f/f}$ mice, I found that GHS-R affects macrophage polarization by regulating PKA-CREB signaling, which promotes gene transcription of IRS2 and AKT signaling. In the final chapter, I discussed conclusions and future directions

regarding the role of macrophage GHS-R as a driver of macrophage programing and metabolic dysregulation.

CHAPTER II

MYELOID-SPECIFIC GHS-R IS AN IMPORTANT IMMUNE REGULATOR

Introduction

Inflammation underlies a wide variety of inflammatory processes. Metabolically triggered inflammation is termed "meta-inflammation," which underlies the pathological processes of many immune-associated metabolic dysfunctions. Macrophages are important cells of the immune system, consisting of two subtypes designated M1 and M2 type (48, 97). M1-like macrophages are characterized by expressing both F4/80, CD11c but not CD206 and responsible for producing pro-inflammatory cytokines such as TNF-α, IL-1β, and IL-6. These M1 type macrophages are associated with obesity and insulin resistance. In contrast, M2-like macrophages express both F4/80, CD206 but not CD11c and release anti-inflammatory cytokines, including IL-10 and Arg1 (48, 97). They are mainly implicated in lean and insulin sensitivity. Thus, M1/M2 macrophage ratio is considered a critical determinant for the state of pro-/anti-inflammatory.

Ghrelin, an endogenous ligand for GHS-R, is the only known circulating orexigenic hormone known to stimulate appetite and promote obesity and insulin resistance (110-113). GHS-R is highly expressed in the hypothalamus but relatively lower in peripheral tissues (83, 114). Historical view of research on ghrelin mainly focused on the roles of ghrelin signaling, primarily with its orexigenic function; very few studies have been done with its non-orexigenic roles. Emerging evidence shows that GHS-R is also expressed in immune cells, including macrophages and monocytes (94, 97). However, the

role of ghrelin signaling in systemic inflammation is controversial (86, 90, 91). The ghrelin/GHS-R signal has been reported to be involved in cholesterol release in human macrophages (86). Elevated cholesterol causes low-grade inflammation in humans (88), and the links between lipid metabolism and immune responses have been documented (86, 89). These observations indicate that ghrelin signaling has important roles in immunity and inflammation, but the direct effects of ghrelin signaling need to be investigated. Here, we have studied the role of GHS-R in myeloid cells using our newly generated myeloid-specific GHS-R deleted mice (*LysM-Cre;Ghsr*$^{f/f}$) and assessed the myeloid-specific functions of GHS-R under normal physiological condition.

Material and Methods

Animals

Previously we reported the generation of fully backcrossed GHS-R floxed mice on C57BL/6J background (115). Using a Cre-Lox system, we generated myeloid-specific GHS-R deficient (*LysM-Cre;Ghsr*$^{f/f}$) mice by breeding *Ghsr*$^{f/f}$ mice with widely used myeloid-specific *LysM-Cre* (JAX stock 4781) (116). Mice were housed in the animal facility of Texas A&M University (college station, Texas), maintained on 12-hour light and 12-hour dark cycles (lights on at 6:00 AM) at 75 F ± 1. Food and water were available ad libitum. RD diet was obtained from Harlan Teklad with the following composition (Fig. 1): RD (2920X): 6.5% fat, 60% carbohydrates, 19.1% protein. All experiments were

conducted in accordance with the NIH guidelines and approved by the institutional animal care and use committee.

Macronutrients		
Crude Protein	%	19.1
Fat (acid hydrolysis)	%	6.5
Carbohydrate (available)	%	47.0
Crude Fiber	%	2.7
Neutral Detergent Fiber	%	12.3
Ash	%	5.1
Selected Nutrient Information		
Energy Density	Kcal/g (kJ/g)	3.1
Calories from Protein	%	24
Calories from Carbohydrate	%	60
Calories from Fat	%	16
Fatty Acids		
Total Saturated Fat	%	0.8
Total Monounsaturated Fat	%	1.1
Total Polyunsaturated Fat	%	2.9
C16:0 Palmitic Acids	%	0.6
C18:0 Stearic Acids	%	0.1
C18:1 Oleic Acids	%	1.1
C18:2 Linoleic Acids	%	2.6
C18:3 Linolenic Acids	%	0.3

Figure 1. The formula and selected nutrient information RD used in this study.

Body composition, indirect calorimetry, and functional tests

All body composition and metabolic parameters data were obtained as we previously described (117). All GTT and ITT were performed as we previously described (117).

Plasma insulin was measured using RIA assay kit (SRI-13K, EMD Millipore, Billerica, MA) or multiplex according to manufactory instruction.

Blood chemistry analysis

Blood was collected by retroorbital bleeding during anesthesia. The blood samples were allowed to clot at room temperature for 30 min before centrifugation (13,000 rpm, 4°C, 15 min), and the serum was collected and stored at -80°C until analyzed for cytokine levels using a commercially available Mouse adipokine kit (Milliplex Map kit, cat# MHSTCMAG-70K, Billerica, MA, USA) and Luminex reader according to the manufacturer's instructions. The serum adiponectin and FFA analysis used Adiponectin Elisa kit (Millipore-Sigma) and FFA Elisa kit (Cayman Chemical) respectively.

eWAT SVF and liver NPC isolation

SVF was isolated as described previously (118, 119). Briefly, 1g of epididymal adipose tissue was dissected and minced in RPMI 1640 media (Gibco) containing 1 mg/ml collagenase Type I (Worthington Chemicals). The solution was incubated in 37°C water bath for 30 minutes. The tissue slurry was then filtered through nylon mesh to remove undigested tissue and centrifuged at 2200 rpm to fractionate adipocytes and SVF.

Liver NPCs were isolated as described previously (120). Briefly, anesthetize the mouse using isoflurane, then perfuse and digest the liver with perfusion buffer via the portal vein. Collect the digested liver and make cell suspension. Purify the cells using Percoll (Sigma) gradient.

Collected SVF cells and NPCs (1×10^6 in a volume of 100 μl of PBS) were incubated with antibodies for flow cytometry analysis.

PM isolation

PMs were obtained from the peritoneum of *Ghsr*$^{f/f}$ or *LysM-Cre;Ghsr*$^{f/f}$ mice as described (121). Briefly, mice were euthanized by rapid cervical dislocation after anesthetization with isoflurane. Then, 3 mL ice-cooled PBS with 2% fetal bovine serum was injected into the abdominal cavity. After gentle shaking for 3 minutes, abdominal fluid was collected into tubes using a syringe with 18G needle. Red blood cells were lysed with ACK lysis buffer for 5 min and quench the reaction by adding two times the volume of PBS. PMs were then collected by centrifugation at 450 g for 10 minutes. The equal number of PMs (2 X 10^5 cells/well) was seeded into 96 well plates in RPMI 1640 media with antibodies for flow cytometry analysis.

Flow cytometry

Cell preparation for flow cytometry was performed as described above. For the cell surface staining, the cells were washed twice with FACS buffer (PBS, pH 7.4, with 2% BSA) and incubated with nonspecific IgG to assess background fluorescence and then stained with a mixture of fluorescently labeled antibodies for 30 min on ice against BV510 anti-mouse CD45 antigen, Alexa Fluor700 anti-mouse Ly6G antigen, APCCy7 anti-mouse CD11b antigen, PeCy7 anti-mouse F4/80 antigen, PE anti-mouse CD38 antigen, Alexa Fluor488 anti-mouse CD206 antigen, and BV421 anti-mouse CX3CR1, and labeled with 7AAD to distinguish live/dead. For the intracellular staining, cells were incubated with BD GolgiPlug for 4 hrs before labeled against live/dead aqua in PBS. Cells were then washed with PBS and then FACS buffer and incubated with nonspecific IgG before labeling against PerCP anti-mouse CD45 antigen, Alexa Fluor700 anti-mouse Ly6G antigen,

APCCy7 anti-mouse CD11b antigen, PeCy7 anti-mouse F4/80 antigen. The cells were washed with FACS buffer and fixed in 2% PFA for 30 min and permeabilized in perm/wash buffer (BD bioscience) for 30 min on ice before labeling against PE-Dazzle594 anti-mouse TNFα antigen for 30 min on ice. Cells washed before data acquisition on ASTRIOS flow cytometry (Beckman Coulter, Indianapolis, IN, USA) and FACS analysis was performed using Flowjo software (Tree Star Inc., OR USA).

Statistical Analysis

Statistical analyses were performed with Graphpad Prism 6.01. Data are presented as the means ± SEM. *$p \leq 0.05$, **$p \leq 0.01$, ***$p \leq 0.001$ vs. *LysM -Cre;Ghsr*$^{f/f}$, #$p<0.05$, ##$p<0.01$, ###$p<0.001$ vs. treatment using t-test or two-way ANOVA.

Results

Generation of myeloid-specific GHS-R ablated mice

In order to investigate the role of GHS-R in myeloid cells, we first generated myeloid-specific GHS-R deletion mouse model by breeding *lysozyme (LysM-Cre*) mice (JAX stock 4781) with our fully backcrossed *Ghsr*$^{f/f}$ mice (control) (116, 122, 123). Heterozygous *LysM-Cre;Ghsr*$^{f/+}$ mice from this breeding were used as a breeder to further generate homozygous *LysM-Cre;Ghsr*$^{f/f}$ mice as the gene targeting strategy shown in diagram Fig. 2A. In *LysM-Cre;Ghsr*$^{f/f}$ mice, GHS-R expression was significantly decreased ~74% in the PM and ~57% SVF of eWAT, the fraction contains adipose tissue macrophages, but not in the brain, Hypo and other peripheral tissues including MA of eWAT, liver, and

GAS (cq value: 37~39) (Fig. 2B). This result demonstrates that GHS-R deletion in *LysM-Cre*;*Ghsr*$^{f/f}$ mice is restricted to myeloid cells.

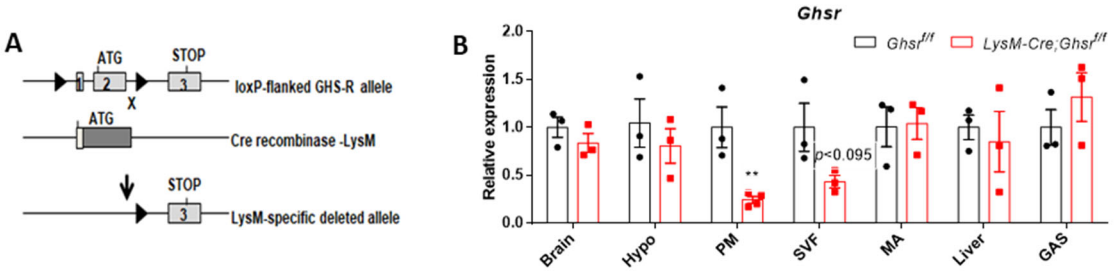

Figure 2. Generation of myeloid-specific GHS-R deleted mice and preliminary validation.
(A) Schematic diagram of the loxP-flanked *Ghsr* allele before and after Cre-derived recombination. Exons 1 and 2 deleted during recombination. Triangle represents loxP sites.
(B) *Ghsr* gene expression in whole brain, hypothalamus (Hypo), peritoneal macrophages (PM), stromal vascular fraction (SVF) from epididymal white adipose tissue, mature adipocytes (MA) from epididymal white adipose tissue, liver, and gastrocnemius muscles (GAS) (n=3-4 mice/group).
Data are presented as the means ± SEM. $^{**}p \leq 0.01$ *vs*. *LysM* -Cre;*Ghsr*$^{f/f}$ using t-test.

Myeloid-specific GHS-R deficiency does not affect metabolic characterization

Under RD, we found that myeloid-specific GHS-R deletion had no significant effect on serum active ghrelin level (Fig. 3A). In line with the active ghrelin level which is involved in meal initiation and appetite stimulation causing weight gain (66), control and *LysM-Cre;Ghsr*$^{f/f}$ mice exhibited indistinguishable weight curves, body fat and lean content, tissue/body weight percentage (Fig. 3B-3E). Additionally, food intake, physical activity, and energy expenditure did not show any difference between both genotypes (Fig. 3F-3H).

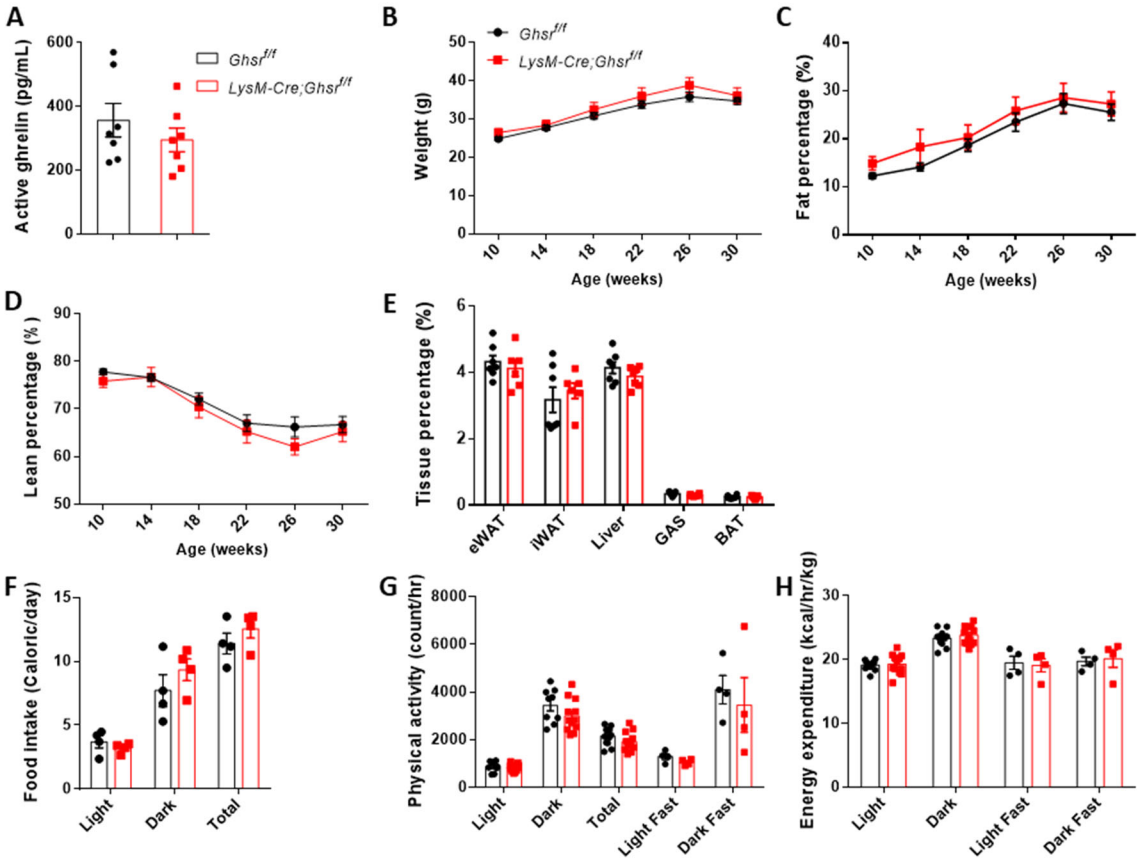

Figure 3. Physiological characterization of myeloid-specific GHS-R knockout mice.
(A) Serum active ghrelin level in RD-fed control and RD-fed *LysM-Cre;Ghsr*$^{f/f}$ mice (n=7 mice/group).
(B-D) Monthly body weight (B), fat body composition (C), and lean body composition (D) of RD-fed control and RD-fed *LysM-Cre;Ghsr*$^{f/f}$ mice under fed condition (n=11 mice/group).
(E) Tissue/body weight percentage of RD-fed control and RD-fed *LysM-Cre;Ghsr*$^{f/f}$ mice under fed condition (n=6-7 mice/group).
(F-H) Food intake (E), physical activity (F), and energy expenditure (G) level of RD-fed control and RD-fed *LysM-Cre;Ghsr*$^{f/f}$ mice (n=4-12).
Data are presented as the means ± SEM. *$p \leq 0.05$ vs. *LysM -Cre;Ghsr*$^{f/f}$ using two-way ANOVA or t-test.

Myeloid-specific GHS-R deficiency does not affect energy homeostasis

Similarly, fed and fasting blood glucose, plasma insulin level, glucose tolerance, and insulin sensitivity were comparable between both groups under RD (Fig. 4A-4D). Taken

together, these data reveal that myeloid-specific GHS-R deficiency does not require metabolic regulation and energy homeostasis under RD feeding.

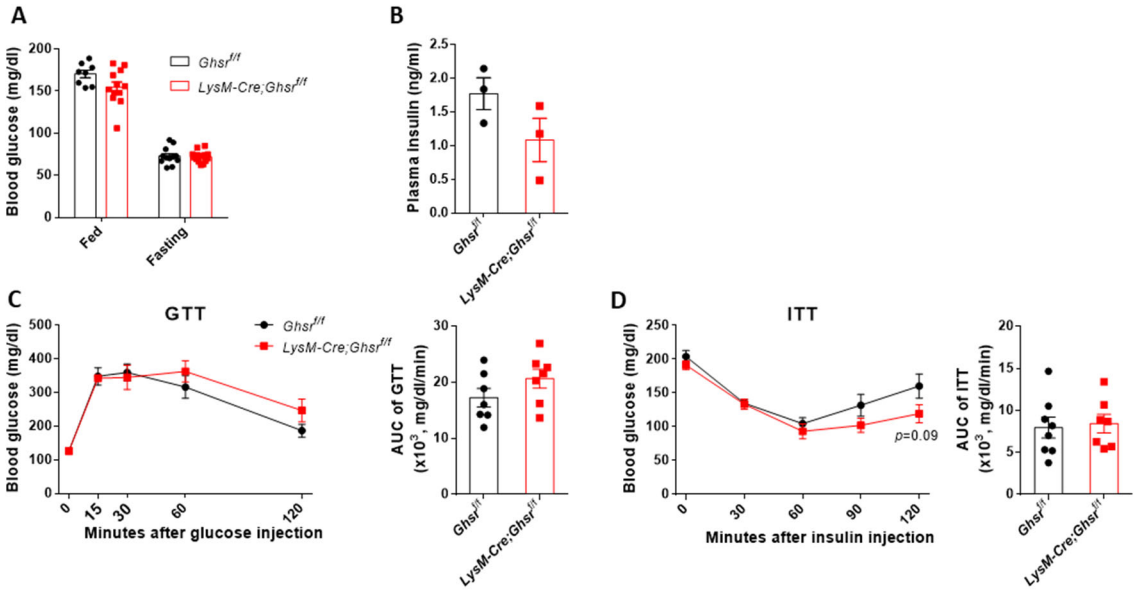

Figure 4. Metabolic characterization of myeloid-specific GHS-R knockout mice.
(A) Blood glucose level under fed or 16 hrs fasting condition in RD-fed control and RD-fed *LysM-Cre;Ghsr*$^{f/f}$ mice (n=8-12 mice/group).
(B) Plasma insulin level in RD-fed control and RD-fed *LysM-Cre;Ghsr*$^{f/f}$ mice after 3 hrs fasting (n=3 mice/group).
(C) GTT in RD-fed control and RD-fed *LysM-Cre;Ghsr*$^{f/f}$ mice after 16 hrs fasting (n=7 mice/group).
(D) ITT in RD-fed control and RD-fed *LysM-Cre;Ghsr*$^{f/f}$ mice after 4 hrs fasting (n=7-8 mice/group).
Data are presented as the means ± SEM. *$p \leq 0.05$ vs. *LysM -Cre;Ghsr*$^{f/f}$ using two-way ANOVA or t-test.

Myeloid-specific GHS-R deficiency shows a profile of reduced inflammation

Although there was no effect of myeloid-specific GHS-R in metabolic characterization or energy homeostasis, significantly alleviated serum pro-inflammatory cytokine level was found in RD-fed *LysM-Cre;Ghsr*$^{f/f}$ mice comparing with RD-fed control mice (Fig. 5A). In line with the alleviated serum pro-inflammatory cytokine level, the mRNA level of pro-inflammatory cytokines in PMs was reduced by GHS-R deficiency (Fig. 5B). PMs were labeled against fluorophore-conjugated antibodies and analyzed by following the gating

strategies (Fig. 5C and 5D). Similarly, myeloid-specific GHS-R deletion showed a mild decrease of TNFα (p<0.083) in PMs without altering the percentage of macrophage subset, M1- or M2-type macrophage subsets (Fig. 5E-5G).

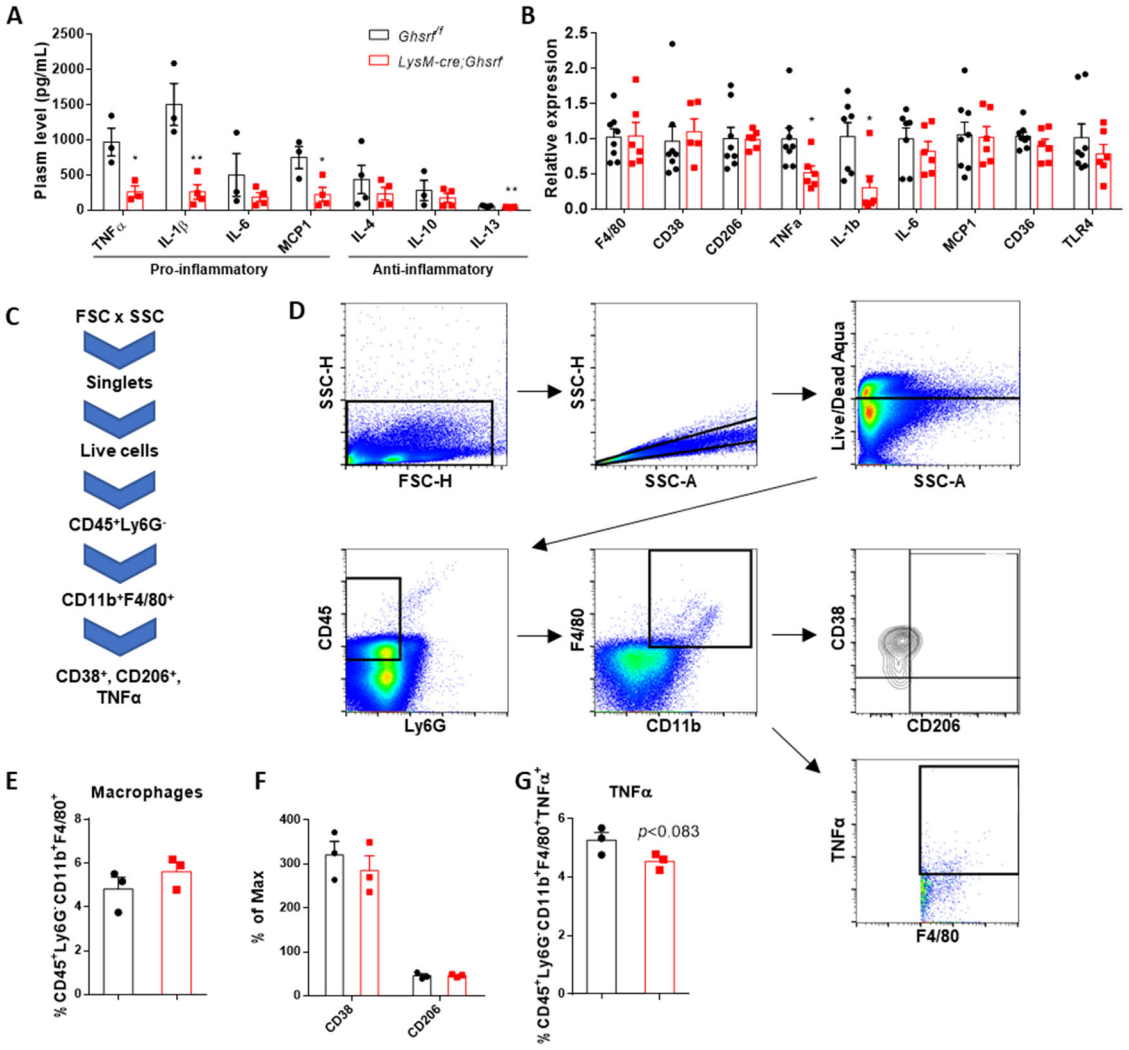

Figure 5. Inflammatory characterization of myeloid-specific GHS-R knockout mice.
(A) Serum inflammatory cytokine level in RD-fed control and RD-fed *LysM-Cre;Ghsr*$^{f/f}$ mice (n=3-4).
(B) mRNA level of macrophage signature and pro-inflammatory cytokine/chemokine related genes in PMs of RD-fed control and RD-fed *LysM-Cre;Ghsr*$^{f/f}$ (n=5-8 mice/group).
(C and D) Flow cytometry gating strategies in PMs
(E-G) Percentage of macrophage subset (E), MFI of CD38 and CD206 (F), and TNFα (G) in PMs of RD-fed control and RD-fed *LysM-Cre;Ghsr*$^{f/f}$ mice (n=3 mice/group).
Data are presented as the means ± SEM. *$p \leq 0.05$, **$p \leq 0.01$ vs. *LysM -Cre;Ghsr*$^{f/f}$ using two-way ANOVA or t-test.

Myeloid-specific GHS-R deficiency does not affect macrophage infiltration in eWAT and liver

Tissue macrophages were labeled against fluorophore-conjugated antibodies and analyzed by following the gating strategies (Fig. 6A and 6B). Under RD condition, percentage of macrophage subset in SVF of eWAT showed a decreased trend (p<0.053) in line with mildly decreased in the percentage of IM subset in RD-fed *LysM-Cre;Ghsr*$^{f/f}$ mice comparing with RD-fed control mice (Fig. 6C and 6D). Interestingly, the percentage of KC subset was increased in RD-fed control while myeloid-specific GHS-R deletion reduced the KC subset (Fig. 6F and 6G). However, the changes of macrophage infiltration to the eWAT (Fig. 6E) and liver (Fig. 6H) were very mild which is confirmed by Mac-2 staining.

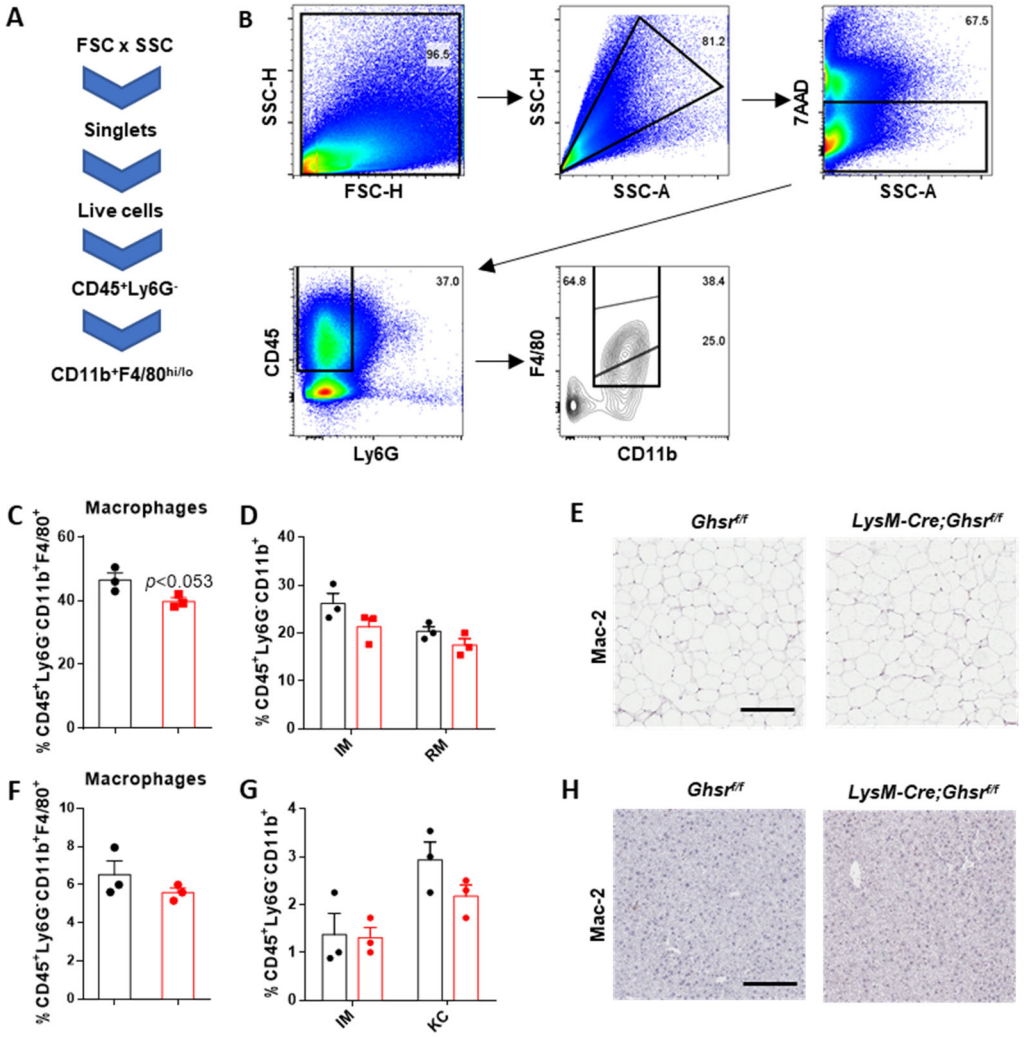

Figure 6. Tissue macrophages in eWAT and liver of myeloid-specific GHS-R knockout mice.
(A and B) Flow cytometry gating strategies in tissue macrophages.
(C and D) Percentage of macrophage subset (B) and IM and RM (C) in eWAT SVF of RD-fed control and *LysM-Cre;Ghsr*$^{f/f}$ mice (n=3 mice/group).
(E) Immunohistochemistry staining of MAC-2 in eWAT (n=3 mice/group).
(F and G) Percentage of macrophage subset (D) and IM and KC (E) in liver NPCs of RD-fed control and *LysM-Cre;Ghsr*$^{f/f}$ mice (n=3 mice/group).
(H) Immunohistochemistry staining of MAC-2 in the liver (n=3 mice/group).
Data are presented as the means ± SEM. *$p \leq 0.05$ vs. *LysM -Cre;Ghsr*$^{f/f}$ using two-way ANOVA or t-test.

Discussion

We previously reported that GHS-R global null mice protect age-associated low-grade inflammatory responses in both WAT and BAT by shifting macrophage phenotype from M1-like to M2-like macrophages (83). To eliminate the possibility of secondary effect from central or other immune cells, the current study using myeloid-specific GHS-R deleted mice has been conducted to examine whether GHS-R in myeloid cells mediates adipose inflammation by regulating macrophage phenotype under physiological conditions.

In physiological conditions, approximately 10% of the cells in adipose tissue stain positive for macrophage marker in humans (CD68) and mice (F4/80) (124). Macrophages play a crucial role in host defense and inflammatory microenvironment (125). Research has shown that macrophages work in efferocytosis, angiogenesis, lipid buffering, and eliminating damaged cells in a lean state (126). The complex crosstalk between adipocytes and macrophages is found in numerous reports, including the ability of preadipocytes to differentiate into macrophages (127) and vice versa (macrophages to differentiate into preadipocytes) (128).

Although there was no difference between genotypes in phenotypical characteristics, energy consumption, and insulin sensitivity on RD feeding (Fig. 3 and 4), myeloid-specific GHS-R deficiency reduced pro-inflammatory cytokines in serum and PMs on RD (Fig. 5A). This data demonstrates that GHS-R deletion in myeloid cells reduces systemic inflammation without changing the insulin sensitivity of RD-fed mice, possibly due to insufficient levels of inflammation on RD to cause insulin resistance to

demonstrate the effect of myeloid-specific GHS-R. Therefore, we further conduct the study in pathological conditions, inducing inflammation using endotoxin LPS.

CHAPTER III

THE ROLE OF MYELOID-SPECIFIC GHS-R IN LPS-INDUCED ACUTE INFLAMMATION (ENDOTOXEMIA)

Introduction

Sepsis and septic shock are unusual systemic inflammatory responses to infection, causing high mortality in intensive care units (129-131). Sepsis is a common condition associated with acute systemic inflammation and oxidative stress, leading to massive terminal organ dysfunction. Under LPS-induced sepsis, the liver plays a vital role in immunological homeostasis and energy (133, 134), and therefore, LPS-induced liver injury in mice has been employed to simulate the course of liver failure in septic endotoxemia (132-134). Although the specific mechanism remains unclear, a consensus has been well reached that hepatic apoptosis caused by inflammatory oxidative stress might make a significant contribution to liver failure.

Growth hormone secretagogue receptor (GHS-R) is the only endogenous receptor for the gut hormone ghrelin identified to date (135). Our previous studies suggest GHS-R to be a driver of inflammatory responses (97, 107). We showed global ablation of GHS-R in mice decreases liver steatosis, adipose inflammation, and GHS-R knockdown in macrophage cells reduces the expression of pro-inflammatory cytokine genes, possibly through regulation of macrophage polarization.

To explore the role of myeloid GHS-R in the pathogenesis of sepsis, we subjected myeloid-specific GHS-R knockout mice (*LysM*-Cre;*Ghsr*$^{f/f}$) to an experimental model of

sepsis, induced by the bacterial toxin LPS and monitored mortality rate and liver inflammation which may regulate by macrophage GHS-R.

Material and Methods

Animals

Previously we reported the generation of fully backcrossed GHS-R floxed mice on C57BL/6J background (115). Using a Cre-Lox system, we generated myeloid-specific GHS-R deficient (*LysM-Cre;Ghsr*$^{f/f}$) mice by breeding *Ghsr*$^{f/f}$ mice with widely used myeloid-specific *LysM-Cre* (JAX stock 4781) (116). Mice were housed in the animal facility of Texas A&M University (college station, Texas), maintained on 12-hour light and 12-hour dark cycles (lights on at 6:00 AM) at 75 F ± 1. Food and water were available ad libitum. All diets were obtained from Harlan Teklad with the following composition: RD (2920X): 6.5% fat, 60% carbohydrates, 19.1% protein.

Endotoxin-induced model of sepsis

Sepsis was induced in age-matched male *Ghsr*$^{f/f}$ (control) and *LysM-Cre;Ghsr*$^{f/f}$ mice (3 month-old, 22-27 g) by *i.p*. injection of bacterial endotoxin (LPS, *Escherichia coli* 055:B5; Sigma-Aldrich) given at a single acute does of 5 mg/kg. Mortality was recorded for up to 72 hours after the onset of sepsis. Blood, PMs, and liver are collected after 24 hrs of LPS administration. All experiments were conducted in accordance with the NIH guidelines and approved by the institutional animal care and use committee.

Blood chemistry analysis

Blood was collected by retroorbital bleeding during anesthesia for serum cytokine analysis. The blood samples were allowed to clot at room temperature for 30 min before centrifugation (13,000 rpm, 4°C, 15 min) and the serum was collected and stored at -80°C until analyzed for cytokine levels using a commercially available Mouse adipokine kit (Milliplex Map kit, cat# MHSTCMAG-70K, Billerica, MA, USA) and Luminex reader according to the manufacturer's instructions.

PM isolation

PMs were obtained from the peritoneum of *Ghsr*$^{f/f}$ or *LysM-Cre;Ghsr*$^{f/f}$ mice after *i.p*. injection of bacterial endotoxin (LPS, *Escherichia coli* 055:B5; Sigma-Aldrich) given at a single acute does of 5 mg/kg as described (121). Briefly, mice were euthanized by rapid cervical dislocation after anesthetization with isoflurane. Then, 3 mL ice-cooled PBS with 2% fetal bovine serum was injected into the abdominal cavity. After gentle shaking for 3 minutes, abdominal fluid was collected into tubes using a syringe with 18G needle. Red blood cells were lysed with ACK lysis buffer for 5 min and quench the reaction by adding two times the volume of PBS. PMs were then collected by centrifugation at 450 g for 10 minutes. The equal number of PMs (1 X 10^6 cells/well) was seeded into 96 well plates in RPMI 1640 media containing L-glutamine, 10% fetal bovine serum, 100U/ml penicillin, 100µg/ml streptomycin as described at 37 °C in a humidified, 5% CO_2 incubator for 4 hr.

BMDM isolation, culture, and treatment

Bone marrow cells were isolated from the tibias and femurs of mice as previously described (136). Cells were seeded into 6-well plates at a density of 1.5 X 10^6 cells/well and cultured in a humidified incubator at 37 and 5% CO_2. The culture medium was RPMI

1640 medium containing L-glutamine, 10% fetal bovine serum, 100U/ml penicillin, and 100 μg/ml streptomycin supplemented with 10 ng/mL macrophage colony-stimulating factor (M-CSF) for 7 days. At the end of the 7 days culture period, >95% of the cells were positive for macrophage markers and bone marrow-derived macrophages (BMDMs) were subjected to inflammatory assays. On the seventh day, cells were counted and replated with either LPS (100 ng/mL) or saline for 4 hours.

Quantitative real-time PCR. Total RNA was isolated using TRIzol® Reagent (Invitrogen, Carlsbad, CA) or Aurum Total RNA mini kit (Bio-Rad Laboratories, Inc., Hercules, CA, USA) according to the manufacturer's instructions. RNA samples were treated with RNase-free DNase (Ambion, Austin, TX) to remove genomic DNA before reverse transcription. Reverse transcription was performed using Superscript III First Strand Synthesis System (Invitrogen, Carlsbad, CA) according to the manufacturer's instructions. Quantitative real-time PCR reaction was performed as we previously described (117). Ghsr-1α primers designed including the intron for distinguishing from the expression of GHS-R 1β as below: sense primer 5′-GGACCAGAACCACAAACAGACA-3′, anti-sense primer 5′-CAGCAGAGGATGAAAGCAAACA-3′ (82). The rest of the primer information is available upon request.

Statistical Analysis

Statistical analyses were performed with Graphpad Prism 6.01. Data were presented as mean ± SEM. Data are presented as the means ± SEM. *$p \leq 0.05$, **$p \leq 0.01$, ***$p \leq 0.001$

vs. *LysM -Cre;Ghsr*$^{f/f}$, #p<0.05, ##p<0.01, ###p<0.001 vs. treatment using t-test or two-way ANOVA.

Results

Myeloid-specific GHS-R deletion protects against lethal endotoxemia and systemic inflammation

To investigate the role of macrophage GHS-R during acute pro-inflammatory responses, we evaluated the effects against lethal endotoxemia in an LPS-induced *in vivo* model. Mice were treated *i.p.* with LPS at 5 mg/kg and mortality was monitored over a 70 hrs period. This high dose of LPS was chosen because it led to a mortality rate of >90% in control mice. Surprisingly, we found significant protection against lethal endotoxemia in myeloid GHS-R deficiency protected against lethal endotoxemia in *LysM-Cre;Ghsr*$^{f/f}$ mice (Fig. 7A). Myeloid-specific GHS-R deficiency simultaneously reduced the serum levels of pro-inflammatory cytokines without affecting serum levels of anti-inflammatory cytokines under LPS-induced endotoxemia (Fig. 7B and 7C).

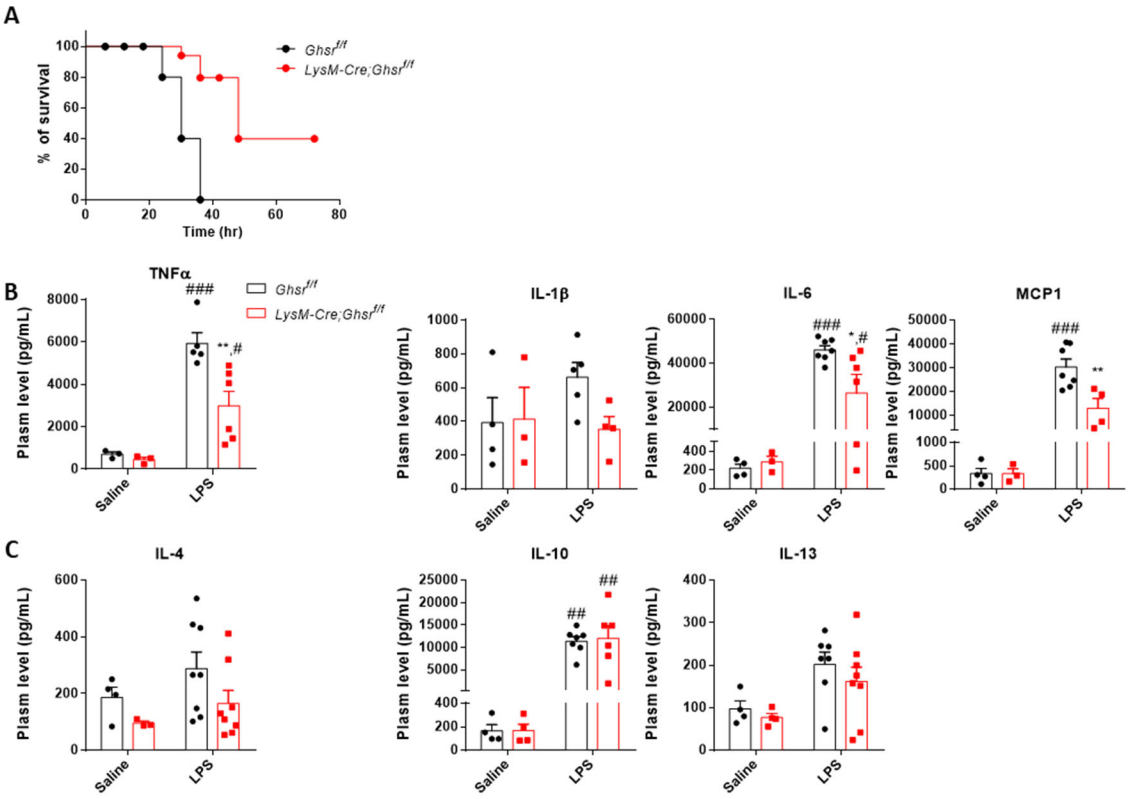

Figure 7. Myeloid-specific GHS-R deletion protects against lethal endotoxemia and attenuates systemic inflammation in LPS-induced endotoxemia.
(A) Survivability rate after LPS (5 mg/kg) *i.p.* administration in control and *LysM-Cre;Ghsr$^{f/f}$* mice (n=13-17 mice/group).
(B and C) Serum pro- (B) and anti- (C) cytokine level after 24 hrs of LPS (5 mg/kg) *i.p.* administration in control and *LysM-Cre;Ghsr$^{f/f}$* mice.
(n=3-8 mice/group).
Data are presented as the means ± SEM. *$p \leq 0.05$ vs. *LysM -Cre;Ghsr$^{f/f}$*, #$p \leq 0.05$, ##$p \leq 0.01$, ###$p \leq 0.001$ vs. treatment using two-way ANOVA.

Myeloid-specific GHS-R deletion attenuates inflammatory responses in liver and hepatocytes

The liver is a major organ that plays a crucial role in immunological homeostasis and metabolism while the system is impaired by a bacterial infection (132, 137). Inducing liver injury with a high dose of LPS in the murine model has been employed as a model for

studying failure or death in septic endotoxemia (132, 134). A currently predominant concept of the underlying mechanism is increased oxidative stress and apoptosis from the hepatic inflammatory response. To investigate the inhibitory effect of macrophage GHS-R against liver failure in LPS-induced endotoxemia, mRNA level of pro-inflammatory cytokines in the liver has been examined. As shown in Fig. 8A, pro-inflammatory responses were dramatically increased by LPS administration in control mice while myeloid-specific GHS-R deficiency protected against the LPS-induced pro-inflammatory response. To explore the direct communication between macrophages and hepatocytes, primary hepatocytes from control mice were co-cultured with conditional media from LPS-treated BMDMs of control and *LysM-Cre;Ghsr*$^{f/f}$ mice. In agree with the result from liver tissue, hepatocytes cultured with conditional media from *LysM-Cre;Ghsr*$^{f/f}$ BMDMs showed significantly lower pro-inflammatory cytokine expression (Fig. 8B).

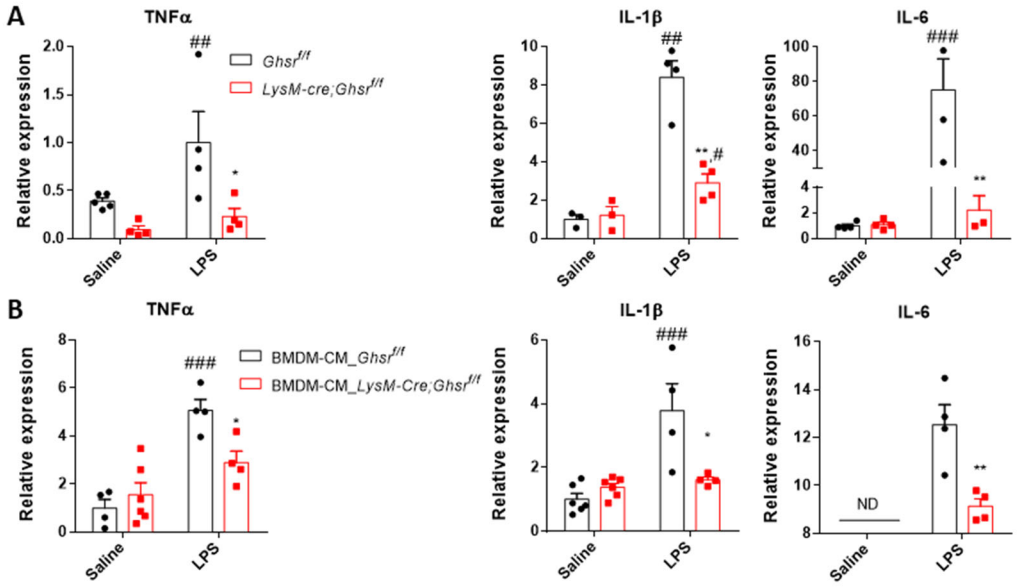

Figure 8. Myeloid-specific GHS-R deletion attenuates inflammation in liver and hepatocytes of LPS-induced endotoxemia and LPS-induced inflammation.
(A) mRNA level of pro-inflammatory cytokine related genes in liver of control and *LysM-Cre;Ghsr$^{f/f}$* mice after LPS (5 mg/kg) *i.p.* administration (n=3-5 mice/group).
(B) mRNA level of pro-inflammatory cytokine related genes in control-hepatocytes incubated with conditional media from 4 hrs of 100 µg/mL LPS treated BMDMs of control and *LysM-Cre;Ghsr$^{f/f}$* (n=4-6 mice/group).
Data are presented as the means ± SEM. *$p \leq 0.05$ vs. *LysM -Cre;Ghsr$^{f/f}$*, #$p \leq 0.05$, ##$p \leq 0.01$, ###$p \leq 0.001$ vs. LPS using two-way ANOVA.

Myeloid-specific GHS-R deletion attenuates pro-inflammatory responses in PMs

To further validate the role of macrophage GHS-R in the inflammatory response under LPS-induced endotoxemia, PMs were obtained from the peritoneum of control or *LysM-Cre*;*Ghsr$^{f/f}$* mice after 24 hrs of LPS administration. qPCR analysis revealed that the mRNA of *TNFα, IL-1β*, and *IL-6* was significantly upregulated in PMs upon LPS stimulation in PMs of control mice and dampened by GHS-R deletion PMs of LPS-injected *LysM-Cre*;*Ghsr$^{f/f}$* mice (Fig. 9A). The reduced protein level of the pro-inflammatory cytokines measured by flow analysis (Fig. 9B and 9C) further supports the regulatory role of myeloid-specific GHS-R in pro-inflammatory response.

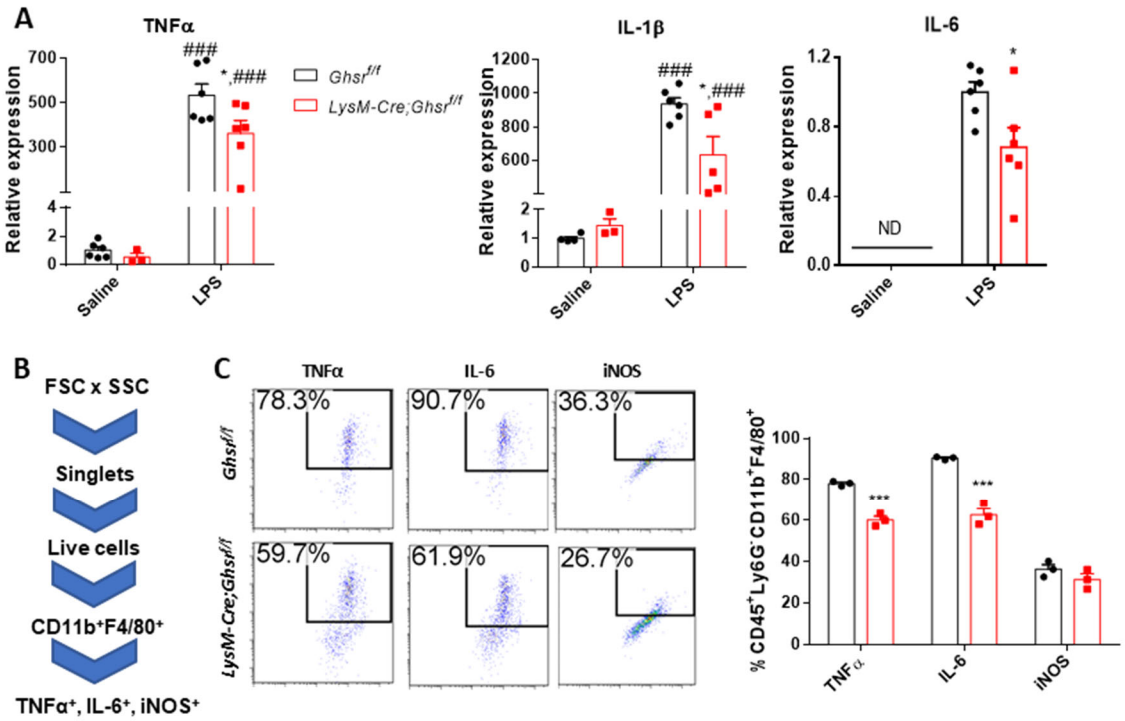

Figure 9. Myeloid-specific GHS-R deletion attenuates inflammation in PMs in LPS-induced endotoxemia.
(A) mRNA level of pro-inflammatory cytokine related genes in PMs of control and *LysM-Cre;Ghsr*$^{f/f}$ mice after LPS (5 mg/kg) *i.p.* administration (n=3-6 mice/group).
(B) Flow cytometry gating strategies in PMs .
(C) Percentage of pro-inflammatory cytokine subsets in PMs of control and *LysM-Cre;Ghsr*$^{f/f}$ mice after LPS (5 mg/kg) *i.p.* administration (n=3 mice/group).
Data are presented as the means ± SEM. *$p \leq 0.05$, * $p \leq 0.001$ vs. *LysM -Cre;Ghsr*$^{f/f}$, ###$p \leq 0.001$ vs. treatment using two-way ANOVA or t-test.

Myeloid-specific GHS-R deletion attenuates LPS-induced pro-inflammatory responses and M1-like polarization in BMDMs

To further study the inflammatory response at a cellular level, we used BMDMs from control and *LysM-Cre;Ghsr*$^{f/f}$ mice. BMDMs were exposed to LPS for 4 hrs and were lysate for mRNA study. The conditional media was collected to measure the cytokine levels. In both control and *LysM-Cre;Ghsr*$^{f/f}$ BMDMs, LPS stimulation led to increased pro-inflammatory cytokine levels in both cells and conditional media (Fig. 10A and 10B).

However, those from *LysM-Cre;Ghsr*$^{f/f}$ mice showed attenuated inflammatory response against LPS exposure which was in agreement with the *in vivo* findings. According to the flow analysis, this is possibly due to the reduction of M1-like macrophage polarization regulated by GHS-R in macrophages (Fig. 10C-10E).

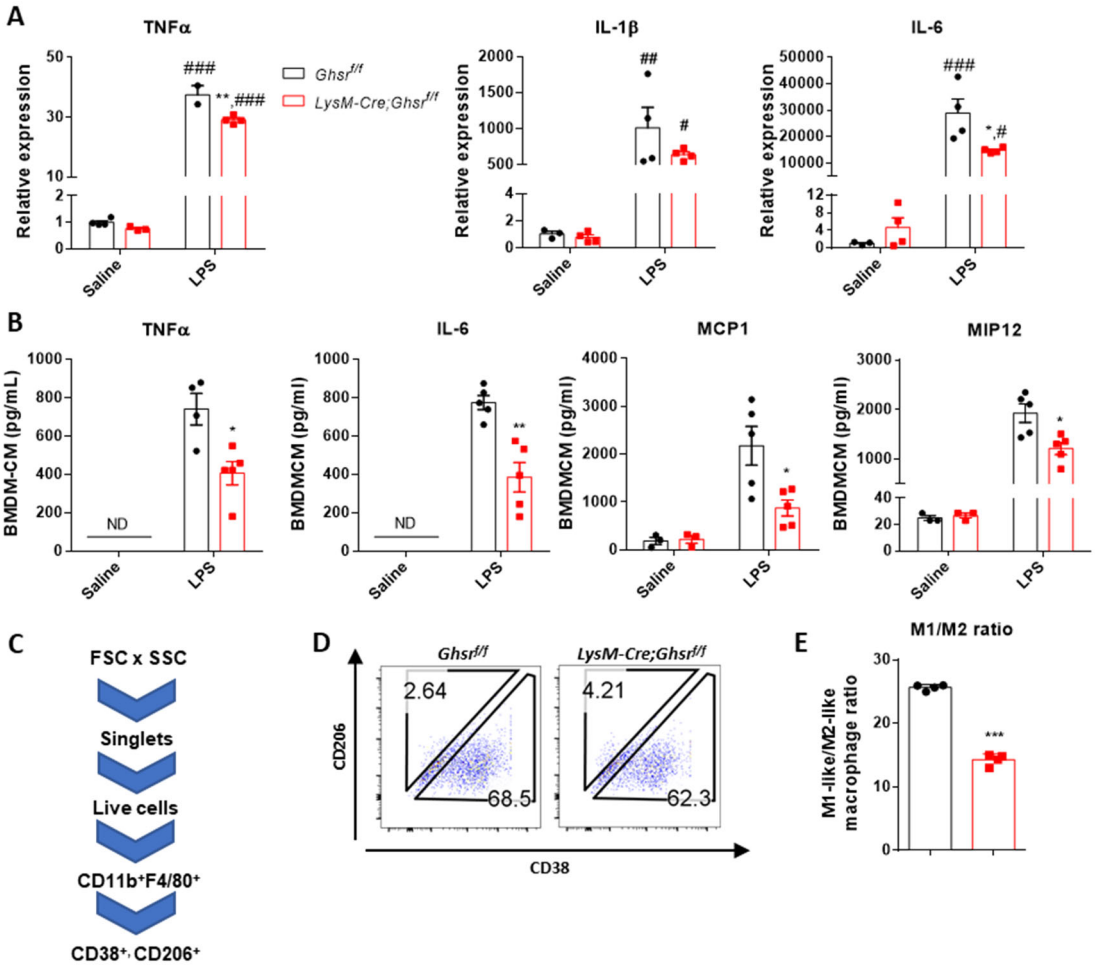

Figure 10. Myeloid-specific GHS-R deletion reduces inflammatory responses in BMDMs against LPS stimulation.
(A) mRNA level of pro-inflammatory cytokines in BMDMs of control and *LysM-Cre;Ghsr*$^{f/f}$ mice after 4 hrs of 100 ng/mL LPS stimulation (n=3-4/group).
(B) Cytokine/chemokine level in the conditioned media from BMDMs of control and *LysM-Cre;Ghsr*$^{f/f}$ mice after 4 hrs of 100 ng/mL LPS stimulation (n=3-5/group).
(C) Flow cytometry gating strategies in BMDMs (n=4 /group).
(D and E) Percentage of CD38 and CD 206 subsets (D) and M1-like/M2-like macrophage ratio.
Data are presented as the means ± SEM. *$p \leq 0.05$, **$p \leq 0.01$, ***$p \leq 0.001$ vs. *LysM -Cre;Ghsr*$^{f/f}$, #$p \leq 0.05$, ##$p \leq 0.01$, ###$p \leq 0.001$ vs. LPS using two-way ANOVA or t-test.

Macrophage GHS-R is an important immune regulator in LPS-induced pro-inflammatory responses and M1-like polarization in BMDMs

In this set of experiments, we sought to determine the role of GHSR in LPS-induced inflammation in the aspects of gain- or loss-of-function achieved by using GHS-R antagonist (JMV2959) in BMDMs and GHS-R overexpression in cultured murine macrophages (Raw264.7 cells). The GHS-R antagonist yield a 60% reduction of Ghsr expression compared with saline-treated cells (control) (Fig. 11A). It clearly shows that pre-treatment with GHS-R antagonist reduced LPS-induced expression of pro-inflammatory markers *TNFα*, *IL-1β*, *IL-6* and *MCP1* (Fig. 11B). Experiment using GHS-R in Raw264.7 cells (Fig. 11C) confirmed the reduced mRNA level of pro-inflammatory cytokines (Fig. 11D). These data suggest that GHS-R directly affects the inflammatory response of macrophages, and a GHS-R antagonist mitigates LPS-induced macrophage inflammation.

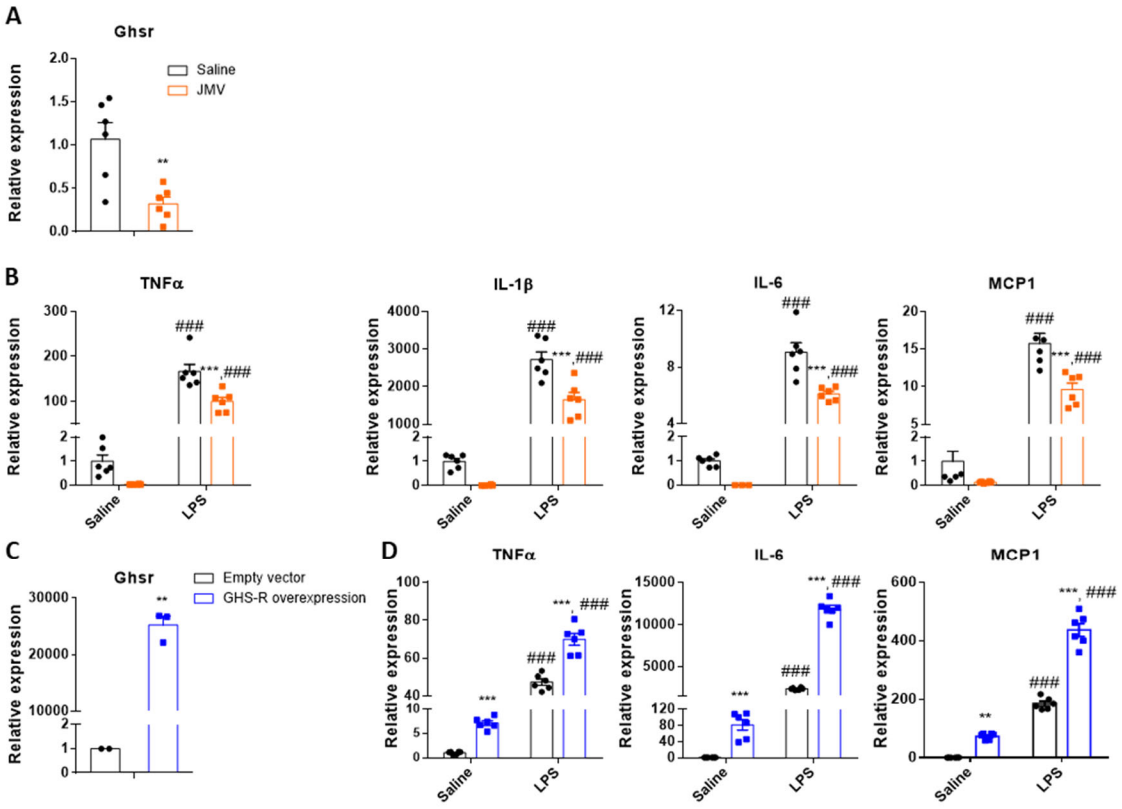

Figure 11. GHS-R affects inflammatory responses in macrophages *in vitro*.
(A and B) mRNA level of *Ghsr* (A) and pro-inflammatory cytokines (B) in BMDMs of control mice with or without 3 μM GHS-R antagonist JMV2959 after 4 hrs of 100 ng/mL LPS stimulation (n=5-6/group).
(C and D) mRNA level of *Ghsr* (C) and pro-inflammatory cytokines (D) in Raw264.7 cells with or without GHS-R overexpression after 4 hrs of 100 ng/mL LPS stimulation (n=2-6/group).
Data are presented as the means ± SEM. $^{**}p \leq 0.01$, $^{***}p \leq 0.001$ vs. *LysM -Cre;Ghsr*$^{f/f}$, $\#\#\#p \leq 0.001$ vs. LPS using two-way ANOVA.

Discussion

Sepsis, caused by the acute systemic inflammatory response (138), requires further study for elucidating the mechanism of mortality to provide promising clinical strategies (139). A recent study suggested that LPS-induced liver damage is associated with inflammatory mediators such as TNFα, IL-1β, and superoxide, contributing to mitochondrial dysfunction (140).

Mitochondrial function is a central determinant of clinical outcome since it is the primary target of acute inflammation-induced oxidative stress. Based on the cellular microenvironment, diverse stress conditions increase ROS generation from prooxidants and NO (141, 142). Several lines of evidence showed that ROS plays a leading role in septic shock and organ failure (143, 144).

Here, we characterized the functional role of GHS-R in macrophages in LPS-induced endotoxemia. We found *LysM*-Cre;*Ghsr*$^{f/f}$ mice displayed a significantly longer survival time, reduced circulating inflammatory cytokine levels, and lower inflammation in liver tissues and hepatocytes in a paracrine manner. To understand the cellular mechanism of macrophage GHS-R in local and systemic inflammation under LPS-induced endotoxemia, we conducted *ex vivo* and *in vitro* studies using bone marrow-derived macrophages (BMDMs) and Raw264.7 cells. GHS-R deficient BMDMs showed reduced pro-inflammatory polarization and decreased expression of pro-inflammatory cytokine genes. This pro-inflammatory effect of GHS-R in macrophages is confirmed in loss- and gain-of-function.

Taken together, our data demonstrated that GHS-R has cell-autonomous effects in macrophages in modulating mitochondrial function and inflammatory response, which in turn modulate systemic inflammation. Our studies suggest GHS-R may be a novel therapeutic target in inflammatory disorders such as sepsis.

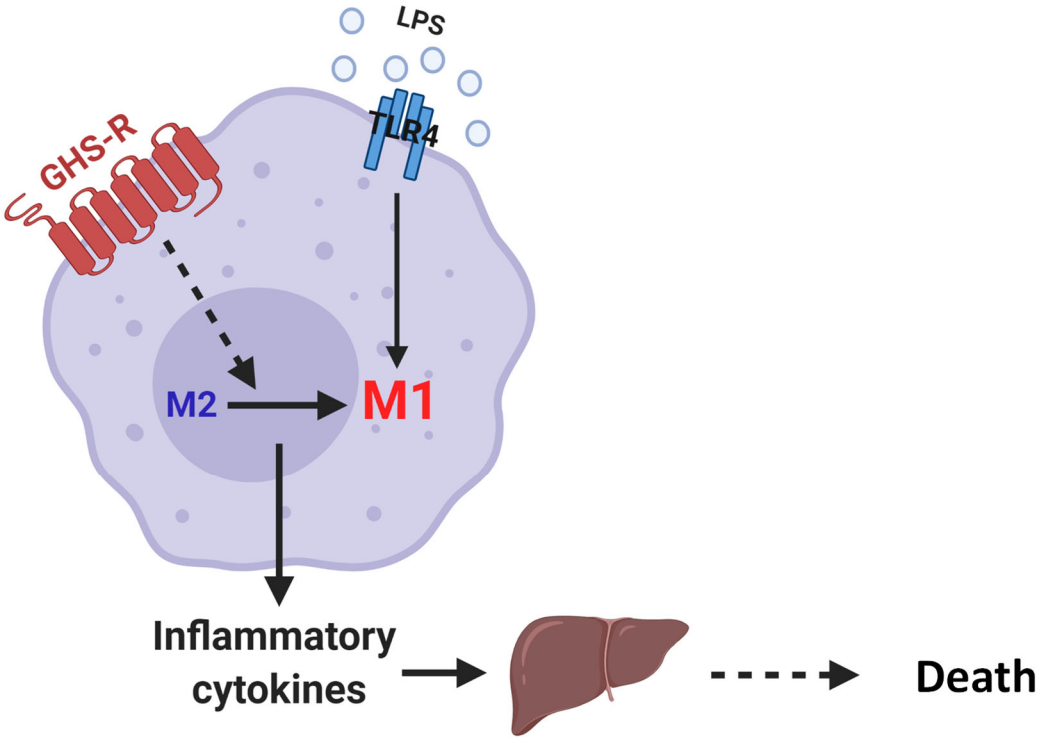

Figure 12. Diagrammatic conclusion of chapter III.
Macrophage GHS-R augments systemic inflammation by programing macrophage polarization to M1. Increased inflammatory cytokines impairs liver in paracrine manner which may lead to liver failure and cause deceases.

CHAPTER IV

THE ROLE OF MYELOID-SPECIFIC GHS-R IN DIET-INDUCED CHRONIC INFLAMMATION

Introduction

Inflammation correlates with increased obesity, which is known to induce low-grade chronic inflammation in adipose tissue and liver tissues. Obesity-associated meta-inflammation can elicit the development of obesity-related insulin resistance (3, 4), dysregulation of fatty acid metabolism (145, 146) and chronic diseases such as NAFLD (1, 2). In the inflammatory processes, chronic inflammation increases circulating inflammatory mediators and induces the recruitment, proliferation, and activation of various immune cells that together regulate the cellular response that orchestrates tissue damage and/or repair (5). Although many immune cell types are involved in tissue damage or repair processes (6), macrophages have been shown to exhibit critical regulatory activity at all stages of inflammatory and tissue reparative responses in different organ systems (7).

Macrophages are a crucial determinant of meta-inflammation and are present as monocytes in circulation or as infiltrated or resident macrophages in tissues (147-149). Phenotypic and functional changes of recruited and resident macrophages play critical roles in local tissue microenvironment and tissue homeostasis (54, 150). Depending on the signals to which macrophages are exposed, they can be polarized into two subtypes; M1 or M2 subtype (48, 97). M1-like macrophages are characterized by expressing both F4/80,

CD38 but not CD206 and responsible for producing pro-inflammatory cytokines such as TNF-α, IL-1β, and IL-6. These M1-like macrophages are associated with obesity and insulin resistance. In contrast, M2-like macrophages express both F4/80, CD206 but not CD38 and release anti-inflammatory cytokines, including IL-10 and arginase 1 (48, 97). They are mainly implicated in lean and insulin sensitivity. Thus, M1/M2 macrophage ratio is considered as a critical determinant for the state of pro-/anti-inflammatory.

Our previous study demonstrated that GHS-R deletion mitigates the effects of high fructose corn syrup (HFCS) on adipose inflammation and liver steatosis (106). Our recent study further demonstrated that antagonism of GHS-R decreases pro-inflammatory gene expression in macrophages in vitro (97). These observations suggest that ghrelin signaling may have important roles in immunity and inflammation, but the direct effects of GHS-R in macrophages are unknown. Here, we have studied the role of GHS-R in macrophages using our newly generated myeloid-specific GHS-R deleted mice (*LysM-Cre;Ghsr*$^{f/f}$) and assess the myeloid-specific functions of GHS-R in macrophage infiltration and polarization under chronic DIO-induced inflammation.

Material and Methods

Animals

Previously we reported the generation of fully backcrossed GHS-R floxed mice on C57BL/6J background (115). Using a Cre-Lox system, we generated myeloid-specific GHS-R deficient (*LysM-Cre;Ghsr*$^{f/f}$) mice by breeding *Ghsr*$^{f/f}$ mice with widely used myeloid-specific *LysM-Cre* (JAX stock 4781) (116). Mice were housed in the animal

facility of Texas A&M University (college station, Texas), maintained on 12-hour light and 12-hour dark cycles (lights on at 6:00 AM) at 75 F ± 1. Food and water were available ad libitum. All diets were obtained from Harlan Teklad with the following composition: HFD (TD 88137): 42% fat, 42.7% carbohydrates, 15.2% protein calories. All experiments were conducted in accordance with the NIH guidelines and approved by the institutional animal care and use committee.

Formula		
Casein	g/kg	195.0
DL-Methionine	g/kg	3.0
Sucrose	g/kg	341.46
Corn Starch	g/kg	150.0
Andydrous Milkfat	g/kg	210.0
Cholesterol	g/kg	1.5
Cellulose	g/kg	50.0
Mineral Mix	g/kg	35.0
Calcium Carbonate	g/kg	4.0
Vitamin Mix	g/kg	10.0
Ethoxyquin	g/kg	0.04
Selected Nutrient Information		
Energy Density	Kcal/g (kJ/g)	4.5
Calories from Protein	%	15.2
Calories from Carbohydrate	%	42.7
Calories from Fat	%	42.0
Fatty Acids		
Total Saturated Fat	%	12.8
Total Monounsaturated Fat	%	5.6
Total Polyunsaturated Fat	%	1.0
C16:0 Palmitic Acids	%	28.9
C18:0 Stearic Acids	%	12.5
C18:1 Oleic Acids	%	20.9
C18:2 Linoleic Acids	%	2.3
C18:3 Linolenic Acids	%	0.7

Figure 13. The formula and selected nutrient information HFD used in this study.

Body composition, indirect calorimetry, and functional tests

All body composition and metabolic parameters data were obtained as we previously described (117). All GTT and ITT were performed as we previously described (117). Plasma insulin was measured using RIA assay kit (SRI-13K, EMD Millipore, Billerica, MA) or multiplex according to manufactory instruction.

Blood chemistry analysis

Blood was collected by retroorbital bleeding during anesthesia. The blood samples were allowed to clot at room temperature for 30 min before centrifugation (13,000 rpm, 4°C, 15 min) and the serum was collected and stored at -80°C until analyzed for cytokine levels using a commercially available Mouse adipokine kit (Milliplex Map kit, cat# MHSTCMAG-70K, Billerica, MA, USA) and Luminex reader according to the manufacturer's instructions. Serum adiponectin and FFA analysis used the Adiponectin Elisa kit (Millipore-Sigma) and FFA Elisa kit (Cayman Chemical).

eWAT SVF and liver NPC isolation

SVF was isolated as described previously (118, 119). Briefly, 1g of epididymal adipose tissue was dissected and minced in RPMI 1640 media (Gibco) containing 1 mg/ml collagenase Type I (Worthington Chemicals). The solution was incubated in 37°C water bath for 30 minutes. The tissue slurry was then filtered through nylon mesh to remove undigested tissue and centrifuged at 2200 rpm to fractionate adipocytes and SVF.

Liver NPCs were isolated as described previously (120). Briefly, anesthetize the mouse by using isoflurane, then perfuse and digest the liver with perfusion buffer via the portal vein. Collect the digested liver and make cell suspension. Purify the cells using Percoll (Sigma) gradient.

Collected SVF cells and NPCs (1×10^6 in a volume of 100 µl of PBS) were incubated with antibodies for flow cytometry analysis.

PM isolation

Peritoneal macrophages (PMs) were obtained from the peritoneum of *Ghsr*$^{f/f}$ or *LysM-Cre;Ghsr* $^{f/f}$ mice as described (121). Briefly, mice were euthanized by rapid cervical dislocation after anesthetization with isoflurane. Then, 3 mL ice-cooled PBS with 2% fetal bovine serum was injected into the abdominal cavity. After gentle shaking for 3 minutes, abdominal fluid was collected into tubes using a syringe with 18G needle. Red blood cells were lysed with ACK lysis buffer for 5 min and quench the reaction by adding two times the volume of PBS. PMs were then collected by centrifugation at 450 g for 10 minutes. The equal number of PMs ($2 \text{ X } 10^5$ cells/well) was seeded into 96 well plates in RPMI 1640 media containing L-glutamine, 10% fetal bovine serum, 100U/ml penicillin, 100µg/ml streptomycin as described at 37 °C in a humidified, 5% CO_2 incubator for 4 hr.

BMDM isolation, culture, and treatment

Bone marrow cells were isolated from the tibias and femurs of mice as previously described (136). Cells were seeded into 6-well plates at a density of $1.5 \text{ X } 10^6$ cells/well and cultured in a humidified incubator at 37 and 5% CO_2. The culture medium was RPMI 1640 medium containing L-glutamine, 10% fetal bovine serum, 100U/ml penicillin, and 100 µg/ml streptomycin supplemented with 10 ng/mL macrophage colony-stimulating factor (M-CSF) for 7 days. At the end of the 7 days culture period, >95% of the cells were positive for macrophage markers and bone marrow-derived macrophages (BMDMs) were

subjected to inflammatory assays. On the seventh day, cells were counted and replated with either PA 150 μM or BSA for 24 hours.

Flow cytometry

Cell preparation for flow cytometry was performed as described above. For the cell surface staining, the cells were washed twice with FACS buffer (PBS, pH 7.4, with 2% BSA) and incubated with nonspecific IgG to assess background fluorescence and then stained with a mixture of fluorescently labeled antibodies for 30 min on ice against BV510 anti-mouse CD45 antigen, Alexa Fluor700 anti-mouse Ly6G antigen, APCCy7 anti-mouse CD11b antigen, PeCy7 anti-mouse F4/80 antigen, PE anti-mouse CD38 antigen, Alexa Fluor488 anti-mouse CD206 antigen, BV421 anti-mouse CX3CR1, and APC anti-mouse CD36 antigen and labeled with 7AAD to distinguish live/dead. For the intracellular staining, cells were incubated with BD GolgiPlug for 4 hrs before labeled against live/dead aqua in PBS. Cells were then washed with PBS and then FACS buffer and incubated with nonspecific IgG before labeling against PerCP anti-mouse CD45 antigen, Alexa Fluor700 anti-mouse Ly6G antigen, APCCy7 anti-mouse CD11b antigen, PeCy7 anti-mouse F4/80 antigen. The cells were washed with FACS buffer and fixed in 2% PFA for 30 min and permeabilized in perm/wash buffer (BD bioscience) for 30 min on ice before labeling against PE-Dazzle594 anti-mouse TNFα antigen, PE anti-mouse IL-1β antigen, APC anti-mouse IL-6 antigen, and Alexa Fluor488 anti-mouse iNOS antigen for 30 min on ice. Cells washed before data acquisition on ASTRIOS flow cytometry (Beckman Coulter,Indianapolis, IN, USA) and FACS analysis was performed using Flowjo software (Tree Star Inc., OR USA).

Immunohistochemistry staining

For detection of Mac-2, 5 μm paraffin-imbedded eWAT or liver sections were fixed and processed for immunohistochemistry using the avidin-biotin peroxidase complex (ABC, ThermoFisher, Waltham, MA) method and diaminobenzidine (DAB)-nickel reactions (Abcam, Cambridge, UK) as previously described (151). Briefly, sections were de-paraffinized and dehydrated. Sections were incubated sequentially with 3% H_2O_2 to block peroxidase, Mac-2 antibody (Abcam), then followed by secondary antibody (anti-rabbit) and ABC solution. After the DAB-nickel reaction, the sections were counterstained with 0.1% neutral red solution, and analyzed using a light microscope (Olympus DX 51, Olympus, Tokyo) and a charge-coupled device camera (Olympus DP12).

Quantitative real-time PCR

Total RNA was isolated using TRIzol® Reagent (Invitrogen, Carlsbad, CA) or Aurum Total RNA mini kit (Bio-Rad Laboratories, Inc., Hercules, CA, USA) according to the manufacturer's instructions. RNA samples were treated with RNase-free DNase (Ambion, Austin, TX) to remove genomic DNA before reverse transcription. Reverse transcription was performed using Superscript III First Strand Synthesis System (Invitrogen, Carlsbad, CA) according to the manufacturer's instructions. Quantitative real-time PCR reaction was performed as we previously described (117). Ghsr-1α primers designed including the intron for distinguishing from the expression of GHS-R 1β as below: sense primer 5′-GGACCAGAACCACAAACAGACA-3′, anti-sense primer 5′-CAGCAGAGGATGAAAGCAAACA-3′ (82). The rest of the primer information is available upon request.

Statistical Analysis

Statistical analyses were performed with Graphpad Prism 6.01. Data were presented as mean ± SEM. Data are presented as the means ± SEM. *$p \leq 0.05$, **$p \leq 0.01$, ***$p \leq 0.001$ vs. *LysM -Cre;Ghsr*$^{f/f}$, #$p<0.05$, ##$p<0.01$, ###$p<0.001$ vs. treatment using t-test or two-way ANOVA.

Results

Myeloid-specific GHS-R deletion alleviates diet-induced insulin resistance and impairment of glucose

To examine the contribution of myeloid-specific GHS-R to metabolic regulation on diet-induced obesity, we fed control and *LysM-Cre*;*Ghsr*$^{f/f}$ mice HFD for 5- to 7-months starting at 8-weeks of age. Similar to RD feeding, serum active ghrelin level, body weight, body fat mass, and tissue/body weight percentage were indistinguishable between control and *LysM-Cre*;*Ghsr*$^{f/f}$ mice under HFD (Fig. 14A-14E). Myeloid-specific GHS-R deletion did not alter food intake, physical activity, and energy expenditure under HFD feeding (Fig. 14F-14H).

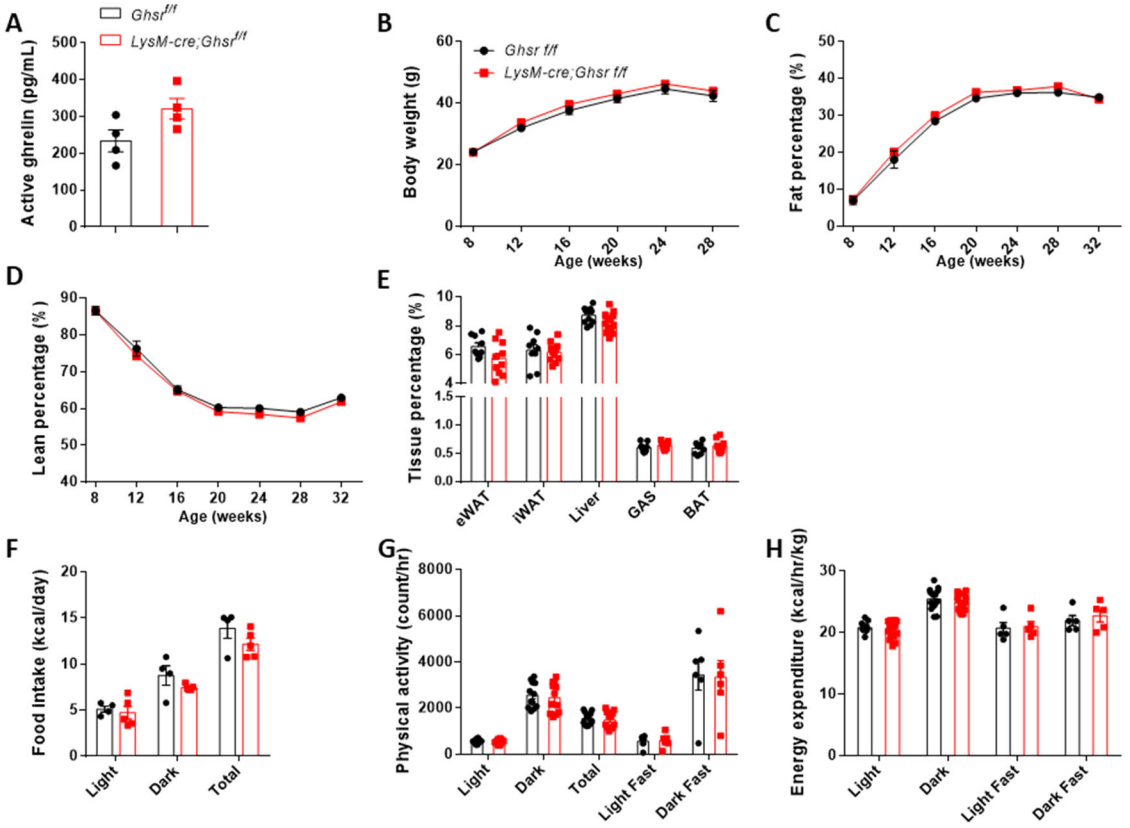

Figure 14. Myeloid-specific GHS-R deletion does not alter phenotypical characterization in HFD-fed mice.

(A) Serum active ghrelin level in HFD-fed control and HFD-fed *LysM-Cre;Ghsr*$^{f/f}$ mice (n=4 mice/group).
(B-D) Monthly body weight (B), fat body composition (C), and lean body composition (D) of HFD-fed control and HFD-fed *LysM-Cre;Ghsr*$^{f/f}$ mice under fed condition (n=11-14 mice/group).
(E) Tissue/body weight percentage of HFD-fed control and HFD-fed *LysM-Cre;Ghsr*$^{f/f}$ mice under fed condition (n=9-14 mice/group).
(E-G) Food intake (E), physical activity (F), and energy expenditure (G) level of HFD-fed control and HFD-fed *LysM-Cre;Ghsr*$^{f/f}$ mice (n=4-12 mice/group).
Data are presented as the means ± SEM. *$p \leq 0.05$ vs. *LysM -Cre;Ghsr*$^{f/f}$ using two-way ANOVA or t-test.

In addition to the metabolic change, obesity is a causative factor for type 2 diabetes through induction of insulin resistance (152). Interestingly, fed or fasting glucose level and plasma insulin concentration under HFD feeding showed lower blood glucose and insulin concentration in *LysM-Cre*;*Ghsr*$^{f/f}$ mice compared to control mice (Fig. 15A and 15B). We further calculated homeostasis model assessment of insulin resistance (HOMA-

IR) in the HFD-fed mice. Consistent with decreased blood glucose and plasma insulin levels, the HOMA-IR values of obese *LysM-Cre*;*Ghsr*$^{f/f}$ mice were <58% lower than those of control mice (Fig. 15C). *LysM-Cre*;*Ghsr*$^{f/f}$ mice were less hyperglycemic with lower plasma insulin concentration during an intraperitoneal glucose tolerance test (Fig. 15D) in line with increased insulin sensitivity as measured by serum insulin level during GTT and insulin tolerance test (Fig. 15E and 15F).

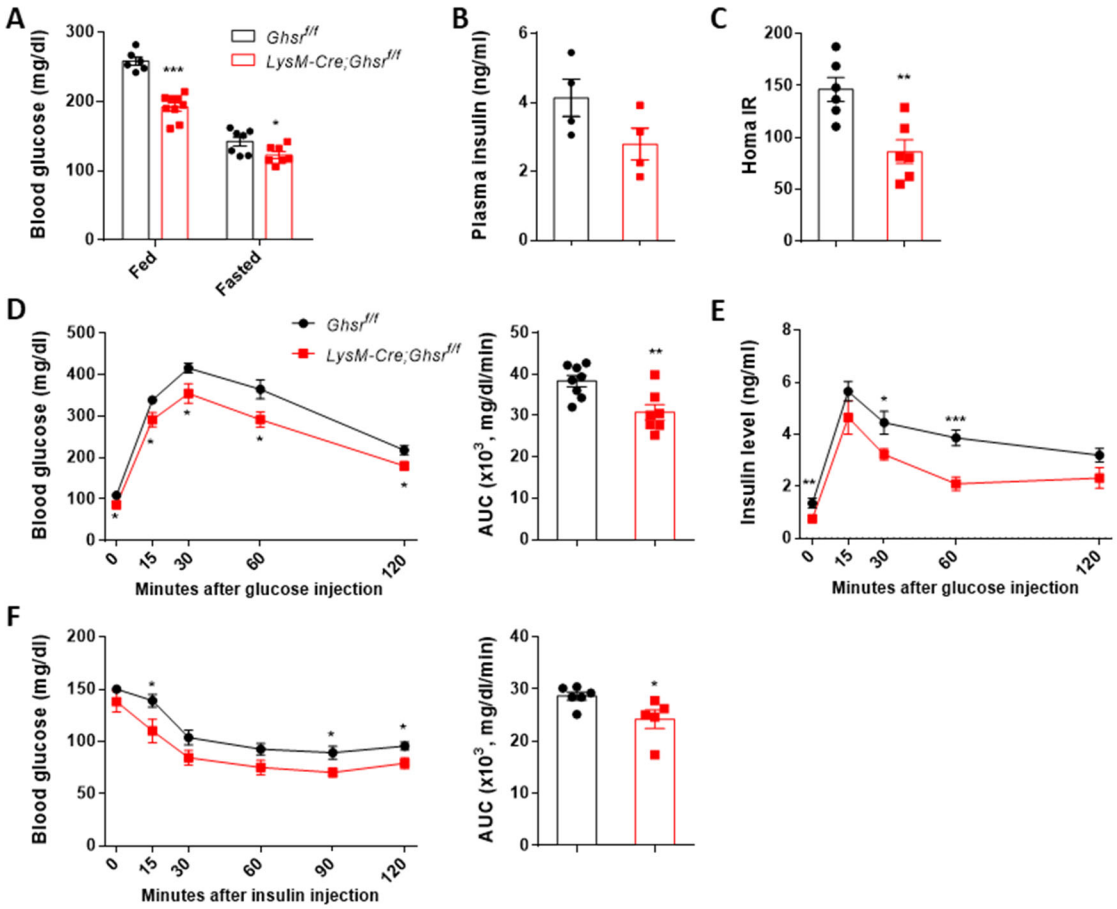

Figure 15. Myeloid-specific GHS-R deletion attenuates insulin resistance in HFD-fed mice.
(A) Blood glucose level under fed or 16 hrs fasting condition in RD-fed control and RD-fed *LysM-Cre;Ghsr*$^{f/f}$ mice (n=6-9 mice/group).
(B) Plasma insulin level in HFD-fed control and HFD-fed *LysM-Cre;Ghsr*$^{f/f}$ mice after 3 hrs fasting (n=4 mice/group).
(C) HOMA-IR was calculated using the following formula: fasting glucose (mg/dl) × fasting insulin (ng/ml) (n=6 mice/group).
(D and E) GTT (D) and serum insulin level (E) from GTT in HFD-fed control and HFD-fed *LysM-Cre;Ghsr*$^{f/f}$ mice after 16 hrs fasting (n=7-8 mice/group).
(F) ITT in HFD-fed control and HFD-fed *LysM-Cre;Ghsr*$^{f/f}$ mice after 4 hrs fasting (n=5-6 mice/group).
Data are presented as the means ± SEM. *$p \leq 0.05$, *$p \leq 0.01$, *$p \leq 0.001$ vs. *LysM-Cre;Ghsr*$^{f/f}$ using two-way ANOVA or t-test.

However, pyruvate tolerance showed no difference between genotypes (Fig. 16A). We next examined the gluconeogenesis-related genes in the liver of HFD-fed control and *LysM-Cre*;*Ghsr*$^{f/f}$ mice but the expression of gluconeogenesis genes was comparable (Fig. 16B). These results indicate that improvement of glucose utilization in the liver may not be the predominant factor causing insulin sensitivity in HFD-fed *LysM-Cre*;*Ghsr*$^{f/f}$ mice.

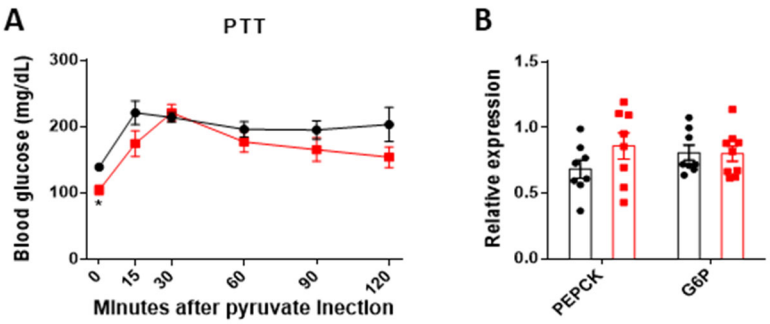

Figure 16. Myeloid-specific GHS-R deletion does not alter gluconeogenesis in liver of HFD-fed mice.
(A) PTT in HFD-fed control and HFD-fed *LysM-Cre;Ghsr*$^{f/f}$ mice after 16 hrs fasting (n=7-8 mice/group).
(B) mRNA level of gluconeogenesis related genes in liver of HFD-fed control and HFD-fed *LysM-Cre;Ghsr*$^{f/f}$ (n=8 mice/group).
Data are presented as the means ± SEM. *$p \leq 0.05$ vs. *LysM-Cre;Ghsr*$^{f/f}$ using t-test.

Myeloid-specific GHS-R deletion reduces systemic inflammation and circulating monocytes with high infiltrative capacity

It is well known that obesity leads to inflammation which further triggers for the development of insulin resistance (153, 154). When exposed to HFD, control mice significantly elevated serum pro-inflammatory cytokine levels over those exposed to RD (Fig. 5A and 17A). Moreover, HFD-fed *LysM-Cre*;*Ghsr*$^{f/f}$ mice showed lower serum levels of TNFα, IL-1β, IL-6, and MCP1 compared to HFD-fed control mice (Fig. 17A). The other measured serum anti-inflammatory cytokines, IL-4, IL-10, and IL-13, were not

significantly different between genotypes on HFD (Fig. 17B). Collectively, these suggest that under RD or HFD feeding, GHS-R deletion in myeloid cells reduces pro-inflammatory cytokine profile and prevents HFD-induced insulin resistance.

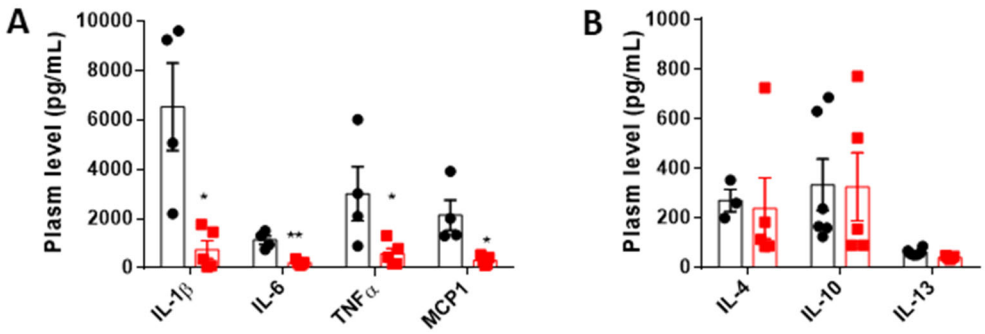

Figure 17. Myeloid-specific GHS-R deletion attenuates serum inflammatory cytokine level in HFD-fed mice.
(A and B) Serum pro- (A) and anti- (B) inflammatory cytokine level in HFD-fed control and HFD-fed *LysM-Cre;Ghsr*$^{f/f}$ mice (n=4-6).
Data are presented as the means ± SEM. *$p \leq 0.05$, *$p \leq 0.01$ vs. *LysM -Cre;Ghsr*$^{f/f}$ using t-test.

Myeloid-specific GHS-R deletion attenuates obesity-associated macrophage recruitment and inflammatory response in eWAT

Because deletion of GHS-R in myeloid cells reduced migratory and infiltrative capacity of monocytes to tissues (data not shown), we next investigated the contribution of myeloid-specific GHS-R to obesity-related accumulation of macrophages and inflammation in eWAT. *Ghsr* expression was significantly down-regulated in myeloid-specific GHS-R deleted eWAT comparing with control eWAT under HFD-feeding (Fig. 18A). Compared to HFD-fed control mice, HFD-fed *LysM*-Cre;*Ghsr*$^{f/f}$ mice had reduced CLS and macrophage infiltration in eWAT as measured by Mac-2 staining (Fig. 18B). To further study phenotypic polarization and inflammation of adipose tissue macrophages, we interrogated the F4/80^{lo} and F4/80^{hi} populations for macrophage phenotypic

polarization as described in Fig. 18C. We used the established markers CD38 for M1-like and CD206 for M2-like macrophages (155, 156). The current finding showed that myeloid-specific GHS-R reduced the percentage of macrophages and macrophage infiltration to the eWAT (Fig. 18D and 18E). The previous study demonstrated that within the $CD11b^{+}F4/80^{+}$ ATM population, two distinct populations ($F4/80^{hi}$ and $F4/80^{lo}$) were distinguished by CX3CR1 expression which indicates that resident ATMs are predominantly $F4/80^{lo}CX3CR1^{-}$ and that ATMs infiltrating during obesity are primarily $F4/80^{hi}CX3CR1^{+}$ (157) as we showed in Fig. 18F. We found that MFI of CX3CR1 was down-regulated by myeloid-specific GHS-R deletion (Fig. 18G).

In addition HFD-fed *LysM-Cre;Ghsr*$^{f/f}$ mice showed reduced expression of pro-inflammatory cytokines in eWAT (Fig. 18H). Together, the dynamics of macrophage infiltration was shown over the course of HFD-induced cell infiltration into the SVF of adipose tissue which alleviates inflammation in eWAT.

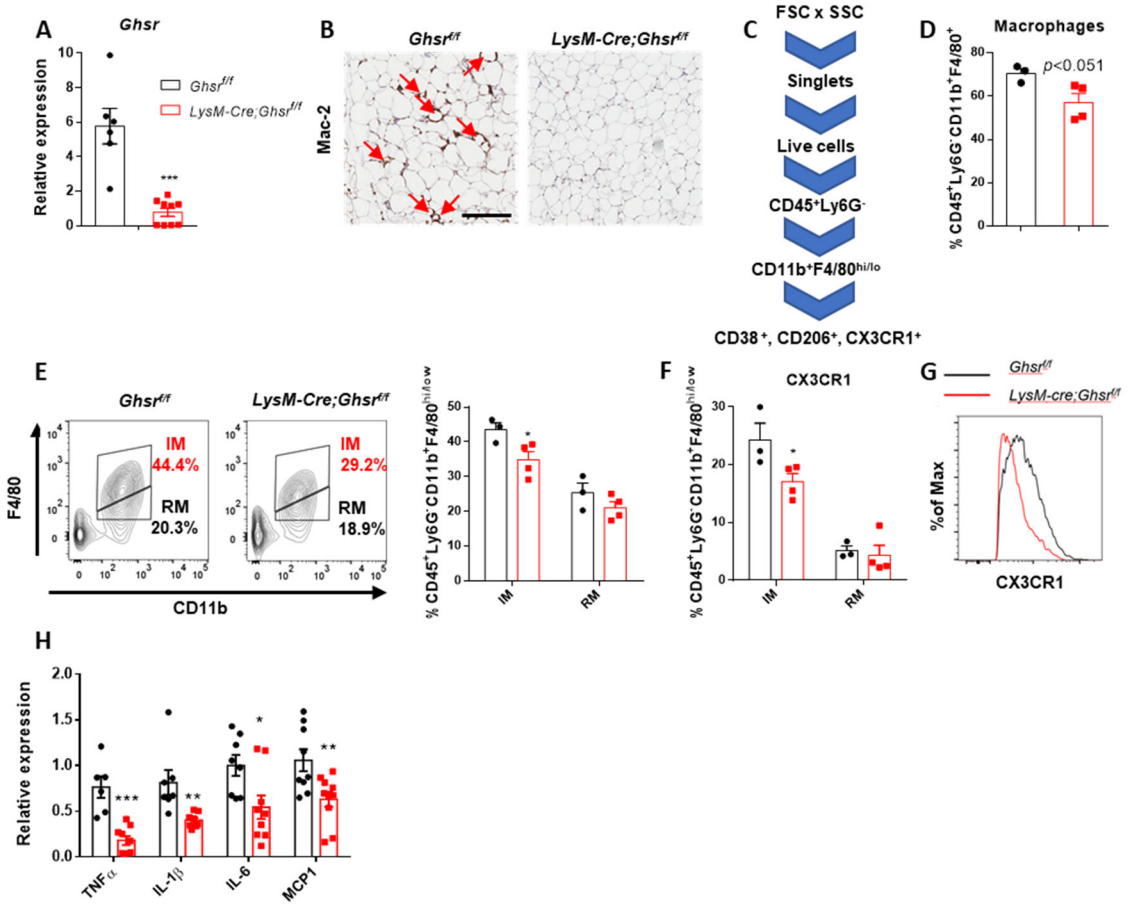

Figure 18. Myeloid-specific GHS-R deletion reduces infiltrated macrophages in eWAT of HFD-fed mice.

(A) mRNA level of *Ghsr* in eWAT of HFD-fed control and HFD-fed *LysM-Cre;Ghsr*$^{f/f}$ (n=6-9 mice/group).

(B) Immunohistochemistry staining of Mac-2 in eWAT of HFD-fed control and HFD-fed *LysM-Cre;Ghsr*$^{f/f}$ (n=3 mice/group).

(C) Flow cytometry gating strategies in eWAT.

(D) Percentage of macrophage subset ($CD45^+Ly6G^-CD11b^+F4/80^+$) in eWAT SVF of HFD-fed control and HFD-fed *LysM-Cre;Ghsr*$^{f/f}$ (n=3-4 mice/group).

(E) Percentage of IM ($CD45^+Ly6G^-CD11b^+F4/80^{hi}$) and RM ($CD45^+Ly6G^-CD11b^+F4/80^{lo}$) subset in eWAT SVF of HFD-fed control and HFD-fed *LysM-Cre;Ghsr*$^{f/f}$ (n=3-4 mice/group).

(F and G) Percentage of CX3CR1 from IM and RM subset (F) and MFI of CX3CR1 from IM (G) in eWAT SVF of HFD-fed control and HFD-fed *LysM-Cre;Ghsr*$^{f/f}$ mice (n=3-4 mice/group).

(H) mRNA level of pro-inflammatory cytokine/chemokine related genes in eWAT of HFD-fed control and HFD-fed *LysM-Cre;Ghsr*$^{f/f}$ (n=6-9 mice/group).

Data are presented as the means ± SEM. *$p \leq 0.05$, *** $p \leq 0.001$, vs. *LysM -Cre;Ghsr*$^{f/f}$ using two-way ANOVA or t-test.

Myeloid-specific GHS-R deletion attenuates serum free fatty acids and elevates serum adiponectin concentration

As obesity-associated low-grade inflammation results in insulin resistance which has been demonstrated to arise from reduced circulating adiponectin concentrations (158, 159) and increased serum FFAs (160-162), we determined the parameters in HFD-fed control and HFD-fed *LysM-Cre*;*Ghsr*$^{f/f}$ mice. Myeloid-specific GHS-R deletion reduced the size of adipocyte and significantly elevated serum adiponectin concentration (Fig. 19A-19C). In HFD, significantly reduced serum FFA concentration along with suppressed lipolysis as measured by lipolysis-related genes was observed in *LysM-Cre*;*Ghsr*$^{f/f}$ mice compared to control mice (Fig. 19D and 19E). Collectively, these data demonstrate that myeloid-specific GHS-R deficiency promotes adiponectin production and suppresses FFA secretion into the blood by reducing lipolysis in eWAT which together leading to insulin sensitivity.

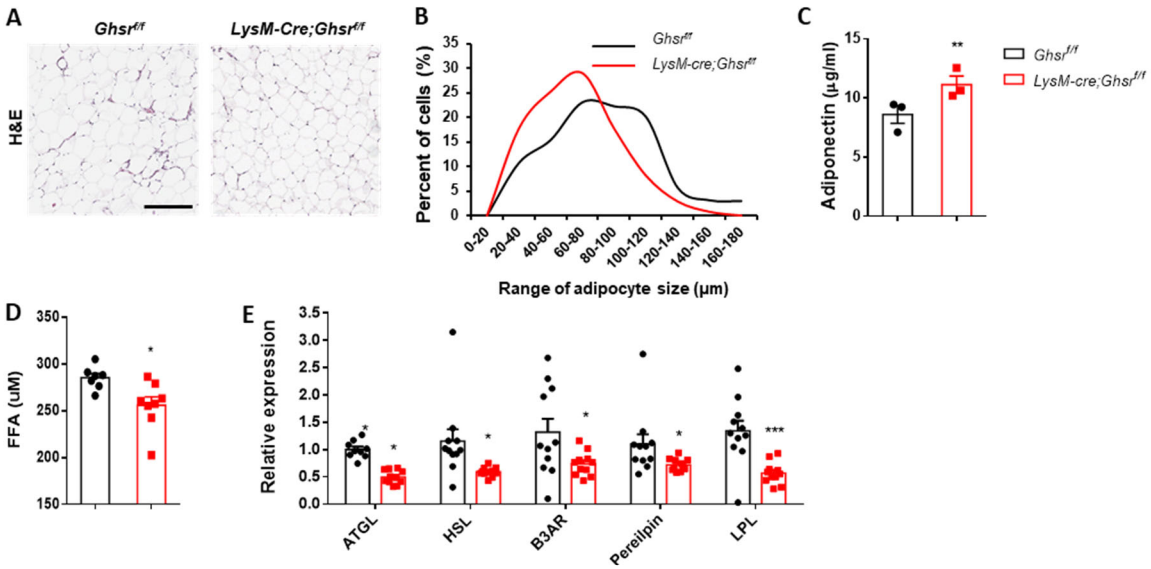

Figure 19. Myeloid-specific GHS-R deletion promotes healthy phenotype of adipose tissues.
(A) Immunohistochemistry staining of H&E in eWAT of HFD-fed control and HFD-fed *LysM-Cre;Ghsr*$^{f/f}$ mice (n=3 mice/group).
(B) Adipocyte size distribution in eWAT of HFD-fed control and HFD-fed *LysM-Cre;Ghsr*$^{f/f}$ mice (n=3 mice/group).
(C and D) Serum adiponectin level (C; n=3 mice/group) and serum FFA level (D; n=7-8 mice/group) in HFD-fed control and HFD-fed *LysM-Cre;Ghsr*$^{f/f}$ mice.
(E) mRNA level of lipolysis related genes in eWAT of HFD-fed control and HFD-fed *LysM-Cre;Ghsr*$^{f/f}$ (n=9-11 mice/group).
Data are presented as the means ± SEM. *$p \leq 0.05$, **$p \leq 0.01$, ***$p \leq 0.001$, vs. *LysM-Cre;Ghsr*$^{f/f}$ using t-test.

Myeloid-specific GHS-R deletion attenuates diet-induced NAFLD by attenuating the hepatic inflammatory response

It has been established that the liver plays a crucial role in lipid metabolism by taking up serum-free fatty acids and storing them as TG (163). Myeloid-specific GHS-R deficiency reduced diet-induced hepatic steatosis, as measured by H&E and Oil-Red-O staining (Fig. 20A). While increased expression of beta-oxidation-related genes was found, the expression of lipid synthesis and storage genes is reduced in the liver of HFD-fed *LysM-Cre;Ghsr*$^{f/f}$ comparing with HFD-fed control (Fig. 20B).

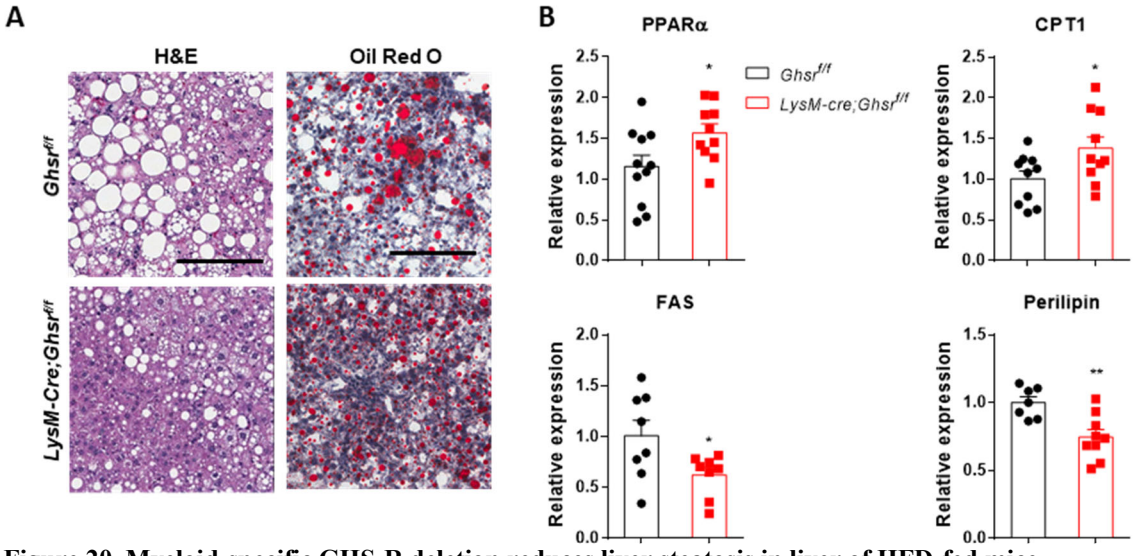

Figure 20. Myeloid-specific GHS-R deletion reduces liver steatosis in liver of HFD-fed mice.
(A) Immunohistochemistry staining of H&E, Oil red O, Mac-2 in liver of HFD-fed control and HFD-fed *LysM-Cre;Ghsr*$^{f/f}$ (n=3 mice/group).
(B) mRNA level of lipid metabolism related genes in liver of HFD-fed control and HFD-fed *LysM-Cre;Ghsr*$^{f/f}$ (n=7-11 mice/group).
Data are presented as the means ± SEM. *$p \leq 0.05$ vs. *LysM-Cre;Ghsr*$^{f/f}$ using t-test.

Further, we observed that *Ghsr* expression was reduced in the liver of HFD-fed *LysM-Cre*;*Ghsr*$^{f/f}$ mice compared to HFD-fed control mice (Fig. 21A). Inflammation is the key factor that drives the progression of simple steatosis to NAFLD. When liver inflammatory status was examined, liver sections from HFD-fed *LysM-Cre*;*Ghsr*$^{f/f}$ mice contained fewer Mac-2-positive cells (infiltrated macrophages and Kupffer cells) compared to those of HFD-fed control mice (Fig. 21B). Percentage of macrophages showed a reduced trend ($p<0.064$) in HFD-fed liver mainly due to the reduction of infiltrated macrophages (Fig. 21C and 21D). Similar to the result of eWAT, CX3CR1 expression in IM showed a decreased trend ($p<0.088$) in liver NPC of HFD-fed *LysM-Cre*;*Ghsr*$^{f/f}$ mice comparing with HFD-fed control mice (Fig. 21E and 21F). mRNA levels

of *F4/80, TNFα* and *IL-6* in the liver of HFD-fed *LysM-Cre*;*Ghsr*$^{f/f}$ mice were significantly lower compared to HFD-fed control mice (Fig. 21G).

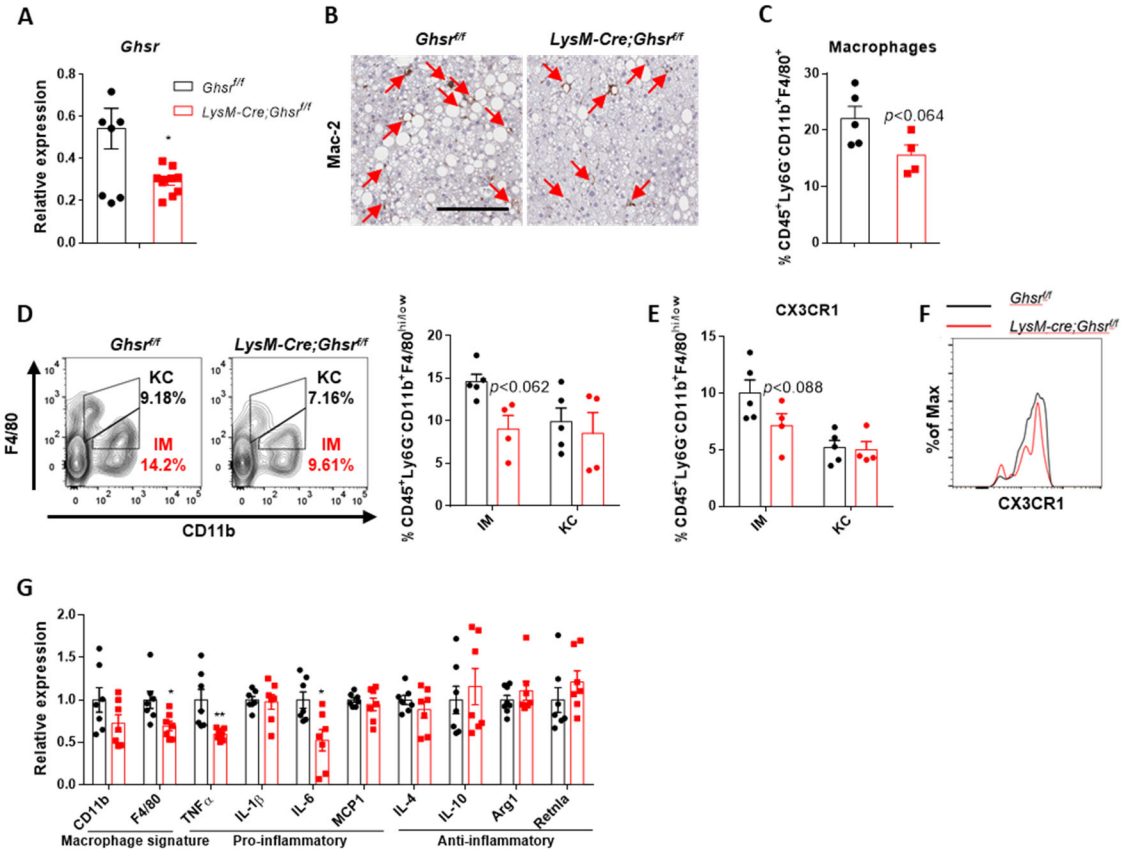

Figure 21. Myeloid-specific GHS-R deletion reduces macrophage infiltration and inflammation in liver of HFD-fed mice.
(A) mRNA level of *Ghsr* in liver of HFD-fed control and HFD-fed *LysM-Cre;Ghsr*$^{f/f}$ (n=7-9 mice/group).
(B) Immunohistochemistry staining of H&E, Oil red O, Mac-2 in liver of HFD-fed control and HFD-fed *LysM-Cre;Ghsr*$^{f/f}$ (n=3 mice/group).
(C) Percentage of macrophage subset ($CD45^+Ly6G^-CD11b^+F4/80^+$) in liver NPC of HFD-fed control and HFD-fed *LysM-Cre;Ghsr*$^{f/f}$ (n=4-5 mice/group).
(D) Percentage of IM ($CD45^+Ly6G^-CD11b^+F4/80^{low}$) and RM ($CD45^+Ly6G^-CD11b^+F4/80^{hi}$) subset in liver NPC of HFD-fed control and HFD-fed *LysM-Cre;Ghsr*$^{f/f}$ (n=4-5 mice/group).
(E and F) Percentage of CX3CR1 from IM and RM subset (E) and MFI of CX3CR1 from IM (F) in liver NPC of HFD-fed control and HFD-fed *LysM-Cre;Ghsr*$^{f/f}$ mice (n=4-5 mice/group).
(G) mRNA level of inflammatory cytokine/chemokine related genes in liver of HFD-fed control and HFD-fed *LysM-Cre;Ghsr*$^{f/f}$ (n=7 mice/group).
Data are presented as the means ± SEM. *$p \leq 0.05$ vs. *LysM-Cre;Ghsr*$^{f/f}$ using two-way ANOVA or t-test.

Next, we performed macrophage and hepatocyte co-cultures to address whether GHS-R facilitates macrophage generation of factors to promote aspects of NAFLD. We incubated control hepatocytes with BMDM-CM (Fig. 22A). When pro-inflammatory response and lipid utilization were examined, hepatocytes incubated with CM of PA-treated *LysM-Cre*;*Ghsr*$^{f/f}$ BMDMs showed significantly decreased mRNA levels of *TNFα*, *IL-6, and MCP1* (Fig. 22B), while those related to beta-oxidation is promoted compared to hepatocytes incubated with PA-treated WT BMDM-CM (Fig. 22C). Together these results suggest that GHS-R activation enables macrophages to generate factors that can enhance hepatocyte pro-inflammatory response and use fatty acids via beta-oxidation.

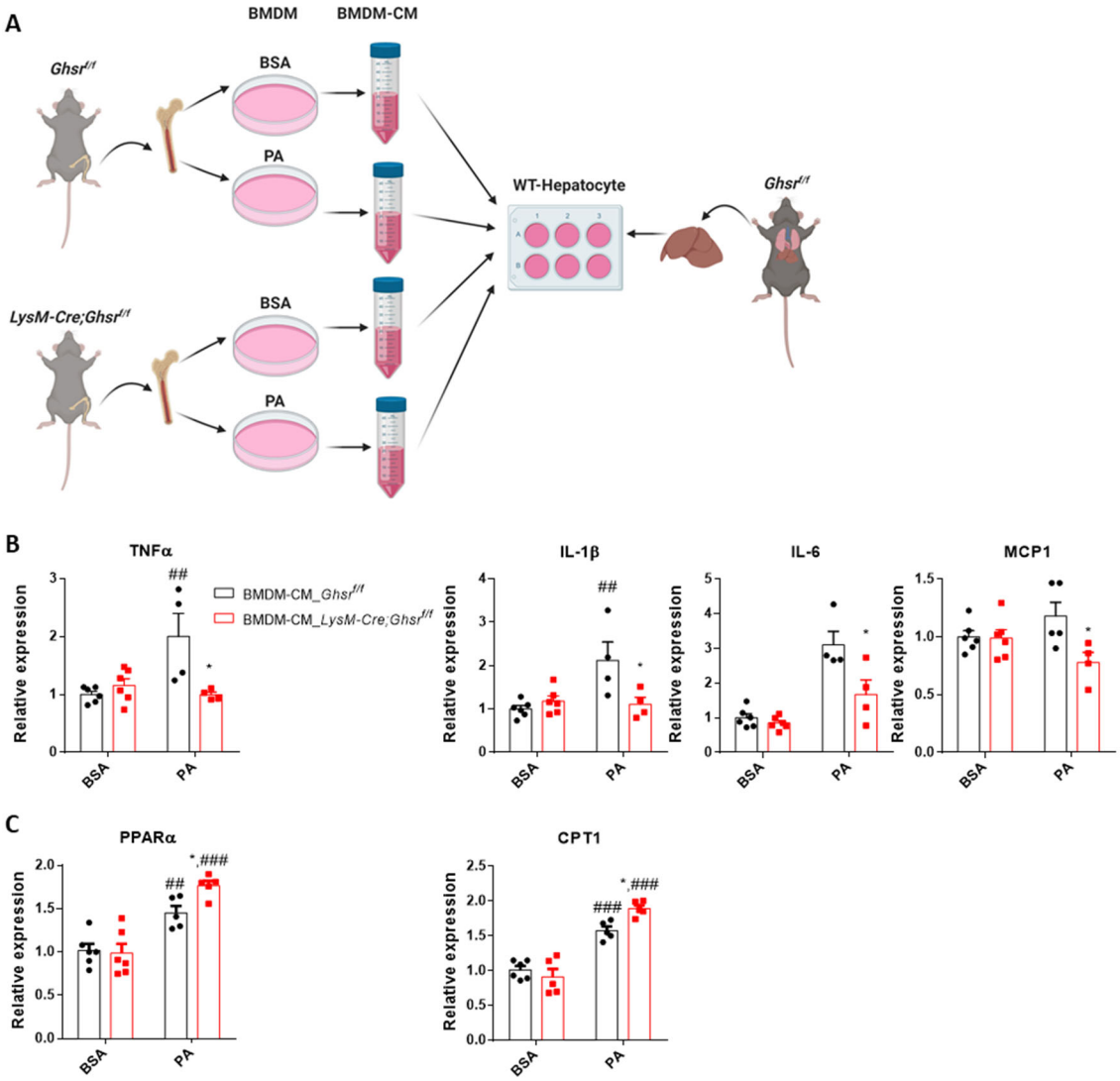

Figure 22. Myeloid-specific GHS-R deletion attenuates inflammatory response and promotes beta-oxidation in hepatocytes.

(A) Diagram of hepatocyte and BMDM-CM co-culture method.

(B and C) mRNA level of pro-inflammatory cytokine/chemokine (B) and beta-oxidation (C) related genes in control-hepatocytes incubated with conditional media from 24 hrs of 150 µM PA/BSA treated BMDMs of control and *LysM-Cre;Ghsr*$^{f/f}$ (n=4-6 mice/group).

Data are presented as the means ± SEM. *$p \leq 0.05$ vs. *LysM-Cre;Ghsr*$^{f/f}$, ##$p \leq 0.01$, ###$p \leq 0.001$ vs. PA using two-way ANOVA.

Myeloid-specific GHS-R deletion attenuates HFD-induced pro-inflammatory response in peritoneal macrophages

We examined alteration of *Ghsr* mRNA expression in peritoneal macrophages (PMs) by HFD-feeding and found that *Ghsr* expression was significantly upregulated under HFD-feeding compared to the level in RD-feeding in control mice (Fig. 23A), indicating that macrophage GHS-R may contribute to the reprogramming of immune microenvironment in DIO. To further validate the role of macrophages GHS-R in response to inflammation, PMs were obtained from the peritoneum of HFD-fed control or HFD-fed *LysM-Cre*;*Ghsr*$^{f/f}$ mice and analyzed following Fig. 23B. We have found that PMs in the circulatory system did not show the difference in the percentage of macrophage subset between genotypes (Fig. 23C). However, the MFI of CD38 was significantly reduced in PMs of HFD-fed *LysM-Cre*;*Ghsr*$^{f/f}$ compared to HFD-fed control, which is in line with a decreased percentage of CD38 (Fig. 23D and 23E), explaining reduced M1/M2 like macrophage ratio (Fig. 23F). As expected, HFD-fed *LysM-Cre*;*Ghsr*$^{f/f}$ PMs exhibited significantly decreased pro-inflammatory cytokine markers in protein and pro-inflammatory gene expression in mRNA levels of IL-6 (Fig. 23G and 23H), suggesting myeloid-specific GHS-R diminished M1 polarization of PMs.

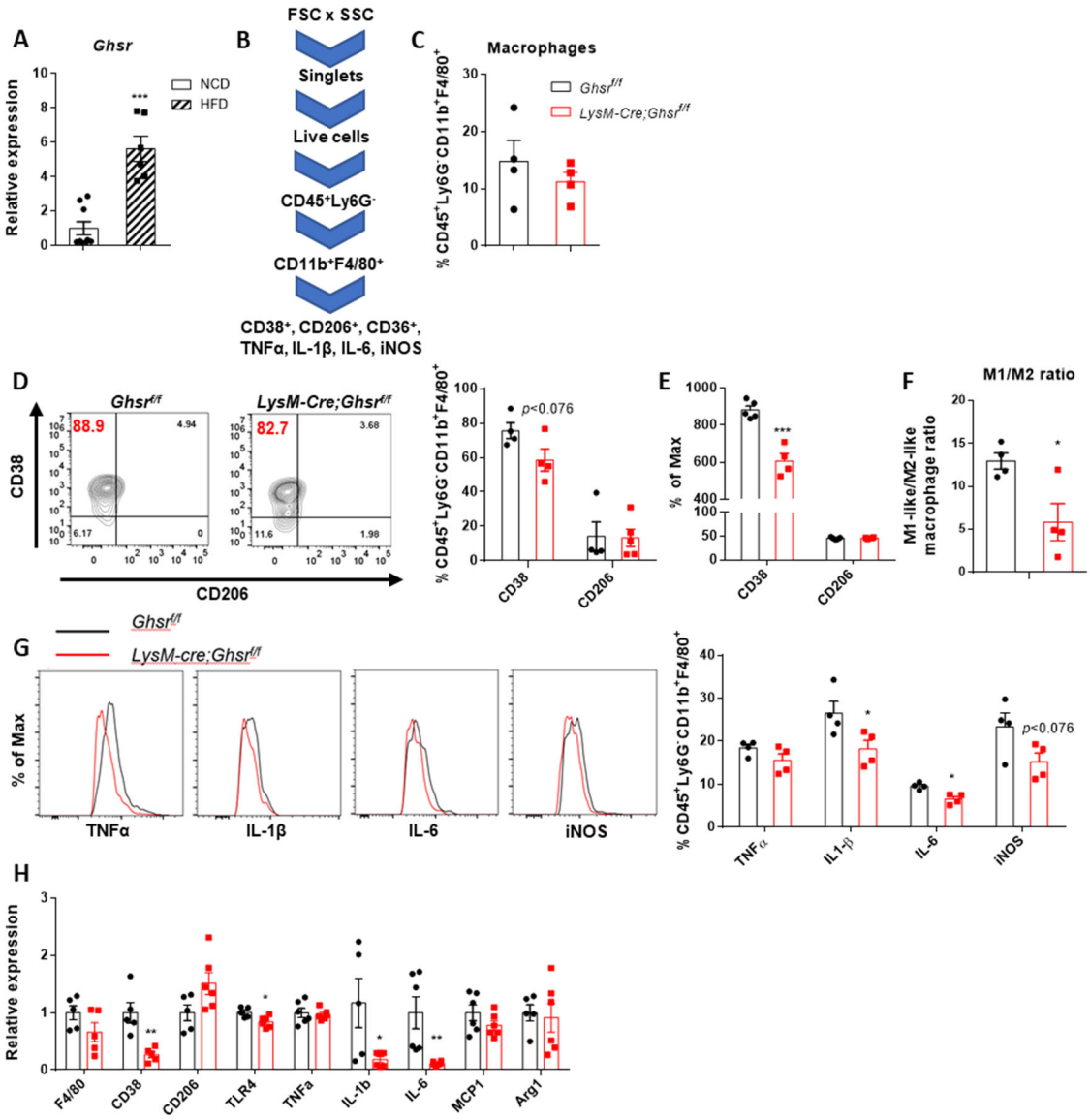

Figure 23. Myeloid-specific GHS-R deletion attenuates inflammatory responses in PMs.
(A) mRNA level of *Ghsr* in PMs of RD-fed and HFD-fed control mice (n=6-9 mice/group).
(B) Flow cytometry gating strategies in PMs.
(C) Percentage of macrophage subset (C) in PMs of HFD-fed control and HFD-fed *LysM-Cre;Ghsr*$^{f/f}$ mice (n=4 mice/group).
(D-F) Percentage (D) and MFI (E) of M1- and M2-like macrophage subsets and ratio of M1-like/M2-like macrophage (F) in PMs of HFD-fed control and HFD-fed *LysM-Cre;Ghsr*$^{f/f}$ mice (n=4-5 mice/group).
(G) Percentage of pro-inflammatory cytokine subsets in PMs of HFD-fed control and HFD-fed *LysM-Cre;Ghsr*$^{f/f}$ mice (n=4-5 mice/group).
(H) mRNA level of pro-inflammatory cytokine/chemokine related genes in PMs of HFD-fed control and HFD-fed *LysM-Cre;Ghsr*$^{f/f}$.
Data are presented as the means ± SEM. *$p \leq 0.05$, **$p \leq 0.01$, ***$p \leq 0.001$ vs. *LysM-Cre;Ghsr*$^{f/f}$ using t-test.

Moreover, HFD-fed *LysM-Cre*;*Ghsr*$^{f/f}$ PMs exhibited significantly reduced production CD36 according to flow analysis (Fig. 24A) and gene expression (Fig. 24B). Macrophage GHS-R deficiency down-regulated lipid synthesis gene and upregulated beta-oxidation and lipolysis-related genes, validating that GHS-R suppression in macrophages decreases lipid accumulation in macrophages by reducing lipid uptake and synthesis gene and increasing beta-oxidation and lipolysis genes. Less accumulation of lipid in macrophages further diminishes the pro-inflammatory response of HFD-fed *LysM*-Cre;*Ghsr*$^{f/f}$ PMs. These data are consistent with previous findings, which suggest that the pro-inflammatory effects of DIO are GHS-R dependent.

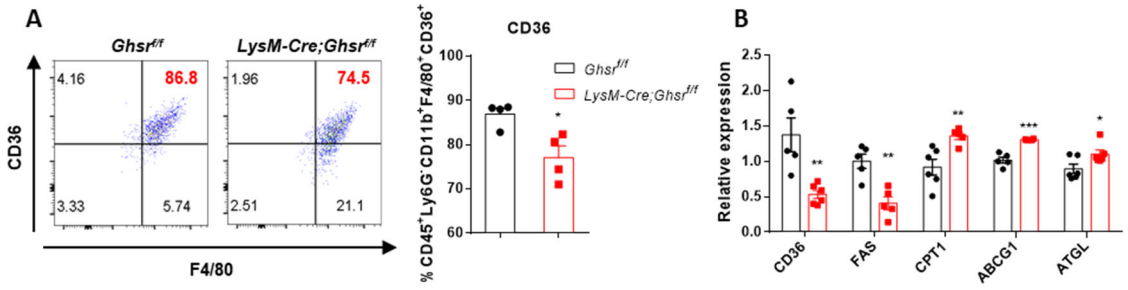

Figure 24. Myeloid-specific GHS-R deletion attenuates PA-related pathway in PMs.
(A) Percentage of CD36 subset in PMs of HFD-fed control and HFD-fed *LysM-Cre;Ghsr*$^{f/f}$ mice (n=4 mice/group).
(B) mRNA level of CD36 and lipid metabolism-related genes in PMs of HFD-fed control and HFD-fed *LysM-Cre;Ghsr*$^{f/f}$ (n=4-6 mice/group).
Data are presented as the means ± SEM. *$p \leq 0.05$, **$p \leq 0.01$, ***$p \leq 0.01$ vs. *LysM-Cre;Ghsr*$^{f/f}$ using t-test.

Myeloid-specific GHS-R deletion attenuates PA-induced pro-inflammatory response in BMDMs

To recapitulate our *in vivo* findings and gain mechanistic insights, we sought to validate GHS-R regulation of macrophage activation *ex vivo* in BMDMs treated with PA to mimic

the HFD condition as described (Fig. 25A). In control BMDMs, PA treatment caused an increase in pro-inflammatory polarization and response (Fig. 25B and 25C). Strikingly, in *LysM-Cre*;*Ghsr*$^{f/f}$ BMDMs, it showed significantly decreased pro-inflammatory activation in PA-induced macrophages in mRNA levels compared with BMDMs control.

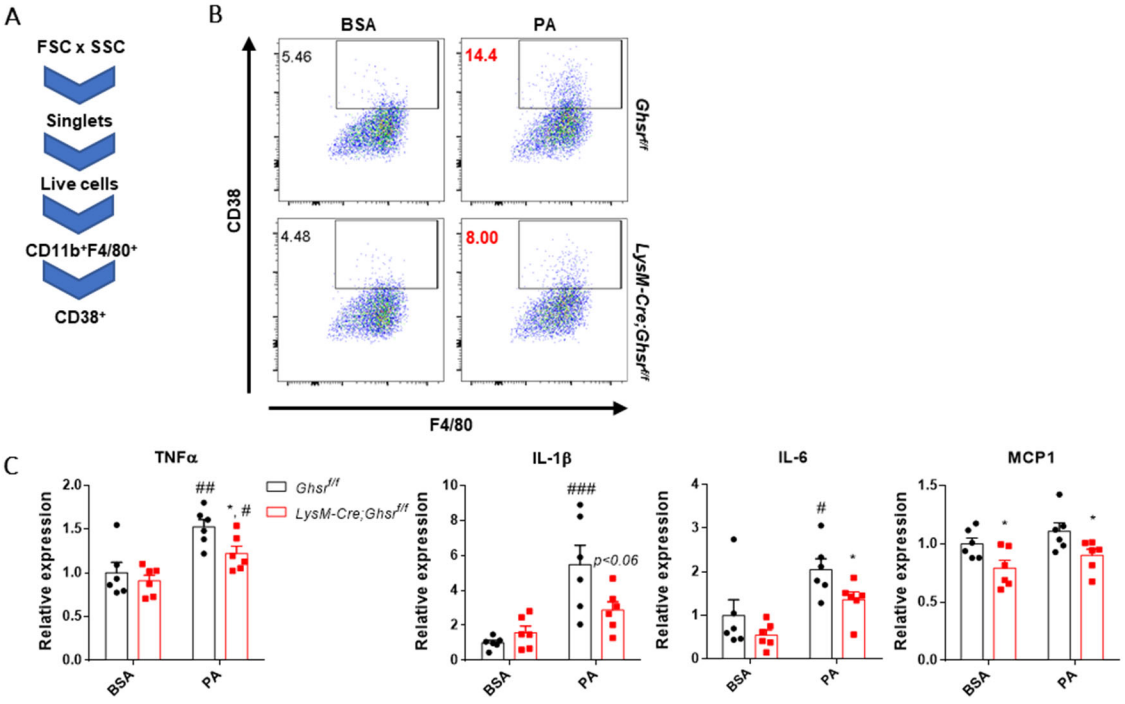

Figure 25. Myeloid-specific GHS-R deletion attenuates PA-induced M1-like polarization and pro-inflammatory response in BMDMs.
(A) Flow cytometry gating strategies in BMDMs.
(B) Percentage of M1-like subset in 24hrs 150 μM PA/BSA-treated BMDMs of control and *LysM-Cre;Ghsr*$^{f/f}$ mice (n=4 mice/group).
(C) mRNA level of pro-inflammatory cytokine/chemokine genes in PA/BSA-treated BMDMs of control and *LysM-Cre;Ghsr*$^{f/f}$ mice (n=6 mice/group).
Data are presented as the means ± SEM. *$p \leq 0.05$ vs. *LysM-Cre;Ghsr*$^{f/f}$, #$p \leq 0.05$, ##$p \leq 0.01$, ###$p \leq 0.001$ vs. PA using two-way ANOVA.

Discussion

Our current data showed that myeloid GHS-R played crucial roles in macrophage accumulation and polarization in adipose tissues of DIO mice. This conclusion is supported by several lines of evidence: First, GHS-R is highly expressed in adipose tissue SVF of DIO mice. Second, studies of GHS-R deletion in vivo or overexpression in vitro demonstrated that myeloid GHS-R contributed to macrophage infiltration and polarization in adipose tissues. Third, monocytes and macrophages of myeloid-specific GHS-R deleted mice expressed lower levels of chemokine receptors, which may reduce macrophage migration.

The adipose tissue is a central metabolic organ in storing excess lipids in the body and suppling free fatty acids as energy. The white adipose tissue functions as a critical endocrine organ, secreting various hormones and cytokines, which are key mediators in normal metabolism and obesity-associated dysfunctions (164, 165). It is well known that obesity induces chronic local inflammation in adipose tissue and increased pro-inflammatory cytokines (124, 166, 167). It has been reported that food intake and body weight are reduced in HFD-fed global GHS-R knockout mice, which may affect insulin sensitivity and inflammatory status. However, it has also been studied that increased fat mass is not always correlated with increased inflammation (168, 169). We have previously reported that GHS-R ablation neither inhibits weight loss nor food intake in aged mice (170), while adipose tissue inflammation and insulin resistance were alleviated (97). In HFCS-feeding mice, severely increased adipose inflammation and insulin resistance were found without causing obesity; interestingly, knockout of GHS-R attenuates HFCS-

induced adipose inflammation and insulin resistance (106). Consistent with the results from GHS-R ablation mice, our current study had shown that myeloid-specific GHS-R ablation mice did not affect the body weight, food intake, or energy expenditure. Thus, the involvement of tissue-infiltrated macrophage polarization might be the critical point in the improvement of insulin sensitivity of GHS-R knockout mice fed with HFD.

A large body of research has provided ample evidence for multiple points of intersection between activation of pro-inflammatory signaling cascades and inhibition of insulin action in different, tissue-specific extent (171-173). A recent study shows that FGF21 enhances insulin sensitivity by regulating the release of adiponectin and fat expansion, accompanied by an increase of M2-like macrophage polarization (174). In our current data, myeloid GHS-R deletion increased serum FGF21 and adiponectin levels while showing no difference in subcutaneous fat mass and polarization of M2-like macrophage, suggesting insulin sensitivity phenotype in myeloid-specific GHS-R deleted mice may not proactively from subcutaneous fat. When hepatic glycogen is depleted by overnight fasting, pyruvate is converted to glucose in the liver to buffer blood glucose (175). Since insulin suppresses hepatic gluconeogenesis, one possible method to assess the hepatic insulin sensitivity is examining the rate of hepatic glucose production in response to pyruvate administration. Here, when sodium pyruvate was administrated after overnight fasting, no differences in hepatic glucose production were observed by myeloid GHS-R ablation. A question raised from here is why epididymal fat is the major insulin target tissue regulating obesity-induced insulin resistance. This might be explained by the findings that in WT mice the obesity-induced macrophage infiltration is several multitudes

higher in eWAT compared to liver and skeletal muscle (176). In addition, our finding indicated GHS-R expression, which is expected to be expressed mainly by macrophages in tissues, is 3~6-fold higher in eWAT than in other insulin target tissues (data not shown). Therefore, the effect of myeloid GHS-R ablation may be particularly predominant in eWAT to regulate the biogenesis and function of the tissue, which results in enhanced insulin sensitivity.

The dynamic change of stromal cells in the adipose tissue during chronic inflammation has led to the coinage of the term "adipose tissue remodeling," indicating the changes in number and phenotype of the stromal cells. Whereas neutrophils with short life spans due to apoptosis transiently infiltrate into adipose tissue early in the course of HFD feeding (177, 178), macrophages have longer life spans and comprise about 50% of the total SVF cells in obese adipose tissues (124, 179, 180). Notably, it is published that the chronic state of insulin resistance from long-term exposure to HFD is heavily related to macrophage-mediated pro-inflammation, while the initial stage of insulin resistance is related to acute tissue lipid overload (181). Over the course of chronic pro-inflammatory state during the development of obesity, excessive macrophage infiltration into WAT influences metabolic disorder by secreting the majority of adipose tissue-derived cytokines and chemokines such as TNFα, IL-1β, IL-6, and MCP-1 (179, 182-185). We found that an increase in total ATMs during HFD feeding (data not shown) and myeloid GHS-R ablation decreased the ratio of M1-like/M2-like macrophages and pro-inflammatory cytokines that decreases macrophage-mediated adipose tissue inflammation during HFD feeding.

Moreover, our current data showed that GHS-R expression in PMs was highly upregulated under HFD feeding compared to RD feeding. PMs of HFD-fed mice or PA stimulated BMDMs were tested in vivo and ex vivo respectively to investigate direct macrophage inflammatory response to chronic low-grade inflammation. Ablation of GHS-R in PMs and BMDMs reduced M1-like/M2-like macrophage ratio and expression of pro-inflammatory cytokines without changing M2 macrophage marker and anti-inflammatory cytokines, which is in line with the trend of circulating cytokines in plasma. This new data underscores that GHS-R in macrophages is an important regulator of macrophage polarization, and GHS-R ablated macrophages exhibit characteristics of alternative activation by reducing M1-like macrophage polarization.

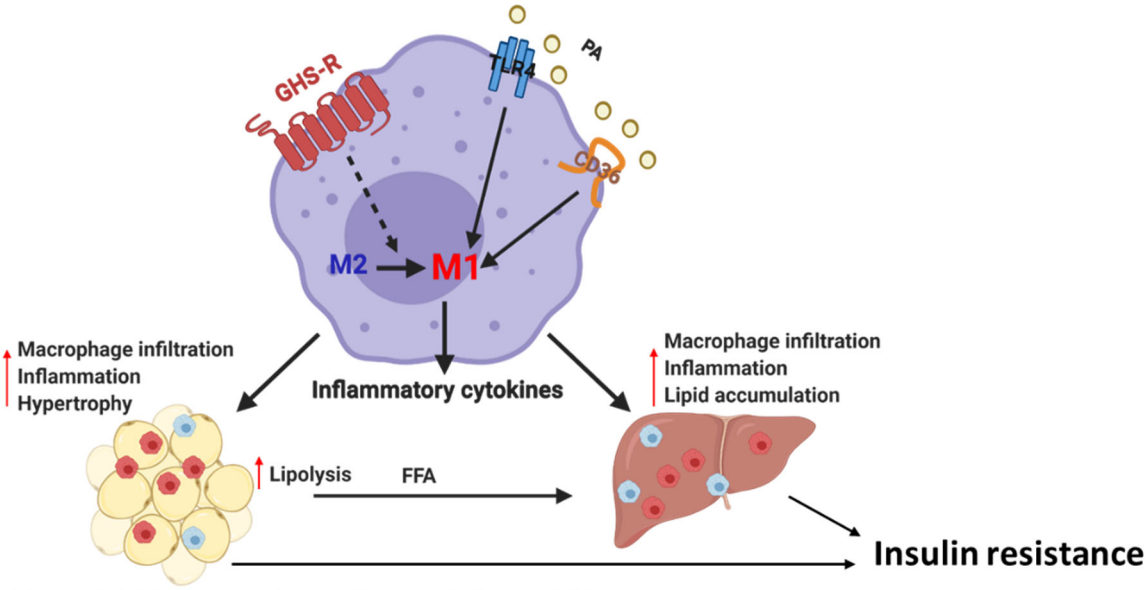

Figure 26. Diagrammatic conclusion of chapter IV.
Macrophage GHS-R impairs tissue homeostasis by increasing macrophage infiltration and M1 polarization in insulin target tissues. Hypertrophy and lipolysis increased in eWAT which promotes FFA secretion in serum and lead liver steatosis. Together, dysfunction in insulin target tissues cause systemic insulin resistance.

CHAPTER V

MECHANISMS UNDERLYING GHS-R ACTIONS IN MACROPHAGE POLARIZATION

Introduction

Macrophage activation and lipid metabolism are intimately linked to metabolic reprogramming in the activation of both M1-like and M2-like macrophages by activating inflammatory pathways (186). Recent publications highlighted the concept that pro-inflammatory M1-like macrophages rely on glycolysis, while anti-inflammatory M2-like macrophages demand fatty acid oxidation (FAO). Recent studies have found that saturated fatty acids (SFAs) polarize macrophages to M1-like by activating NLRP3 inflammasome mediated by activated endoribonuclease inositol-requiring kinase 1α (IRE1α) in myeloid cells (187). Our current findings show that GHS-R deficient BMDMs indicate increased FAO under palmitic acid (PA) treatment comparing with control BMDMs. This result indicates that under the same amount of SFA substrates, GHS-R deficient macrophages possess a higher potential to utilize FAs via FAO and decrease M1-polarization by activating pro-inflammatory pathways with the overload of FA. The beneficial effects were found that enhancing FAO which promotes macrophage FA catabolism attenuates inflammatory and ER stress responses to palmitate (188, 189). However, the role of oxidative metabolism, in particular FAO in macrophage polarization, is less well clarified as compared to the impact of glycolysis.

Early studies demonstrated that insulin receptors, mainly IRS2 but not IRS1 (190, 191), are expressed in macrophages (192). However, the physiological function of these receptors in macrophages is unclear. Among the different signaling cascades, the PI3K/AKT pathway, downstream of IRS1/2, has emerged as a central regulator of macrophage polarization. Predominant isoforms of PI3K are PI3Kδ and PI3Kγ in cells of the hematopoietic lineage (193). AKT is three serine/threonine-specific protein kinases (AKT1, AKT2, and AKT3) that regulate multiple cellular processes, including cell proliferation, migration, and intermediary metabolism (194-196). Although it is not yet elucidated that individual AKT isoforms are activated by specific PI3K in macrophages, isoform-specific effects on macrophage function have been reported for both AKT and PI3K. In the recent study, AKT isoforms differentially contribute to macrophage polarization; AKT1 and AKT2 ablation result in M1 and M2 phenotype, respectively (197).

Material and Methods

Animals

Previously we reported the generation of fully backcrossed GHS-R floxed mice on C57BL/6J background (115). Using a Cre-Lox system, we generated myeloid-specific GHS-R deficient (*LysM-Cre;Ghsr*$^{f/f}$) mice by breeding *Ghsr*$^{f/f}$ mice with widely used myeloid-specific *LysM-Cre* (JAX stock 4781) (116). Mice were housed in the animal facility of Texas A&M University (college station, Texas), maintained on 12-hour light

and 12-hour dark cycles (lights on at 6:00 AM) at 75 F ± 1. Food and water were available ad libitum. All diets were obtained from Harlan Teklad with the following composition: RD (2920X): 6.5% fat, 60% carbohydrates, 19.1% protein. All experiments were conducted in accordance with the NIH guidelines and approved by the institutional animal care and use committee.

BMDM isolation, culture, and treatment

Bone marrow cells were isolated from the tibias and femurs of mice as previously described (136). Cells were seeded into 6-well plates at a density of 1.5 X 10^6 cells/well and cultured in a humidified incubator at 37 and 5% CO_2. The culture medium was RPMI 1640 medium containing L-glutamine, 10% fetal bovine serum, 100U/ml penicillin, and 100 µg/ml streptomycin supplemented with 10 ng/mL macrophage colony-stimulating factor (M-CSF) for 7 days. At the end of the 7 days culture period, >95% of the cells were positive for macrophage markers and bone marrow-derived macrophages (BMDMs) were subjected to inflammatory assays. On the seventh day, cells were counted and replated with either 4 hrs of LPS (100 ng/mL) for glycolysis, OXPHOS, and mitochondrial superoxide experiments or 24 hrs of PA (150 µM) for FAO experiment.

Measurement of glycolysis and OXPHOS

An XF96 analyzer (Seahorse Biosciences, North Billerica, MA, USA) was used to measure bioenergetics function in intact BMDMs in real-time. BMDMs were seeded into Seahorse Bioscience XF 96 cell culture plates at the seeding density of 80,000 cells in 200 µL medium and allowed to adhere and grow for 24 h in a 37 °C humidified incubator with 5% CO2. Measurements of extracellular flux were made in unbuffered media. ECAR was

calculated at baseline to compare the rate of glycolysis. OCR was used to analyze OXPHOS by sequentially adding pharmacological inhibitors of oxidative phosphorylation. The resultant bioenergetics profile provides detailed information on individual components of mitochondrial bioenergetics components.

Fatty acid oxidation (FAO) measurement

FAO was measured by adding XF Palmitate-BSA FAO substrate (Seahorse Bioscience, North Billerica, MA, USA) and monitoring OCR of cells without exogenous glucose or glutamine. The experiments were performed according to the manufacturer's protocol (#102720-100 Seahorse Bioscience) to determine the ability of cells to oxidize added exogenously added fatty acids. Analysis of results utilized XFe Wave software (Seahorse Bioscience). The number of cells in each well is measured using a DNA-based stain (CyQUANT Cell Proliferation Assay Kit, Invitrogen) to normalize the data.

Measurement of mitochondrial superoxide in BMDMs

The mitochondrial superoxide was determined using MitoSOX and MitoTracker Green. BMDMs were cultured in 35 mm round dish at a density of 800,000 cells per dish. After 1 hr of LPS treatment, the medium was changed and MitoTracker Green (final concentration 175 μM) and MitoSOX (final concentration 2.5 μM) were added. After the staining, cells were washed twice and suspended in live-cell solution and fluorescence was read at ex 510/em 580 nm for MitoSOX and ex 490/em 516 nm for MitoTracker Green. The Mitochondrial superoxide data were normalized to the nuclear stain and quantified.

Western blotting

BMDMs (3 x 10^6 per well in six-well cell culture plates) or Raw 264.7 cells (2 x 10^5) were treated with LPS 100 or 10 ng/mL respectively for 30 min and washed twice with DPBS before making the lysate. The total cellular lysate was prepared using RIPA buffer (50 mM Tris-HCl, pH 7.4/150 mM NaCl/1%TritonX-100/1% deoxycholate/0.1% SDS/1% aprotinin) with protease and phosphatase inhibitor (Roche, Nutley, NJ). Samples were centrifuged at 12,000 × g for 10 min at 4°C. The concentrations of the protein samples were measured by the BCA-protein assay. Western blot analyses were performed using 65 μg of cell lysate. Proteins were resolved by 10-15% SDS-PAGE gel and transferred to NC membranes. Blots were blocked 5% bovine serum albumin (BSA) (5% BSA were dissolved in phosphate-buffered saline with 0.1% Tween 20) for 1 hr, and then incubated with primary antibody (anti-phospho-S133 CREB, anti-phospho-S247 AKT, anti-CREB, anti-AKT, anti-IRS2, and anti-GAPDH antibodies were purchased from Cell Signaling Technology). in BSA-PBST for overnight. Blots were washed with PBST three times (10 min each time) and then incubated in HRP-coupled secondary antibody for 1hr. Blots were washed with PBST three times (10 min each time) and then subjected to ECL (Amersham Biosciences) before detecting the chemiluminescence. The intensity of the signal was analyzed and quantified by Image J software.

Statistical Analysis

Statistical analyses were performed with Graphpad Prism 6.01. Data were presented as mean ± SEM. Data are presented as the means ± SEM. *$p \leq 0.05$, **$p \leq 0.01$, ***$p \leq 0.001$ vs. *LysM -Cre;Ghsr*$^{f/f}$, #$p<0.05$, ##$p<0.01$, ###$p<0.001$ vs. treatment using t-test or two-way ANOVA.

Results

Myeloid-specific GHS-R deletion attenuates glycolysis and enhances OXPHOS in BMDMs

In the previous chapters, we have shown that macrophage GHS-R deficiency attenuates pro-inflammatory response by regulating M1/M2 macrophage polarization under different inflammatory circumstances. As macrophage polarization is highly regulated by GHS-R in macrophages, we explored the mechanism by which macrophage GHS-R deletion in myeloid-specific GHS-R ablated mice reduces inflammatory response. Since M1-like and M2- like macrophages display distinct functions and regulates different genes, specific metabolic activities are involved (198). M1-like macrophages are associated with increased glycolysis and production of ROS (199, 200). On the other hand, the M2 macs rely on fatty acid oxidation and OXPHOS for generating ATP (201). It is shown that *LysM-Cre*;*Ghsr*$^{f/f}$ BMDMs showed reduced glycolysis and enhanced OXPHOS under LPS stimulated inflammation (Fig. 27). This suggests that GHS-R ablation in macrophages protects LPS-induced mitochondrial dysfunction and utilizes energy via mitochondrial involved pathways.

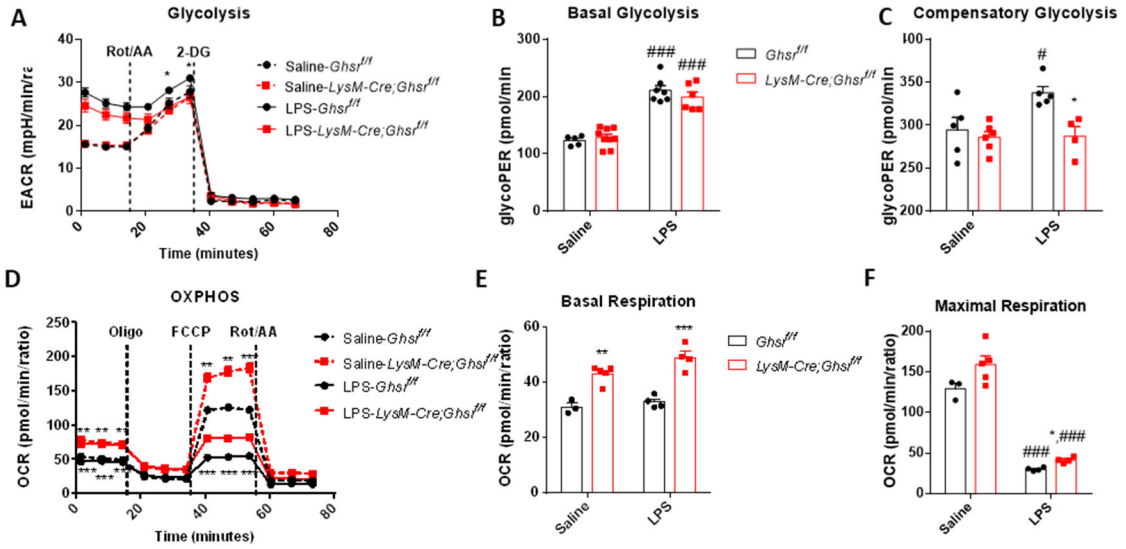

Figure 27. Macrophage GHS-R deficiency suppressed LPS-induced glycolysis and protects LPS-induced mitochondrial dysfunction in BMDMs.
(A-C) ECAR indicating glycolytic rate in LPS-treated BMDMs of control and *LysM-Cre*;*Ghsr*$^{f/f}$ (n=4-9/group).
(D-F) OCR indicating mitochondrial bioenergetic rate in LPS-treated BMDMs of control and *LysM-Cre*;*Ghsr*$^{f/f}$ (n=3-5/group).
Data are presented as the means ± SEM. *$p \leq 0.05$, **$p \leq 0.01$, ***$p \leq 0.001$ vs. *LysM-Cre;Ghsr*$^{f/f}$, #$p \leq 0.05$, ###$p \leq 0.001$ vs. LPS using two-way ANOVA.

Myeloid-specific GHS-R deletion enhances fatty acid oxidation in BMDMs

Mitochondria provide the main source of energy to eukaryotic cells, oxidizing fats and sugars to generate ATP. Mitochondrial fatty acid β-oxidation (FAO) and oxidative phosphorylation (OXPHOS) are two metabolic pathways which are central to this process.

To understand the role of mitochondrial function in the inflammatory response, we investigated fatty acid oxidation (FAO) by measuring oxygen consumption rate (OCR) in *LysM-Cre*;*Ghsr*$^{f/f}$ and control BMDMs using a Seahorse Biosciences extracellular flux analyzer. We observed higher OCR in *LysM-Cre*;*Ghsr*$^{f/f}$ BMDMs compared to control (Fig. 28A). We analyzed the basal and maximal respiration rate that both of which were

significantly higher in PA-treated BMDMs of *LysM-Cre*;*Ghsr*$^{f/f}$ than those of control (Fig. 28B and 28C). These results indicate a higher metabolic rate in *LysM-Cre*;*Ghsr*$^{f/f}$ BMDMs, which correlates with higher beta-oxidation in PMs of HFD-fed *LysM-Cre*;*Ghsr*$^{f/f}$ (Fig. 24B).

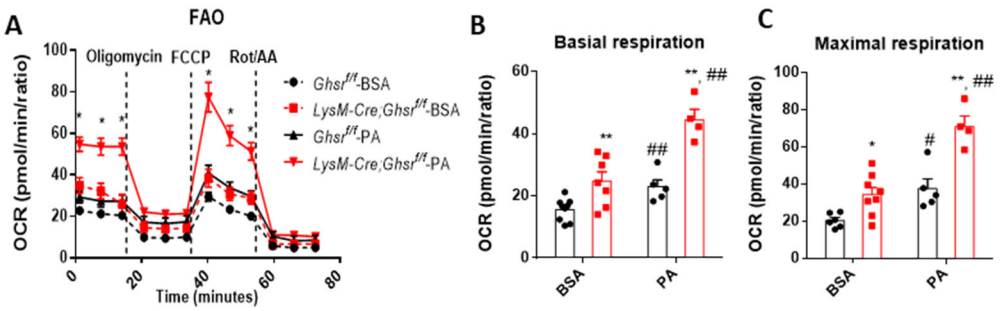

Figure 28. Macrophage GHS-R deficiency increased FAO in BMDMs.
(A-C) FAO measured as OCR in LPS-treated BMDMs of control and *LysM-Cre*;*Ghsr*$^{f/f}$ (n=4-8/group). Data are presented as the means ± SEM. *$p \leq 0.05$, **$p \leq 0.01$ vs. *LysM Cre;Ghsr*$^{f/f}$, #$p \leq 0.05$, ##$p \leq 0.01$ vs. PA using two-way ANOVA.

Myeloid-specific GHS-R deletion decreases LPS-induced mitochondrial superoxide in BMDMs

To compare the difference in oxidant levels in GHS-R deficient and control BMDMs, we measured mitochondrial ROS after LPS exposure. Control BMDMs showed a significant increase in mitochondrial ROS level but not the cells from *LysM-Cre*;*Ghsr*$^{f/f}$ mice (Fig. 29A)

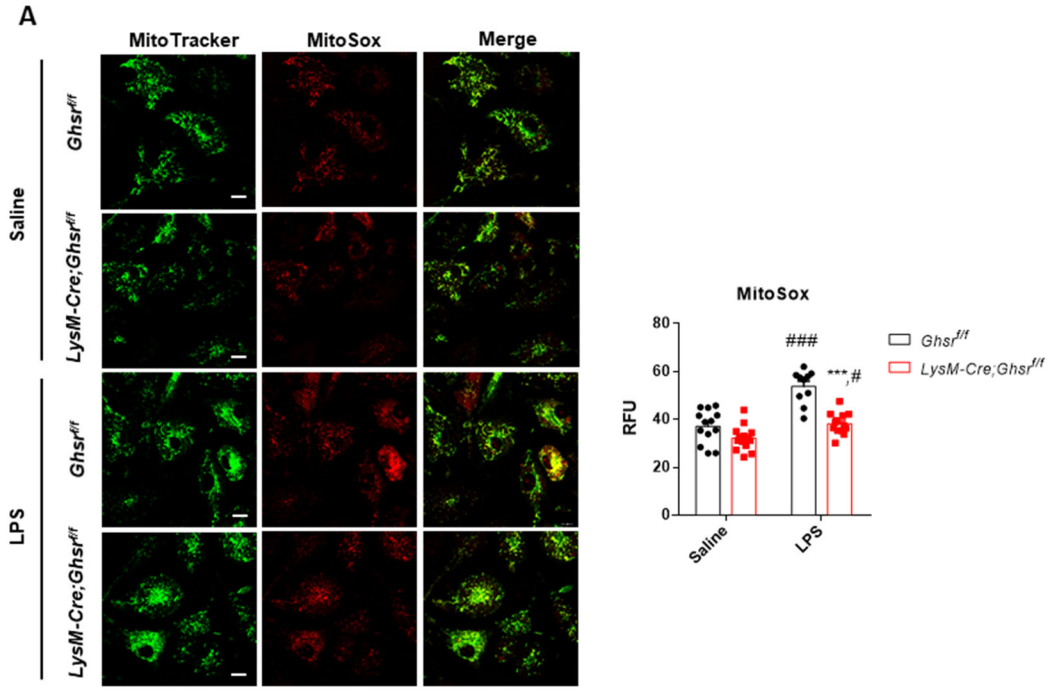

Figure 29. Macrophage GHS-R deficiency attenuates LPS-induced mitochondrial superoxide in BMDMs.
(A) Immunofluorescence staining with MitoTracker and MitoSox in BMDMs of control and *LysM-Cre;Ghsr*$^{f/f}$ mice. Image with confocal microscopy and quantified using ImageJ software. (n=10-14/group).
Data are presented as the means ± SEM. ***$p \leq 0.001$ vs. *LysM-Cre;Ghsr*$^{f/f}$, #$p \leq 0.05$, ###$p \leq 0.001$ vs. LPS using two-way ANOVA.

Myeloid-specific GHS-R deletion attenuates PKA and insulin signaling and blunts the inflammatory response to inflammatory challenge via PKA signaling. It is known that PKA-CREB signaling pathway is one of the major G protein-coupled receptor (GPCR) pathways, which activates the insulin pathway (202). As a member of GPCRs, the PKA-CREB signaling pathway of GHS-R has been studied, but the mechanism by which GHS-R in macrophages activates PKA remains poorly understood. We investigated the role of GHS-R in macrophages in PKA-CREB signaling by stimulating BMDMs with LPS. Data showed that deletion of GHS-R in BMDMs significantly decreases IRS2, p-CREB, and p-AKT (Fig. 30A).

Moreover, we examined the involvement of PKA signaling in macrophage pro-inflammatory response induced by LPS or PA. In inhibiting the PKA signaling group, LPS-stimulated BMDMs of WT mice showed significantly reduced pro-inflammatory cytokine expression comparing with scramble, while those of *LysM-Cre*;*Ghsr*$^{f/f}$ mice did not show the difference (Fig. 30B). Next, we also challenged mice with PA then determined inflammatory sensitivity change in PKA inhibition. In line with PA-induced inflammation, pro-inflammatory cytokines of *LysM-Cre*;*Ghsr*$^{f/f}$ mice reduced compared to that of control mice (Fig. 30C). Taken together, these results indicate that myeloid-specific GHS-R deletion suppresses macrophage pro-inflammatory response in the challenge of LPS or PA insult via inhibiting PKA signaling pathways.

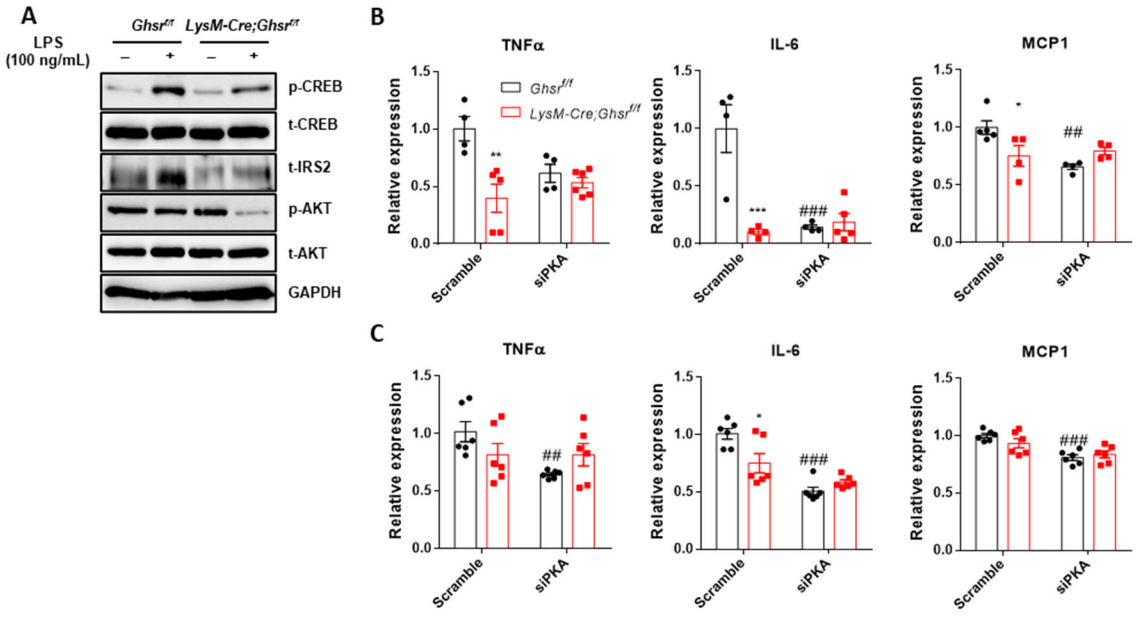

Figure 30. Macrophage GHS-R blunts the inflammatory response to LPS or PA challenge via PKA signaling.
(A) CREB and IRS2 signaling in LPS-stimulated BMDMs of control and *LysM-Cre*;*Ghsr*$^{f/f}$ mice.
(B) Inhibiting PKA signaling with siPKA in LPS-stimulated BMDMs of control and *LysM-Cre*;*Ghsr*$^{f/f}$ mice (4-6/groups).
(C) Inhibiting PKA signaling with siPKA in PA-stimulated BMDMs of control and *LysM-Cre*;*Ghsr*$^{f/f}$ mice (6/groups).
Data are presented as the means ± SEM. *$p \leq 0.05$, **$p \leq 0.01$, ***$p \leq 0.001$ vs *LysM-Cre*;*Ghsr*$^{f/f}$, ##$p \leq 0.01$, ###$p \leq 0.001$ vs. treatment two-way ANOVA.

Myeloid-specific GHS-R deletion blunts the inflammatory response to inflammatory challenge and attenuates inflammatory response via PKA signaling

To further examine whether myeloid-specific GHS-R deletion on response to inflammation regulated by PKA signaling, we stimulated Raw264.7 murine macrophages with LPS to induce inflammation. We have observed that GHS-R overexpression promoted the mRNA level of IRS2 but not IRS1 (Fig. 31A). The expression of AKT1 and AKT2 was upregulated by GHS-R overexpression in macrophages (Fig. 31A). In the protein level, overexpressing GHS-R in macrophages enhanced LPS-stimulated IRS2 and

PI3K p110δ and phosphorylation of CREB, AKT, and AKT2 but not AKT1 (Fig. 31B). These results indicate that GHS-R deletion regulates PKA-CREB and insulin signaling, especially IRS2-PI3K 110δ-AKT2 in macrophages.

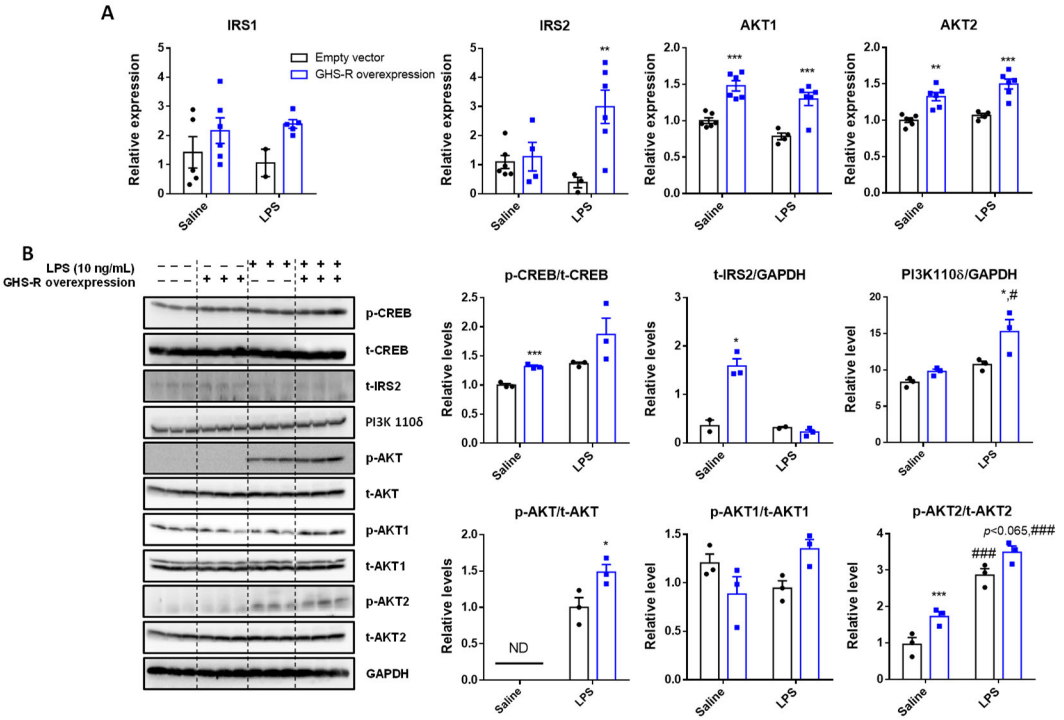

Figure 31. Overexpressing GHS-R in macrophages increase CREB and IRS2 signaling in macrophages.
(A) mRNA level of insulin insulin signal related genes (n=2-6/groups).
(B) CREB and IRS2 signaling in BMDMs of control and *LysM-Cre*;*Ghsr*$^{f/f}$ mice (n=3 mice/groups).
Data are presented as the means ± SEM. *$p \leq 0.05$, **$p \leq 0.01$, ***$p \leq 0.001$ vs *LysM-Cre*;*Ghsr*$^{f/f}$, #$p \leq 0.05$, ###$p \leq 0.001$ vs. LPS using two-way ANOVA.

Discussion

Under metabolic stress, macrophages undergo extensive changes in glycolysis and oxidative phosphorylation, resulting in inflammatory cytokine production (8). The activation of macrophages by pro-inflammatory signals, such as LPS, results in metabolic

reprogramming of macrophages by exhibiting a glycolytic burst and a suppressed OXPHOS (199). To achieve these phenotypes, LPS activates two metabolic regulators, the mTOR and HIF1α, and suppresses AMPK (203). **(i)** Under LPS or LPS/IFNγ-induced inflammation, TLR4 activates hypoxia regulator HIF1α, which in turn activates Glut1, resulting in increased glycolysis and decreased oxidative phosphorylation (8, 204, 205)**.** This metabolic switch from OXPHOS towards glycolysis results in an increase of NADPH levels which can be used as a substrate for NO and iNOS to generate ROS and NO, respectively (200). The metabolic shift in macrophages under inflammatory conditions results in robust electron donors entering the ETC, thus causing electron leakage and formation of ROS (206). NO reacts with superoxide to form peroxynitrite, which causes the accumulation of ROS (200). NO also suppresses OXPHOS in mitochondria, while ROS stabilizes HIF-1α, which further enhances glycolysis. **(ii)** AMPKa2 deficiency results in altered mitochondrial structure, decreased oxidative capacity, and hyper-physiological ROS (207, 208). The recent study shows that IRS2 inhibits AMPK activity to reduce FAO in the muscle (209) and contributes to mitochondrial functions in aging neurons (210). However, the role of IRS2 in macrophages as a metabolic regulator is currently not clear.

It has also been reported that cAMP regulates IRS2 in pancreatic β-cells (68) and critical features of macrophages via PKA, such as macrophage recruitment and reprogramming (69). Myeloid insulin receptor deficiency has a protective effect against inflammation and insulin resistance (70). PI3K-Akt–ERK signaling promotes macrophage differentiation and polarization (71). Macrophage reprogramming and meta-inflammation

are major metabolic signatures causing macrophage response during macrophage polarization (72). Our current study showed that GHS-R deficient macrophages have reduced FAO and inflammatory regulator CD36 (Fig. 24). We found that GHS-R modulates inflammation and FAO and ultimately reprograms macrophages, possibly via IRS2-PI3K 110δ-AKT2 pathway regulated by PKA-CREB signaling (Fig. 31). IRS2 expression in β-cells is stimulated by the transcription factor CREB (73), which is downstream of Gαs/cAMP/PKA signaling pathway employed by GHS-R.

Lack of IR-mediated downregulation of IRS2 expression in macrophages was observed (191), while myeloid-specific IR deficiency reduces pro-inflammatory response and systemic insulin resistance (176). A recent concept suggests that AKT/mTORC1 signaling in macrophages modulates polarization, and the M1-like phenotype is generated by a switch to high anaerobic glycolysis, while oxidative phosphorylation is specific for M2 macrophages (211, 212). This is in line with our findings that macrophage GHS-R ablation showed a reduction in pro-inflammatory response and glycolysis and an enhancement of mitochondrial OXPHOS and FAO. Collectively, macrophage GHS-R could potentially serve as a critical mediator that links the dysregulations of the meta-inflammatory diseases by regulating macrophage polarization and energy metabolism via PKA-CREB mediated IRS2- PI3K 110δ-AKT2 signaling.

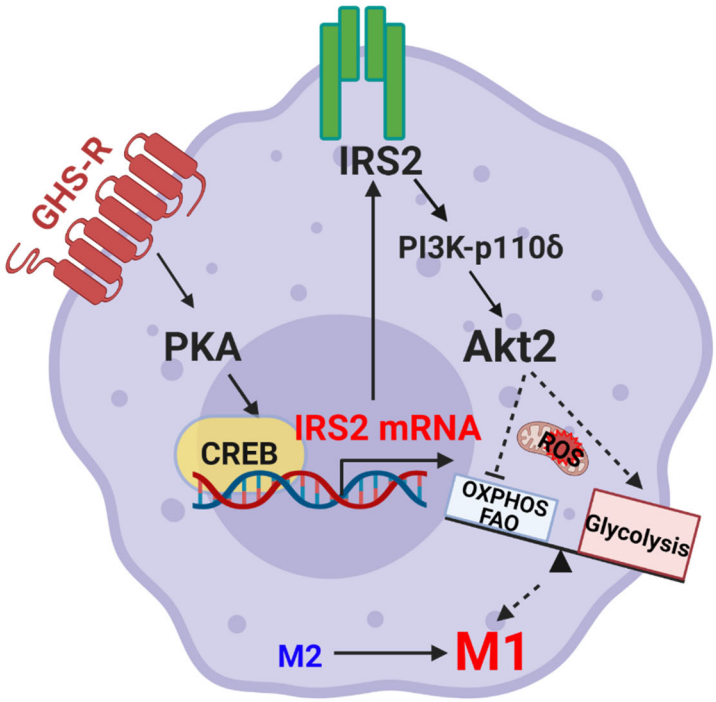

Figure 32. Diagrammatic conclusion of chapter V.
Macrophage GHS-R programs macrophage polarization towards M1-like macrophages via activating PKA-CREB signaling. CREB increases the mRNA level of IRS2 and activates downstream signaling such as PI3K-AKT, a central regulator of activation phenotype in macrophages. This phenotype change in macrophages regulates energy metabolism to prefer glycolysis over OXPHOS and FAO by promoting mitochondrial ROS production.

CHAPTER VI

CONCLUSIONS

In this study, we first provided genetic and biochemical evidence, demonstrating the critical role of myeloid-specific GHS-R served as an essential immunological regulator that causes insulin resistance by promoting macrophage infiltration to tissue and impairing tissue homeostasis. We demonstrated that 1) Myeloid-specific GHS-R deficiency suppresses systemic and macrophage inflammatory response in physiological conditions without altering phenotypic and metabolic characterization. 2) Myeloid-specific GHS-R protects against LPS-induced lethal endotoxemia and liver injury by alleviating inflammatory response and regulating M1 polarization. 3) Myeloid-specific GHS-R deficiency maintains glucose homeostasis and insulin sensitivity via downregulating inflammatory response in insulin target tissues which have reduced macrophage infiltration in diet-induced obesity. 4) Ablation of GHS-R in myeloid cells suppresses TLR4- and CD36-mediated inflammatory response and inhibits fat accumulation by reducing de novo lipogenesis in the liver. 5) Ablation of macrophage GHS-R, a novel therapeutic target to regulate the inflammatory response in macrophages, diminishes the onset of M1 polarization, which downregulates glycolysis while enhancing OXPHOS and FAO by reducing ROS production. This may via PKA-CREB signaling, which is downstream of GHS-R. Taken together, our study showed that myeloid-specific GHS-R deletion improves systemic insulin sensitivity by reducing macrophage infiltration and suppressing inflammatory response, possibly by regulating IRS2-AKT signaling.

Furthermore, these novel findings can provide fundamental information in pharmaceutical aspects. Most of the studies on GHS-R signaling are for its primary function, stimulating appetite. Although a few research discovered the role of GHS-R in immune response, the studies are examined in the global GHS-R ablated system, and the specific mechanism remains to be elucidated. Recent studies highlighted macrophage programming as an exciting concept, especially crosstalk with tissues. Our observations in this study suggest that suppressing GHS-R signaling in macrophages may serve as a novel strategy for alleviates pro-inflammatory response and tissue dysfunction. Since about 40% of medicaments in the pharmaceutical market target GPCRs, GHS-R antagonists may serve as a novel therapeutic means of meta-inflammatory diseases.

We have examined myeloid-specific GHS-R deletion by employing *LysM-Cre;Ghsr*$^{f/f,}$ which showed prevention of pro-inflammatory response leading to healthy inflammatory states. Given that *LysM-Cre* affects immune cells derived from myeloid cells, we cannot rule out the possibility that other immune cells contribute to the regulation of systemic inflammation and metabolic homeostasis such as neutrophils.

Another limitation of this study is that the role of macrophage GHS-R in regulating macrophage infiltration was mainly studied in male mice. Whether macrophage GHS-R could regulate macrophage infiltration and polarization in female mice is unclear. Our previous study showed that female *LysM-Cre;Ghsr*$^{f/f}$ mice displayed normal body weight and body composition during HFD feeding in line with the results from the male. Therefore, to reduce animal usage, we used only male mice for the rest of the study. The recent study shows that GHS-R and ER are co-expressed in the hypothalamic site, and

ghrelin binding to GHS-R increases intracellular Ca^{2+} content in the estrogen-dependent manner (213). However, studies of GHS-R and estrogen/estrogen receptor are not known in macrophages/myeloid-cells. Our preliminary study has shown that myeloid-specific GHS-R regulates a sub-population in myeloid linage differently between males and females, suggesting that there is a possibility that estrogen/estrogen receptor affects GHS-R activity in terms of the myeloid cell differentiation.

The traditional view of metabolism and immunity is recognized as two separate fields, but burgeoning evidence supporting an interaction has resulted in the emerging concept of immunometabolism. Metabolically triggered inflammation is termed "meta-inflammation," which underlies pathological processes of many immune-associated metabolic dysfunctions. Early studies with disrupted NFκB pathway in myeloid cells and CCR2 ablated mice reported alleviated obesity-induced insulin resistance due to reduced WAT pro-inflammatory phenotype, highlighting the association between activation of innate immune response and obesity-induced insulin resistance (214, 215). More recent and in-depth studies of adipose tissue macrophages (ATMs) distinguish two populations of ATMs ($CD45^{+}CD11b^{+}F4/80^{+}$) based on differential F4/80 and CX3CR1 expression (216, 217). CX3CR1 is considered a marker of monocyte-derived macrophages and highly expressed in $F4/80^{hi}$ ATMs. The $F4/80^{hi}$ population significantly increased in number after HFD feeding, identifying them as the infiltrating population by chronic low-grade inflammation (218). The present results exhibit that PBMC of myeloid-specific GHS-R deleted mice exhibited a reduction of CCR2 expression (data not shown), which could thus be central to the decreased CR1 expression of infiltrated macrophages in eWAT. This

was shown with a decreased infiltrating population of ATMs which included fewer M1-like macrophages. This was accompanied by a relatively less number of monocytes in PBMC, as well as adipose tissues of myeloid-specific GHS-R deleted mice (data not shown). This defined potential mechanisms: increased apoptosis and decreased proliferation of myeloid lineage cells. Since the presence and frequency of immune cells in tissues are an important indicator of metabolic health, two mechanisms are heavily associated with dramatic changes affecting immuno-metabolism. Therefore, further studies are needed to investigate the role of myeloid-specific GHS-R in cell apoptosis or proliferation.

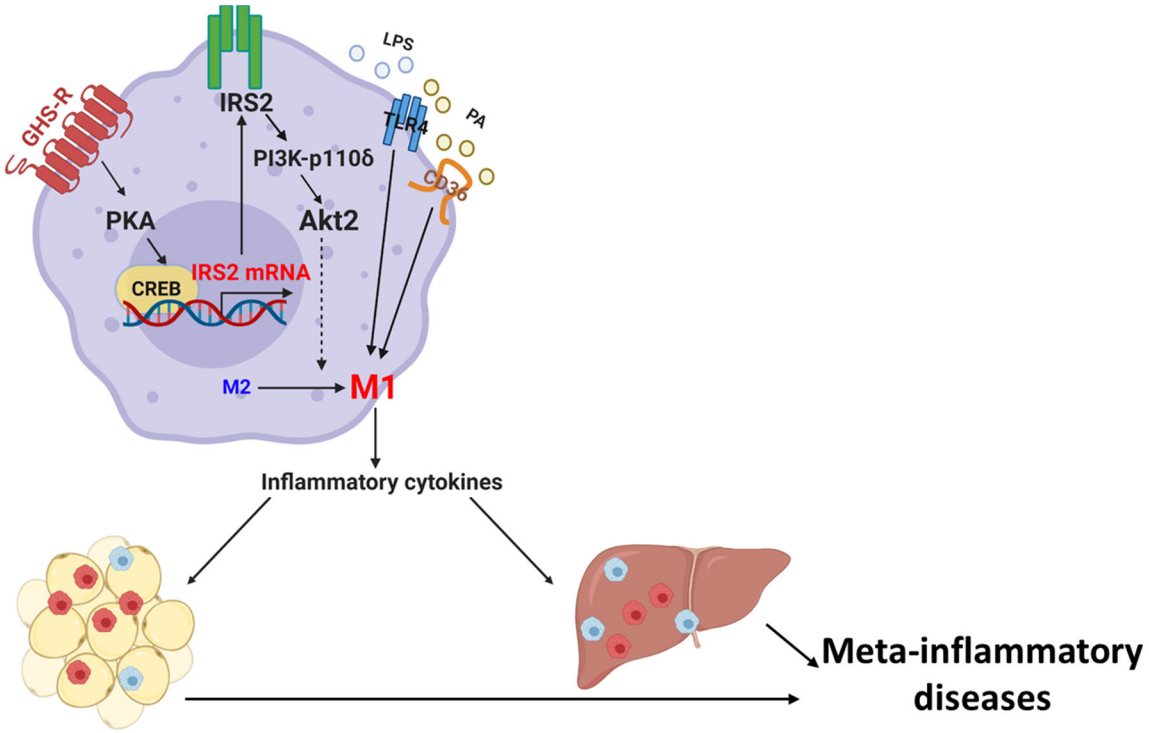

Figure 33. Diagrammatic conclusion of the dissertation.
Macrophages GHS-R accelerates meta-inflammatory diseases by increasing macrophage infiltration and pro-inflammatory response in tissues by promoting M1 polarization, possibly via activating PKA-CREB, which regulates IRS2-PI3K p110δ-AKT2 signaling.

REFERENCES

1. Czaja AJ, Manns MP. Advances in the diagnosis, pathogenesis, and management of autoimmune hepatitis. Gastroenterology. 2010;139(1):58-72 e4. doi: 10.1053/j.gastro.2010.04.053. PubMed PMID: 20451521.

2. Weber A, Boege Y, Reisinger F, Heikenwalder M. Chronic liver inflammation and hepatocellular carcinoma: persistence matters. Swiss Med Wkly. 2011;141:w13197. doi: 10.4414/smw.2011.13197. PubMed PMID: 21557112.

3. Xu H, Barnes GT, Yang Q, Tan G, Yang D, Chou CJ, Sole J, Nichols A, Ross JS, Tartaglia LA, Chen H. Chronic inflammation in fat plays a crucial role in the development of obesity-related insulin resistance. J Clin Invest. 2003;112(12):1821-30. Epub 2003/12/18. doi: 10.1172/JCI19451

112/12/1821 [pii]. PubMed PMID: 14679177; PMCID: 296998.

4. Uysal KT, Wiesbrock SM, Marino MW, Hotamisligil GS. Protection from obesity-induced insulin resistance in mice lacking TNF-alpha function. Nature. 1997;389(6651):610-4. doi: 10.1038/39335. PubMed PMID: 9335502.

5. Wynn TA. Cellular and molecular mechanisms of fibrosis. J Pathol. 2008;214(2):199-210. doi: 10.1002/path.2277. PubMed PMID: 18161745; PMCID: PMC2693329.

6. Mosser DM, Edwards JP. Exploring the full spectrum of macrophage activation. Nat Rev Immunol. 2008;8(12):958-69. doi: 10.1038/nri2448. PubMed PMID: 19029990; PMCID: PMC2724991.

7. Wynn TA, Barron L. Macrophages: master regulators of inflammation and fibrosis. Semin Liver Dis. 2010;30(3):245-57. doi: 10.1055/s-0030-1255354. PubMed PMID: 20665377; PMCID: PMC2924662.

8. Covarrubias AJ, Aksoylar HI, Horng T. Control of macrophage metabolism and activation by mTOR and Akt signaling. Seminars in immunology. 2015;27(4):286-96. doi: 10.1016/j.smim.2015.08.001. PubMed PMID: 26360589; PMCID: 4682888.

9. Akashi K, Traver D, Miyamoto T, Weissman IL. A clonogenic common myeloid progenitor that gives rise to all myeloid lineages. Nature. 2000;404(6774):193-7.

10. Pronk CJ, Rossi DJ, Månsson R, Attema JL, Norddahl GL, Chan CKF, Sigvardsson M, Weissman IL, Bryder D. Elucidation of the phenotypic, functional, and molecular topography of a myeloerythroid progenitor cell hierarchy. Cell stem cell. 2007;1(4):428-42.

11. Samokhvalov IM. Deconvoluting the ontogeny of hematopoietic stem cells. Cellular and molecular life sciences. 2014;71(6):957-78.

12. Nakorn TN, Miyamoto T, Weissman IL. Characterization of mouse clonogenic megakaryocyte progenitors. Proceedings of the National Academy of Sciences. 2003;100(1):205-10.

13. Geissmann F, Manz MG, Jung S, Sieweke MH, Merad M, Ley K. Development of monocytes, macrophages, and dendritic cells. Science. 2010;327(5966):656-61.

14. Hettinger J, Richards DM, Hansson J, Barra MM, Joschko A-C, Krijgsveld J, Feuerer M. Origin of monocytes and macrophages in a committed progenitor. Nature immunology. 2013;14(8):821-30.

15. Shi C, Pamer EG. Monocyte recruitment during infection and inflammation. Nature reviews immunology. 2011;11(11):762-74.

16. Auffray C, Fogg DK, Narni-Mancinelli E, Senechal B, Trouillet C, Saederup N, Leemput J, Bigot K, Campisi L, Abitbol M. CX3CR1+ CD115+ CD135+ common macrophage/DC precursors and the role of CX3CR1 in their response to inflammation. Journal of Experimental Medicine. 2009;206(3):595-606.

17. Fong AM, Robinson LA, Steeber DA, Tedder TF, Yoshie O, Imai T, Patel DD. Fractalkine and CX3CR1 mediate a novel mechanism of leukocyte capture, firm adhesion, and activation under physiologic flow. The Journal of experimental medicine. 1998;188(8):1413-9.

18. Haldar M, Kohyama M, So AY-L, Wumesh K, Wu X, Briseño CG, Satpathy AT, Kretzer NM, Arase H, Rajasekaran NS. Heme-mediated SPI-C induction promotes monocyte differentiation into iron-recycling macrophages. Cell. 2014;156(6):1223-34.

19. Mouchemore KA, Pixley FJ. CSF-1 signaling in macrophages: pleiotrophy through phosphotyrosine-based signaling pathways. Critical reviews in clinical laboratory sciences. 2012;49(2):49-61.

20. Pixley FJ, Stanley ER. CSF-1 regulation of the wandering macrophage: complexity in action. Trends in cell biology. 2004;14(11):628-38.

21. Chopin M, Seillet C, Chevrier S, Wu L, Wang H, Morse III HC, Belz GT, Nutt SL. Langerhans cells are generated by two distinct PU. 1-dependent transcriptional networks. Journal of Experimental Medicine. 2013;210(13):2967-80.

22. Gosselin D, Link VM, Romanoski CE, Fonseca GJ, Eichenfield DZ, Spann NJ, Stender JD, Chun HB, Garner H, Geissmann F. Environment drives selection and function of enhancers controlling tissue-specific macrophage identities. Cell. 2014;159(6):1327-40.

23. Lavin Y, Winter D, Blecher-Gonen R, David E, Keren-Shaul H, Merad M, Jung S, Amit I. Tissue-resident macrophage enhancer landscapes are shaped by the local microenvironment. Cell. 2014;159(6):1312-26.

24. Mass E, Ballesteros I, Farlik M, Halbritter F, Günther P, Crozet L, Jacome-Galarza CE, Händler K, Klughammer J, Kobayashi Y. Specification of tissue-resident macrophages during organogenesis. Science. 2016;353(6304).

25. Butovsky O, Jedrychowski MP, Moore CS, Cialic R, Lanser AJ, Gabriely G, Koeglsperger T, Dake B, Wu PM, Doykan CE. Identification of a unique TGF-β–dependent molecular and functional signature in microglia. Nature neuroscience. 2014;17(1):131-43.

26. Epelman S, Lavine KJ, Beaudin AE, Sojka DK, Carrero JA, Calderon B, Brija T, Gautier EL, Ivanov S, Satpathy AT. Embryonic and adult-derived resident cardiac macrophages are maintained through distinct mechanisms at steady state and during inflammation. Immunity. 2014;40(1):91-104.

27. Greter M, Lelios I, Pelczar P, Hoeffel G, Price J, Leboeuf M, Kündig TM, Frei K, Ginhoux F, Merad M. Stroma-derived interleukin-34 controls the development and maintenance of langerhans cells and the maintenance of microglia. Immunity. 2012;37(6):1050-60.

28. Amit I, Winter DR, Jung S. The role of the local environment and epigenetics in shaping macrophage identity and their effect on tissue homeostasis. Nature immunology. 2016;17(1):18.

29. McDonald B, Pittman K, Menezes GB, Hirota SA, Slaba I, Waterhouse CC, Beck PL, Muruve DA, Kubes P. Intravascular danger signals guide neutrophils to sites of sterile inflammation. Science. 2010;330(6002):362-6.

30. Bain CC, Bravo-Blas A, Scott CL, Perdiguero EG, Geissmann F, Henri S, Malissen B, Osborne LC, Artis D, Mowat AM. Constant replenishment from circulating monocytes maintains the macrophage pool in the intestine of adult mice. Nature immunology. 2014;15(10):929-37.

31. Miyabe C, Miyabe Y, Bricio-Moreno L, Lian J, Rahimi RA, Miura NN, Ohno N, Iwakura Y, Kawakami T, Luster AD. Dectin-2-induced CCL2 production in tissue-resident macrophages ignites cardiac arteritis. J Clin Invest. 2019;129(9):3610-24. Epub 2019/06/07. doi: 10.1172/jci123778. PubMed PMID: 31169521; PMCID: PMC6715376.

32. Kim Y-G, Kamada N, Shaw MH, Warner N, Chen GY, Franchi L, Núñez G. The Nod2 sensor promotes intestinal pathogen eradication via the chemokine CCL2-dependent recruitment of inflammatory monocytes. Immunity. 2011;34(5):769-80.

33. Zigmond E, Varol C, Farache J, Elmaliah E, Satpathy AT, Friedlander G, Mack M, Shpigel N, Boneca IG, Murphy KM, Shakhar G, Halpern Z, Jung S. Ly6C hi monocytes in the inflamed colon give rise to proinflammatory effector cells and migratory antigen-presenting cells. Immunity. 2012;37(6):1076-90. doi: 10.1016/j.immuni.2012.08.026. PubMed PMID: 23219392.

34. Hanna RN, Carlin LM, Hubbeling HG, Nackiewicz D, Green AM, Punt JA, Geissmann F, Hedrick CC. The transcription factor NR4A1 (Nur77) controls bone marrow differentiation and the survival of Ly6C− monocytes. Nature immunology. 2011;12(8):778.

35. Heinz S, Benner C, Spann N, Bertolino E, Lin YC, Laslo P, Cheng JX, Murre C, Singh H, Glass CK. Simple combinations of lineage-determining transcription factors prime cis-regulatory elements required for macrophage and B cell identities. Molecular cell. 2010;38(4):576-89.

36. Nakamura A, Ebina-Shibuya R, Itoh-Nakadai A, Muto A, Shima H, Saigusa D, Aoki J, Ebina M, Nukiwa T, Igarashi K. Transcription repressor Bach2 is required for pulmonary surfactant homeostasis and alveolar macrophage function. Journal of Experimental Medicine. 2013;210(11):2191-204.

37. Guilliams M, De Kleer I, Henri S, Post S, Vanhoutte L, De Prijck S, Deswarte K, Malissen B, Hammad H, Lambrecht BN. Alveolar macrophages develop from fetal monocytes that differentiate into long-lived cells in the first week of life via GM-CSF. Journal of Experimental Medicine. 2013;210(10):1977-92.

38. Kohyama M, Ise W, Edelson BT, Wilker PR, Hildner K, Mejia C, Frazier WA, Murphy TL, Murphy KM. Role for Spi-C in the development of red pulp macrophages and splenic iron homeostasis. Nature. 2009;457(7227):318-21.

39. Noelia A, Guillen JA, Gallardo G, Diaz M, De La Rosa JV, Hernandez IH, Casanova-Acebes M, Lopez F, Tabraue C, Beceiro S. The nuclear receptor LXRα controls

the functional specialization of splenic macrophages. Nature immunology. 2013;14(8):831-9.

40. Joseph SB, Bradley MN, Castrillo A, Bruhn KW, Mak PA, Pei L, Hogenesch J, O'Connell RM, Cheng G, Saez E. LXR-dependent gene expression is important for macrophage survival and the innate immune response. Cell. 2004;119(2):299-309.

41. Serbina NV, Jia T, Hohl TM, Pamer EG. Monocyte-mediated defense against microbial pathogens. Annu Rev Immunol. 2008;26:421-52.

42. Hacker C, Kirsch RD, Ju X-S, Hieronymus T, Gust TC, Kuhl C, Jorgas T, Kurz SM, Rose-John S, Yokota Y. Transcriptional profiling identifies Id2 function in dendritic cell development. Nature immunology. 2003;4(4):380-6.

43. He K, Dai ZY, Li PZ, Zhu XW, Gong JP. Association between liver X receptor-α and neuron-derived orphan nuclear receptor-1 in Kupffer cells of C57BL/6 mice during inflammation. Mol Med Rep. 2015;12(4):6098-104. Epub 2015/08/05. doi: 10.3892/mmr.2015.4155. PubMed PMID: 26239564.

44. Suganami T, Ogawa Y. Adipose tissue macrophages: their role in adipose tissue remodeling. J Leukoc Biol. 2010;88(1):33-9. doi: 10.1189/jlb.0210072. PubMed PMID: 20360405.

45. Thakur V, McMullen MR, Pritchard MT, Nagy LE. Regulation of macrophage activation in alcoholic liver disease. J Gastroenterol Hepatol. 2007;22 Suppl 1:S53-6. doi: 10.1111/j.1440-1746.2006.04650.x. PubMed PMID: 17567466.

46. Hashimoto D, Chow A, Noizat C, Teo P, Beasley MB, Leboeuf M, Becker CD, See P, Price J, Lucas D, Greter M, Mortha A, Boyer SW, Forsberg EC, Tanaka M, van

Rooijen N, Garcia-Sastre A, Stanley ER, Ginhoux F, Frenette PS, Merad M. Tissue-resident macrophages self-maintain locally throughout adult life with minimal contribution from circulating monocytes. Immunity. 2013;38(4):792-804. doi: 10.1016/j.immuni.2013.04.004. PubMed PMID: 23601688; PMCID: PMC3853406.

47. Murray PJ, Wynn TA. Protective and pathogenic functions of macrophage subsets. Nat Rev Immunol. 2011;11(11):723-37. doi: 10.1038/nri3073. PubMed PMID: 21997792; PMCID: PMC3422549.

48. Chawla A, Nguyen KD, Goh YP. Macrophage-mediated inflammation in metabolic disease. Nat Rev Immunol. 2011;11(11):738-49. doi: 10.1038/nri3071. PubMed PMID: 21984069; PMCID: PMC3383854.

49. Xu J, Chi F, Guo T, Punj V, Lee WN, French SW, Tsukamoto H. NOTCH reprograms mitochondrial metabolism for proinflammatory macrophage activation. J Clin Invest. 2015;125(4):1579-90. doi: 10.1172/JCI76468. PubMed PMID: 25798621; PMCID: PMC4396469.

50. Imamura M, Ogawa T, Sasaguri Y, Chayama K, Ueno H. Suppression of macrophage infiltration inhibits activation of hepatic stellate cells and liver fibrogenesis in rats. Gastroenterology. 2005;128(1):138-46. doi: 10.1053/j.gastro.2004.10.005. PubMed PMID: 15633130.

51. Antoniades CG, Quaglia A, Taams LS, Mitry RR, Hussain M, Abeles R, Possamai LA, Bruce M, McPhail M, Starling C, Wagner B, Barnardo A, Pomplun S, Auzinger G, Bernal W, Heaton N, Vergani D, Thursz MR, Wendon J. Source and characterization of

hepatic macrophages in acetaminophen-induced acute liver failure in humans. Hepatology. 2012;56(2):735-46. doi: 10.1002/hep.25657. PubMed PMID: 22334567.

52. Holt MP, Cheng L, Ju C. Identification and characterization of infiltrating macrophages in acetaminophen-induced liver injury. J Leukoc Biol. 2008;84(6):1410-21. doi: 10.1189/jlb.0308173. PubMed PMID: 18713872; PMCID: PMC2614594.

53. Ju C, Reilly TP, Bourdi M, Radonovich MF, Brady JN, George JW, Pohl LR. Protective role of Kupffer cells in acetaminophen-induced hepatic injury in mice. Chem Res Toxicol. 2002;15(12):1504-13. doi: 10.1021/tx0255976. PubMed PMID: 12482232.

54. Jenkins SJ, Ruckerl D, Cook PC, Jones LH, Finkelman FD, van Rooijen N, MacDonald AS, Allen JE. Local macrophage proliferation, rather than recruitment from the blood, is a signature of TH2 inflammation. Science. 2011;332(6035):1284-8. doi: 10.1126/science.1204351. PubMed PMID: 21566158; PMCID: PMC3128495.

55. Davies LC, Rosas M, Jenkins SJ, Liao CT, Scurr MJ, Brombacher F, Fraser DJ, Allen JE, Jones SA, Taylor PR. Distinct bone marrow-derived and tissue-resident macrophage lineages proliferate at key stages during inflammation. Nat Commun. 2013;4:1886. doi: 10.1038/ncomms2877. PubMed PMID: 23695680; PMCID: PMC3842019.

56. Soehnlein O, Lindbom L. Phagocyte partnership during the onset and resolution of inflammation. Nat Rev Immunol. 2010;10(6):427-39. doi: 10.1038/nri2779. PubMed PMID: 20498669.

57. Kang S, Kumanogoh A. The spectrum of macrophage activation by immunometabolism. Int Immunol. 2020;32(7):467-73. doi: 10.1093/intimm/dxaa017. PubMed PMID: 32179900.

58. Sica A, Mantovani A. Macrophage plasticity and polarization: in vivo veritas. J Clin Invest. 2012;122(3):787-95. doi: 10.1172/JCI59643. PubMed PMID: 22378047; PMCID: PMC3287223.

59. Gordon S, Martinez FO. Alternative activation of macrophages: mechanism and functions. Immunity. 2010;32(5):593-604. doi: 10.1016/j.immuni.2010.05.007. PubMed PMID: 20510870.

60. Ferrante CJ, Leibovich SJ. Regulation of Macrophage Polarization and Wound Healing. Adv Wound Care (New Rochelle). 2012;1(1):10-6. doi: 10.1089/wound.2011.0307. PubMed PMID: 24527272; PMCID: PMC3623587.

61. Rigoni TS, Vellozo NS, Cabral-Piccin M, Fabiano-Coelho L, Lopes UG, Filardy AA, DosReis GA, Lopes MF. RANK Ligand Helps Immunity to Leishmania major by Skewing M2-Like Into M1 Macrophages. Front Immunol. 2020;11:886. doi: 10.3389/fimmu.2020.00886. PubMed PMID: 32477357; PMCID: PMC7235166.

62. Batista-Gonzalez A, Vidal R, Criollo A, Carreno LJ. New Insights on the Role of Lipid Metabolism in the Metabolic Reprogramming of Macrophages. Front Immunol. 2019;10:2993. doi: 10.3389/fimmu.2019.02993. PubMed PMID: 31998297; PMCID: PMC6966486.

63. Fujisaka S, Usui I, Bukhari A, Ikutani M, Oya T, Kanatani Y, Tsuneyama K, Nagai Y, Takatsu K, Urakaze M, Kobayashi M, Tobe K. Regulatory mechanisms for adipose

tissue M1 and M2 macrophages in diet-induced obese mice. Diabetes. 2009;58(11):2574-82. Epub 2009/08/20. doi: 10.2337/db08-1475. PubMed PMID: 19690061; PMCID: PMC2768159.

64. Hung YL, Fang SH, Wang SC, Cheng WC, Liu PL, Su CC, Chen CS, Huang MY, Hua KF, Shen KH, Wang YT, Suzuki K, Li CY. Corylin protects LPS-induced sepsis and attenuates LPS-induced inflammatory response. Sci Rep. 2017;7:46299. doi: 10.1038/srep46299. PubMed PMID: 28397806; PMCID: PMC5387730.

65. Cheng Y, Marion TN, Cao X, Wang W, Cao Y. Park 7: A Novel Therapeutic Target for Macrophages in Sepsis-Induced Immunosuppression. Front Immunol. 2018;9:2632. doi: 10.3389/fimmu.2018.02632. PubMed PMID: 30542343; PMCID: PMC6277877.

66. Cummings DE, Purnell JQ, Frayo RS, Schmidova K, Wisse BE, Weigle DS. A preprandial rise in plasma ghrelin levels suggests a role in meal initiation in humans. Diabetes. 2001;50(8):1714-9.

67. Erdmann J, Topsch R, Lippl F, Gussmann P, Schusdziarra V. Postprandial response of plasma ghrelin levels to various test meals in relation to food intake, plasma insulin, and glucose. The Journal of Clinical Endocrinology & Metabolism. 2004;89(6):3048-54.

68. English P, Ghatei M, Malik I, Bloom S, Wilding J. Food fails to suppress ghrelin levels in obese humans. The Journal of Clinical Endocrinology & Metabolism. 2002;87(6):2984-7.

69. Havel PJ. Control of energy homeostasis and insulin action by adipocyte hormones: leptin, acylation stimulating protein, and adiponectin. Current opinion in lipidology. 2002;13(1):51-9.

70. Teff KL, Elliott SS, Tschöp M, Kieffer TJ, Rader D, Heiman M, Townsend RR, Keim NL, D'Alessio D, Havel PJ. Dietary fructose reduces circulating insulin and leptin, attenuates postprandial suppression of ghrelin, and increases triglycerides in women. The Journal of Clinical Endocrinology & Metabolism. 2004;89(6):2963-72.

71. Abdemur A, Slone J, Berho M, Gianos M, Szomstein S, Rosenthal RJ. Morphology, localization, and patterns of ghrelin-producing cells in stomachs of a morbidly obese population. Surgical Laparoscopy Endoscopy & Percutaneous Techniques. 2014;24(2):122-6.

72. Mani V, Hollis JH, Gabler NK. Dietary oil composition differentially modulates intestinal endotoxin transport and postprandial endotoxemia. Nutr Metab (Lond). 2013;10(1):6. doi: 10.1186/1743-7075-10-6. PubMed PMID: 23305038; PMCID: PMC3577458.

73. Lu X, Zhao X, Feng J, Liou AP, Anthony S, Pechhold S, Sun Y, Lu H, Wank S. Postprandial inhibition of gastric ghrelin secretion by long-chain fatty acid through GPR120 in isolated gastric ghrelin cells and mice. American Journal of Physiology-Gastrointestinal and Liver Physiology. 2012;303(3):G367-G76.

74. Silveira BKS, Oliveira TMS, Andrade PA, Hermsdorff HHM, Rosa COB, Franceschini S. Dietary Pattern and Macronutrients Profile on the Variation of

Inflammatory Biomarkers: Scientific Update. Cardiol Res Pract. 2018;2018:4762575. doi: 10.1155/2018/4762575. PubMed PMID: 29725543; PMCID: PMC5872610.

75. Smeets AJ, Soenen S, Luscombe-Marsh ND, Ueland Ø, Westerterp-Plantenga MS. Energy expenditure, satiety, and plasma ghrelin, glucagon-like peptide 1, and peptide tyrosine-tyrosine concentrations following a single high-protein lunch. The Journal of nutrition. 2008;138(4):698-702.

76. Naznin F, Toshinai K, Waise TZ, NamKoong C, Moin ASM, Sakoda H, Nakazato M. Diet-induced obesity causes peripheral and central ghrelin resistance by promoting inflammation. The Journal of endocrinology. 2015;226(1):81.

77. Engelstoft MS, Park W-m, Sakata I, Kristensen LV, Husted AS, Osborne-Lawrence S, Piper PK, Walker AK, Pedersen MH, Nøhr MK. Seven transmembrane G protein-coupled receptor repertoire of gastric ghrelin cells. Molecular metabolism. 2013;2(4):376-92.

78. Banks WA, Burney BO, Robinson SM. Effects of triglycerides, obesity, and starvation on ghrelin transport across the blood–brain barrier. Peptides. 2008;29(11):2061-5.

79. Briggs DI, Enriori PJ, Lemus MB, Cowley MA, Andrews ZB. Diet-induced obesity causes ghrelin resistance in arcuate NPY/AgRP neurons. Endocrinology. 2010;151(10):4745-55.

80. Briggs DI, Lockie SH, Benzler J, Wu Q, Stark R, Reichenbach A, Hoy AJ, Lemus MB, Coleman HA, Parkington HC. Evidence that diet-induced hyperleptinemia, but not

hypothalamic gliosis, causes ghrelin resistance in NPY/AgRP neurons of male mice. Endocrinology. 2014;155(7):2411-22.

81. Gnanapavan S, Kola B, Bustin SA, Morris DG, McGee P, Fairclough P, Bhattacharya S, Carpenter R, Grossman AB, Korbonits M. The tissue distribution of the mRNA of ghrelin and subtypes of its receptor, GHS-R, in humans. J Clin Endocrinol Metab. 2002;87(6):2988. doi: 10.1210/jcem.87.6.8739. PubMed PMID: 12050285.

82. Sun Y, Garcia JM, Smith RG. Ghrelin and growth hormone secretagogue receptor expression in mice during aging. Endocrinology. 2007;148(3):1323-9. doi: 10.1210/en.2006-0782. PubMed PMID: 17158206.

83. Lin L, Saha PK, Ma X, Henshaw IO, Shao L, Chang BH, Buras ED, Tong Q, Chan L, McGuinness OP, Sun Y. Ablation of ghrelin receptor reduces adiposity and improves insulin sensitivity during aging by regulating fat metabolism in white and brown adipose tissues. Aging Cell. 2011;10(6):996-1010. doi: 10.1111/j.1474-9726.2011.00740.x. PubMed PMID: 21895961; PMCID: PMC3215833.

84. Granado M, Martin AI, Lopez-Menduina M, Lopez-Calderon A, Villanua MA. GH-releasing peptide-2 administration prevents liver inflammatory response in endotoxemia. Am J Physiol Endocrinol Metab. 2008;294(1):E131-41. doi: 10.1152/ajpendo.00308.2007. PubMed PMID: 17986630.

85. Dolgor Baatar JHL, Margaret Brill, Ana Lustig, Arnell Carter, and Dennis Taub. An orexigenic hormone ghrelin enhances LPS-induced IL-10 production in human peripheral blood-derived macrophages. The Journal of Immunology. 2010;184.

86. Demers A, Caron V, Rodrigue-Way A, Wahli W, Ong H, Tremblay A. A concerted kinase interplay identifies PPARgamma as a molecular target of ghrelin signaling in macrophages. PLoS One. 2009;4(11):e7728. doi: 10.1371/journal.pone.0007728. PubMed PMID: 19888469; PMCID: PMC2766837.

87. Hosomi S, Oshitani N, Kamata N, Sogawa M, Yamagami H, Watanabe K, Tominaga K, Watanabe T, Fujiwara Y, Maeda K, Hirakawa K, Arakawa T. Phenotypical and functional study of ghrelin and its receptor in the pathogenesis of Crohn's disease. Inflamm Bowel Dis. 2008;14(9):1205-13. doi: 10.1002/ibd.20477. PubMed PMID: 18425803.

88. Varbo A, Benn M, Tybjaerg-Hansen A, Nordestgaard BG. Elevated remnant cholesterol causes both low-grade inflammation and ischemic heart disease, whereas elevated low-density lipoprotein cholesterol causes ischemic heart disease without inflammation. Circulation. 2013;128(12):1298-309. doi: 10.1161/CIRCULATIONAHA.113.003008. PubMed PMID: 23926208.

89. Tall AR, Yvan-Charvet L. Cholesterol, inflammation and innate immunity. Nature reviews Immunology. 2015;15(2):104-16. doi: 10.1038/nri3793. PubMed PMID: 25614320; PMCID: PMC4669071.

90. Li WG, Gavrila D, Liu X, Wang L, Gunnlaugsson S, Stoll LL, McCormick ML, Sigmund CD, Tang C, Weintraub NL. Ghrelin inhibits proinflammatory responses and nuclear factor-kappaB activation in human endothelial cells. Circulation. 2004;109(18):2221-6. doi: 10.1161/01.CIR.0000127956.43874.F2. PubMed PMID: 15117840.

91. Zhao D, Zhan Y, Zeng H, Moyer MP, Mantzoros CS, Pothoulakis C. Ghrelin stimulates interleukin-8 gene expression through protein kinase C-mediated NF-kappaB pathway in human colonic epithelial cells. Journal of cellular biochemistry. 2006;97(6):1317-27. doi: 10.1002/jcb.20744. PubMed PMID: 16552751.

92. Liu C, Huang J, Li H, Yang Z, Zeng Y, Liu J, Hao Y, Li R. Ghrelin accelerates wound healing through GHS-R1a-mediated MAPK-NF-kappaB/GR signaling pathways in combined radiation and burn injury in rats. Sci Rep. 2016;6:27499. Epub 2016/06/09. doi: 10.1038/srep27499. PubMed PMID: 27271793; PMCID: 4895129.

93. Siegl D, Midura EF, Annecke T, Conzen P, Caldwell CC, Tschoep J. The effect of ghrelin upon the early immune response in lean and obese mice during sepsis. PLoS One. 2015;10(4):e0122211. Epub 2015/04/07. doi: 10.1371/journal.pone.0122211. PubMed PMID: 25844479; PMCID: 4386814.

94. Dixit VD, Schaffer EM, Pyle RS, Collins GD, Sakthivel SK, Palaniappan R, Lillard JW, Jr., Taub DD. Ghrelin inhibits leptin- and activation-induced proinflammatory cytokine expression by human monocytes and T cells. The Journal of clinical investigation. 2004;114(1):57-66. doi: 10.1172/JCI21134. PubMed PMID: 15232612; PMCID: 437970.

95. Dixit VD, Yang H, Sun Y, Weeraratna AT, Youm YH, Smith RG, Taub DD. Ghrelin promotes thymopoiesis during aging. The Journal of clinical investigation. 2007;117(10):2778-90. Epub 2007/09/08. doi: 10.1172/JCI30248. PubMed PMID: 17823656; PMCID: 1964507.

96. Zeng M, He W, Li L, Li B, Luo L, Huang X, Guan K, Chen W. Ghrelin attenuates sepsis-associated acute lung injury oxidative stress in rats. Inflammation. 2015;38(2):683-90. Epub 2014/07/20. doi: 10.1007/s10753-014-9977-z. PubMed PMID: 25037094.

97. Lin L, Lee JH, Buras ED, Yu K, Wang R, Smith CW, Wu H, Sheikh-Hamad D, Sun Y. Ghrelin receptor regulates adipose tissue inflammation in aging. Aging. 2016;8(1):178-91. doi: 10.18632/aging.100888. PubMed PMID: 26837433; PMCID: 4761721.

98. Mear Y, Enjalbert A, Thirion S. GHS-R1a constitutive activity and its physiological relevance. Front Neurosci. 2013;7:87. Epub 2013/06/12. doi: 10.3389/fnins.2013.00087. PubMed PMID: 23754971; PMCID: 3665924.

99. Kern A, Mavrikaki M, Ullrich C, Albarran-Zeckler R, Brantley AF, Smith RG. Hippocampal Dopamine/DRD1 Signaling Dependent on the Ghrelin Receptor. Cell. 2015;163(5):1176-90. doi: 10.1016/j.cell.2015.10.062. PubMed PMID: 26590421; PMCID: 4937825.

100. Sun Y, Wang P, Zheng H, Smith RG. Ghrelin stimulation of growth hormone release and appetite is mediated through the growth hormone secretagogue receptor. Proc Natl Acad Sci U S A. 2004;101(13):4679-84. doi: 10.1073/pnas.0305930101. PubMed PMID: 15070777; PMCID: PMC384806.

101. Davies JS, Kotokorpi P, Eccles SR, Barnes SK, Tokarczuk PF, Allen SK, Whitworth HS, Guschina IA, Evans BA, Mode A, Zigman JM, Wells T. Ghrelin induces abdominal obesity via GHS-R-dependent lipid retention. Mol Endocrinol.

2009;23(6):914-24. doi: 10.1210/me.2008-0432. PubMed PMID: 19299444; PMCID: PMC2691683.

102. Ma X, Lin L, Qin G, Lu X, Fiorotto M, Dixit VD, Sun Y. Ablations of ghrelin and ghrelin receptor exhibit differential metabolic phenotypes and thermogenic capacity during aging. PLoS One. 2011;6(1):e16391. Epub 2011/02/08. doi: 10.1371/journal.pone.0016391. PubMed PMID: 21298106; PMCID: 3027652.

103. Delhanty PJ, van der Eerden BC, van der Velde M, Gauna C, Pols HA, Jahr H, Chiba H, van der Lely AJ, van Leeuwen JP. Ghrelin and unacylated ghrelin stimulate human osteoblast growth via mitogen-activated protein kinase (MAPK)/phosphoinositide 3-kinase (PI3K) pathways in the absence of GHS-R1a. J Endocrinol. 2006;188(1):37-47. Epub 2006/01/06. doi: 10.1677/joe.1.06404. PubMed PMID: 16394173.

104. Gauna C, Delhanty PJ, Hofland LJ, Janssen JA, Broglio F, Ross RJ, Ghigo E, van der Lely AJ. Ghrelin stimulates, whereas des-octanoyl ghrelin inhibits, glucose output by primary hepatocytes. J Clin Endocrinol Metab. 2005;90(2):1055-60. Epub 2004/11/13. doi: 10.1210/jc.2004-1069. PubMed PMID: 15536157.

105. Damian M, Marie J, Leyris JP, Fehrentz JA, Verdie P, Martinez J, Baneres JL, Mary S. High constitutive activity is an intrinsic feature of ghrelin receptor protein: a study with a functional monomeric GHS-R1a receptor reconstituted in lipid discs. The Journal of biological chemistry. 2012;287(6):3630-41. Epub 2011/11/26. doi: 10.1074/jbc.M111.288324. PubMed PMID: 22117076; PMCID: 3281683.

106. Ma X, Lin L, Yue J, Pradhan G, Qin G, Minze LJ, Wu H, Sheikh-Hamad D, Smith CW, Sun Y. Ghrelin receptor regulates HFCS-induced adipose inflammation and insulin

resistance. Nutr Diabetes. 2013;3:e99. doi: 10.1038/nutd.2013.41. PubMed PMID: 24366371; PMCID: PMC3877431.

107. Ma X, Lin L, Yue J, Wu CS, Guo CA, Wang R, Yu KJ, Devaraj S, Murano P, Chen Z, Sun Y. Suppression of Ghrelin Exacerbates HFCS-Induced Adiposity and Insulin Resistance. International journal of molecular sciences. 2017;18(6). doi: 10.3390/ijms18061302. PubMed PMID: 28629187; PMCID: 5486123.

108. Langston PK, Shibata M, Horng T. Metabolism supports macrophage activation. Frontiers in immunology. 2017;8:61.

109. Van den Bossche J, O'Neill LA, Menon D. Macrophage immunometabolism: where are we (going)? Trends in immunology. 2017;38(6):395-406.

110. Tschop M, Lahner H, Feldmeier H, Grasberger H, Morrison KM, Janssen OE, Attanasio AF, Strasburger CJ. Effects of growth hormone replacement therapy on levels of cortisol and cortisol-binding globulin in hypopituitary adults. Eur J Endocrinol. 2000;143(6):769-73. doi: 10.1530/eje.0.1430769. PubMed PMID: 11124860.

111. Cowley SC, Elkins KL. Multiple T cell subsets control Francisella tularensis LVS intracellular growth without stimulation through macrophage interferon gamma receptors. J Exp Med. 2003;198(3):379-89. doi: 10.1084/jem.20030687. PubMed PMID: 12885873; PMCID: PMC2194083.

112. Shimbara T, Mondal MS, Kawagoe T, Toshinai K, Koda S, Yamaguchi H, Date Y, Nakazato M. Central administration of ghrelin preferentially enhances fat ingestion. Neurosci Lett. 2004;369(1):75-9. doi: 10.1016/j.neulet.2004.07.060. PubMed PMID: 15380311.

113. Kojima M, Kangawa K. Ghrelin: structure and function. Physiol Rev. 2005;85(2):495-522. doi: 10.1152/physrev.00012.2004. PubMed PMID: 15788704.

114. Zigman JM, Jones JE, Lee CE, Saper CB, Elmquist JK. Expression of ghrelin receptor mRNA in the rat and the mouse brain. J Comp Neurol. 2006;494(3):528-48. Epub 2005/12/02. doi: 10.1002/cne.20823. PubMed PMID: 16320257.

115. Lee JH, Lin L, Xu P, Saito K, Wei Q, Meadows AG, Bongmba OYN, Pradhan G, Zheng H, Xu Y, Sun Y. Neuronal Deletion of Ghrelin Receptor Almost Completely Prevents Diet-Induced Obesity. Diabetes. 2016;65(8):2169-78. Epub 2016/05/10. doi: 10.2337/db15-1587. PubMed PMID: 27207529.

116. Clausen BE, Burkhardt C, Reith W, Renkawitz R, Forster I. Conditional gene targeting in macrophages and granulocytes using LysMcre mice. Transgenic Res. 1999;8(4):265-77. Epub 2000/01/06. PubMed PMID: 10621974.

117. Meadows A, Lee JH, Wu CS, Wei Q, Pradhan G, Yafi M, Lu HC, Sun Y. Deletion of G-protein-coupled receptor 55 promotes obesity by reducing physical activity. International journal of obesity. 2016;40(3):417-24. doi: 10.1038/ijo.2015.209. PubMed PMID: 26447738.

118. Wu H, Ghosh S, Perrard XD, Feng L, Garcia GE, Perrard JL, Sweeney JF, Peterson LE, Chan L, Smith CW. T-cell accumulation and regulated on activation, normal T cell expressed and secreted upregulation in adipose tissue in obesity. Circulation. 2007;115(8):1029.

119. Brake DK, Smith EOB, Mersmann H, Smith CW, Robker RL. ICAM-1 expression in adipose tissue: effects of diet-induced obesity in mice. American Journal of Physiology-Cell Physiology. 2006;291(6):C1232-C9.

120. Holt MP, Cheng L, Ju C. Identification and characterization of infiltrating macrophages in acetaminophen-induced liver injury. Journal of leukocyte biology. 2008;84(6):1410-21.

121. Zhang X, Goncalves R, Mosser DM. The isolation and characterization of murine macrophages. Current protocols in immunology. 2008;83(1):14.1. 1-.1. .

122. Verhulst PJ, De Smet B, Saels I, Thijs T, Ver Donck L, Moechars D, Peeters TL, Depoortere I. Role of ghrelin in the relationship between hyperphagia and accelerated gastric emptying in diabetic mice. Gastroenterology. 2008;135(4):1267-76. PubMed PMID: 18657539.

123. Lee JH, Lin L, Xu P, Saito K, Wei Q, Meadows AG, Bongmba OY, Pradhan G, Zheng H, Xu Y, Sun Y. Neuronal Deletion of Ghrelin Receptor Almost Completely Prevents Diet-Induced Obesity. Diabetes. 2016;65(8):2169-78. doi: 10.2337/db15-1587. PubMed PMID: 27207529; PMCID: 4955988.

124. Weisberg SP, McCann D, Desai M, Rosenbaum M, Leibel RL, Ferrante AW. Obesity is associated with macrophage accumulation in adipose tissue. The Journal of clinical investigation. 2003;112(12):1796-808.

125. Odegaard JI, Chawla A. Alternative macrophage activation and metabolism. Annual Review of Pathology: Mechanisms of Disease. 2011;6:275-97.

126. Schipper HS, Prakken B, Kalkhoven E, Boes M. Adipose tissue-resident immune cells: key players in immunometabolism. Trends in Endocrinology & Metabolism. 2012;23(8):407-15.

127. Charrière G, Cousin B, Arnaud E, André M, Bacou F, Pénicaud L, Casteilla L. Preadipocyte conversion to macrophage: evidence of plasticity. Journal of Biological Chemistry. 2003;278(11):9850-5.

128. Chazenbalk G, Bertolotto C, Heneidi S, Jumabay M, Trivax B, Aronowitz J, Yoshimura K, Simmons CF, Dumesic DA, Azziz R. Novel pathway of adipogenesis through cross-talk between adipose tissue macrophages, adipose stem cells and adipocytes: evidence of cell plasticity. PloS one. 2011;6(3):e17834.

129. Angus DC, Linde-Zwirble WT, Lidicker J, Clermont G, Carcillo J, Pinsky MR. Epidemiology of severe sepsis in the United States: analysis of incidence, outcome, and associated costs of care. Read Online: Critical Care Medicine| Society of Critical Care Medicine. 2001;29(7):1303-10.

130. Baue AE. SEMMELWEIS LECTURE SEPSIS RESEARCH: WHAT DID WE DO WRONG? WHAT WOULD SEMMELWEIS DO TODAY? Shock. 2001;16(1):1-8.

131. Cohen J, Guyatt G, Bernard GR, Calandra T, Cook D, Elbourne D, Marshall J, Nunn A, Opal S. New strategies for clinical trials in patients with sepsis and septic shock. Critical care medicine. 2001;29(4):880-6.

132. Yan J, Li S, Li S. The role of the liver in sepsis. International reviews of immunology. 2014;33(6):498-510.

133. Zhang Z, Bagby GJ, Stoltz D, Oliver P, Schwarzenberger PO, Kolls JK. Prolonged ethanol treatment enhances lipopolysaccharide/phorbol myristate acetate-induced tumor necrosis factor-α production in human monocytic cells. Alcoholism: Clinical and Experimental Research. 2001;25(3):444-9.

134. Bernal W. Acute liver failure: review and update. International anesthesiology clinics. 2017;55(2):92-106.

135. Kojima M, Hosoda H, Date Y, Nakazato M, Matsuo H, Kangawa K. Ghrelin is a growth-hormone-releasing acylated peptide from stomach. Nature. 1999;402(6762):656-60.

136. Weischenfeldt J, Porse B. Bone marrow-derived macrophages (BMM): isolation and applications. Cold Spring Harbor Protocols. 2008;2008(12):pdb. prot5080.

137. Canabal JM, Kramer DJ. Management of sepsis in patients with liver failure. Current opinion in critical care. 2008;14(2):189-97.

138. Sriskandan S, Altmann D. The immunology of sepsis. The Journal of Pathology: A Journal of the Pathological Society of Great Britain and Ireland. 2008;214(2):211-23.

139. Jaeschke H. Reactive oxygen and mechanisms of inflammatory liver injury. Journal of gastroenterology and hepatology. 2000;15(7):718-24.

140. Raval CM, Zhong JL, Mitchell SA, Tyrrell RM. The role of Bach1 in ultraviolet A-mediated human heme oxygenase 1 regulation in human skin fibroblasts. Free Radical Biology and Medicine. 2012;52(1):227-36.

141. Belhadj Slimen I, Najar T, Ghram A, Dabbebi H, Ben Mrad M, Abdrabbah M. Reactive oxygen species, heat stress and oxidative-induced mitochondrial damage. A review. International journal of hyperthermia. 2014;30(7):513-23.

142. Funato Y, Michiue T, Asashima M, Miki H. The thioredoxin-related redox-regulating protein nucleoredoxin inhibits Wnt–β-catenin signalling through dishevelled. Nature cell biology. 2006;8(5):501-8.

143. Zapelini PH, Rezin GT, Cardoso MR, Ritter C, Klamt F, Moreira JC, Streck EL, Dal-Pizzol F. Antioxidant treatment reverses mitochondrial dysfunction in a sepsis animal model. Mitochondrion. 2008;8(3):211-8.

144. Fink MP. Reactive oxygen species as mediators of organ dysfunction caused by sepsis, acute respiratory distress syndrome, or hemorrhagic shock: potential benefits of resuscitation with Ringer's ethyl pyruvate solution. Curr Opin Clin Nutr Metab Care. 2002;5(2):167-74. Epub 2002/02/15. doi: 10.1097/00075197-200203000-00009. PubMed PMID: 11844984.

145. McGarry JD. Banting lecture 2001: dysregulation of fatty acid metabolism in the etiology of type 2 diabetes. Diabetes. 2002;51(1):7-18. PubMed PMID: 11756317.

146. Sachithanandan N, Graham KL, Galic S, Honeyman JE, Fynch SL, Hewitt KA, Steinberg GR, Kay TW. Macrophage deletion of SOCS1 increases sensitivity to LPS and palmitic acid and results in systemic inflammation and hepatic insulin resistance. Diabetes. 2011;60(8):2023-31. doi: 10.2337/db11-0259. PubMed PMID: 21646388; PMCID: PMC3142066.

147. Davies LC, Jenkins SJ, Allen JE, Taylor PR. Tissue-resident macrophages. Nature immunology. 2013;14(10):986.

148. Murray RZ, Stow JL. Cytokine secretion in macrophages: SNAREs, Rabs, and membrane trafficking. Frontiers in immunology. 2014;5:538.

149. Gordon S, Plüddemann A, Martinez Estrada F. Macrophage heterogeneity in tissues: phenotypic diversity and functions. Immunological reviews. 2014;262(1):36-55.

150. Jenkins SJ, Ruckerl D, Thomas GD, Hewitson JP, Duncan S, Brombacher F, Maizels RM, Hume DA, Allen JE. IL-4 directly signals tissue-resident macrophages to proliferate beyond homeostatic levels controlled by CSF-1. J Exp Med. 2013;210(11):2477-91. doi: 10.1084/jem.20121999. PubMed PMID: 24101381; PMCID: PMC3804948.

151. Kojima H, Fujimiya M, Matsumura K, Nakahara T, Hara M, Chan L. Extrapancreatic insulin-producing cells in multiple organs in diabetes. Proceedings of the National Academy of Sciences. 2004;101(8):2458-63.

152. Wondmkun YT. Obesity, insulin resistance, and type 2 diabetes: associations and therapeutic implications. Diabetes, Metabolic Syndrome and Obesity: Targets and Therapy. 2020;13:3611.

153. Shoelson SE, Lee J, Goldfine AB. Inflammation and insulin resistance. J Clin Invest. 2006;116(7):1793-801. doi: 10.1172/JCI29069. PubMed PMID: 16823477; PMCID: PMC1483173.

154. Qatanani M, Lazar MA. Mechanisms of obesity-associated insulin resistance: many choices on the menu. Genes Dev. 2007;21(12):1443-55. doi: 10.1101/gad.1550907. PubMed PMID: 17575046.

155. Jablonski KA, Amici SA, Webb LM, Ruiz-Rosado Jde D, Popovich PG, Partida-Sanchez S, Guerau-de-Arellano M. Novel Markers to Delineate Murine M1 and M2 Macrophages. PLoS One. 2015;10(12):e0145342. Epub 2015/12/25. doi: 10.1371/journal.pone.0145342. PubMed PMID: 26699615; PMCID: PMC4689374.

156. Nawaz A, Aminuddin A, Kado T, Takikawa A, Yamamoto S, Tsuneyama K, Igarashi Y, Ikutani M, Nishida Y, Nagai Y, Takatsu K, Imura J, Sasahara M, Okazaki Y, Ueki K, Okamura T, Tokuyama K, Ando A, Matsumoto M, Mori H, Nakagawa T, Kobayashi N, Saeki K, Usui I, Fujisaka S, Tobe K. CD206(+) M2-like macrophages regulate systemic glucose metabolism by inhibiting proliferation of adipocyte progenitors. Nat Commun. 2017;8(1):286. Epub 2017/08/19. doi: 10.1038/s41467-017-00231-1. PubMed PMID: 28819169; PMCID: PMC5561263.

157. Serbulea V, Upchurch CM, Schappe MS, Voigt P, DeWeese DE, Desai BN, Meher AK, Leitinger N. Macrophage phenotype and bioenergetics are controlled by oxidized phospholipids identified in lean and obese adipose tissue. Proceedings of the National Academy of Sciences. 2018;115(27):E6254-E63.

158. Arita Y, Kihara S, Ouchi N, Takahashi M, Maeda K, Miyagawa J-i, Hotta K, Shimomura I, Nakamura T, Miyaoka K. Paradoxical decrease of an adipose-specific protein, adiponectin, in obesity. Biochemical and biophysical research communications. 1999;257(1):79-83.

159. Faraj M, Havel PJ, Phélis S, Blank D, Sniderman AD, Cianflone K. Plasma acylation-stimulating protein, adiponectin, leptin, and ghrelin before and after weight loss induced by gastric bypass surgery in morbidly obese subjects. The Journal of Clinical Endocrinology & Metabolism. 2003;88(4):1594-602.

160. Reaven GM, Hollenbeck C, Jeng C-Y, Wu MS, Chen Y-DI. Measurement of plasma glucose, free fatty acid, lactate, and insulin for 24 h in patients with NIDDM. Diabetes. 1988;37(8):1020-4.

161. Boden G. Free fatty acids as target for therapy. Current Opinion in Endocrinology, Diabetes and Obesity. 2004;11(5):258-63.

162. Boden G, She P, Mozzoli M, Cheung P, Gumireddy K, Reddy P, Xiang X, Luo Z, Ruderman N. Free Fatty Acids Produce Insulin Resistance and Activate the Proinflammatory Nuclear Factor-κB Pathway in Rat Liver. Diabetes. 2005;54(12):3458-65. doi: 10.2337/diabetes.54.12.3458.

163. Musso G, Gambino R, Cassader M. Recent insights into hepatic lipid metabolism in non-alcoholic fatty liver disease (NAFLD). Progress in lipid research. 2009;48(1):1-26.

164. Sun K, Kusminski CM, Scherer PE. Adipose tissue remodeling and obesity. J Clin Invest. 2011;121(6):2094-101. Epub 2011/06/03. doi: 10.1172/jci45887. PubMed PMID: 21633177; PMCID: PMC3104761.

165. Grant RW, Stephens JM. Fat in flames: influence of cytokines and pattern recognition receptors on adipocyte lipolysis. Am J Physiol Endocrinol Metab. 2015;309(3):E205-13. Epub 2015/06/11. doi: 10.1152/ajpendo.00053.2015. PubMed PMID: 26058863.

166. Lumeng CN, Bodzin JL, Saltiel AR. Obesity induces a phenotypic switch in adipose tissue macrophage polarization. The Journal of clinical investigation. 2007;117(1):175-84.

167. Clément K, Viguerie N, Poitou C, Carette C, Pelloux V, Curat CA, Sicard A, Rome S, Benis A, Zucker JD. Weight loss regulates inflammation-related genes in white adipose tissue of obese subjects. The FASEB Journal. 2004;18(14):1657-69.

168. Luo N, Liu J, Chung BH, Yang Q, Klein RL, Garvey WT, Fu Y. Macrophage adiponectin expression improves insulin sensitivity and protects against inflammation and atherosclerosis. Diabetes. 2010;59(4):791-9.

169. Law IK, Xu A, Lam KS, Berger T, Mak TW, Vanhoutte PM, Liu JT, Sweeney G, Zhou M, Yang B. Lipocalin-2 deficiency attenuates insulin resistance associated with aging and obesity. Diabetes. 2010;59(4):872-82.

170. Sun Y, Butte NF, Garcia JM, Smith RG. Characterization of adult ghrelin and ghrelin receptor knockout mice under positive and negative energy balance. Endocrinology. 2008;149(2):843-50.

171. Hirosumi J, Tuncman G, Chang L, Görgün CZ, Uysal KT, Maeda K, Karin M, Hotamisligil GS. A central role for JNK in obesity and insulin resistance. Nature. 2002;420(6913):333-6.

172. Röhl M, Pasparakis M, Baudler S, Baumgartl J, Gautam D, Huth M, De Lorenzi R, Krone W, Rajewsky K, Brüning JC. Conditional disruption of IκB kinase 2 fails to prevent obesity-induced insulin resistance. The Journal of clinical investigation. 2004;113(3):474-81.

173. Wunderlich FT, Luedde T, Singer S, Schmidt-Supprian M, Baumgartl J, Schirmacher P, Pasparakis M, Brüning JC. Hepatic NF-κB essential modulator deficiency prevents obesity-induced insulin resistance but synergizes with high-fat feeding in tumorigenesis. Proceedings of the national academy of sciences. 2008;105(4):1297-302.

174. Li H, Wu G, Fang Q, Zhang M, Hui X, Sheng B, Wu L, Bao Y, Li P, Xu A. Fibroblast growth factor 21 increases insulin sensitivity through specific expansion of subcutaneous fat. Nature communications. 2018;9(1):1-16.

175. Cherrington A. Control of glucose uptake and release by the liver in vivo. Banting Lecture 1997. Diabetes. 1999;48:1198-214.

176. Mauer J, Chaurasia B, Plum L, Quast T, Hampel B, Blüher M, Kolanus W, Kahn CR, Brüning JC. Myeloid Cell-Restricted Insulin Receptor Deficiency Protects Against Obesity-Induced Inflammation and Systemic Insulin Resistance. PLOS Genetics. 2010;6(5):e1000938. doi: 10.1371/journal.pgen.1000938.

177. Lam D, Harris D, Qin Z. Inflammatory mediator profiling reveals immune properties of chemotactic gradients and macrophage mediator production inhibition during thioglycollate elicited peritoneal inflammation. Mediators of inflammation. 2013;2013.

178. Elgazar-Carmon V, Rudich A, Hadad N, Levy R. Neutrophils transiently infiltrate intra-abdominal fat early in the course of high-fat feeding. Journal of lipid research. 2008;49(9):1894-903.

179. Kanda H, Tateya S, Tamori Y, Kotani K, Hiasa K-i, Kitazawa R, Kitazawa S, Miyachi H, Maeda S, Egashira K. MCP-1 contributes to macrophage infiltration into

adipose tissue, insulin resistance, and hepatic steatosis in obesity. The Journal of clinical investigation. 2006;116(6):1494-505.

180. Amano SU, Cohen JL, Vangala P, Tencerova M, Nicoloro SM, Yawe JC, Shen Y, Czech MP, Aouadi M. Local proliferation of macrophages contributes to obesity-associated adipose tissue inflammation. Cell metabolism. 2014;19(1):162-71.

181. Lee YS, Li P, Huh JY, Hwang IJ, Lu M, Kim JI, Ham M, Talukdar S, Chen A, Lu WJ. Inflammation is necessary for long-term but not short-term high-fat diet–induced insulin resistance. Diabetes. 2011;60(10):2474-83.

182. Bouloumié A, Curat CA, Sengenès C, Lolmède K, Miranville A, Busse R. Role of macrophage tissue infiltration in metabolic diseases. Current Opinion in Clinical Nutrition & Metabolic Care. 2005;8(4):347-54.

183. Granado M, Martin AI, Lopez-Menduina M, López-Calderón A, Villanúa MA. GH-releasing peptide-2 administration prevents liver inflammatory response in endotoxemia. American Journal of Physiology-Endocrinology and Metabolism. 2008;294(1):E131-E41.

184. Bie J, Zhao B, Song J, Ghosh S. Improved Insulin Sensitivity in High Fat-and High Cholesterol-fed Ldlr−/− Mice with Macrophage-specific Transgenic Expression of Cholesteryl Ester Hydrolase ROLE OF MACROPHAGE INFLAMMATION AND INFILTRATION INTO ADIPOSE TISSUE. Journal of Biological Chemistry. 2010;285(18):13630-7.

185. Sartipy P, Loskutoff DJ. Monocyte chemoattractant protein 1 in obesity and insulin resistance. Proceedings of the National Academy of Sciences. 2003;100(12):7265-70.

186. Prieur X, Mok CY, Velagapudi VR, Núñez V, Fuentes L, Montaner D, Ishikawa K, Camacho A, Barbarroja N, O'Rahilly S. Differential lipid partitioning between adipocytes and tissue macrophages modulates macrophage lipotoxicity and M2/M1 polarization in obese mice. Diabetes. 2011;60(3):797-809.

187. Robblee MM, Kim CC, Abate JP, Valdearcos M, Sandlund KL, Shenoy MK, Volmer R, Iwawaki T, Koliwad SK. Saturated fatty acids engage an IRE1α-dependent pathway to activate the NLRP3 inflammasome in myeloid cells. Cell reports. 2016;14(11):2611-23.

188. Namgaladze D, Lips S, Leiker TJ, Murphy RC, Ekroos K, Ferreiros N, Geisslinger G, Brüne B. Inhibition of macrophage fatty acid β-oxidation exacerbates palmitate-induced inflammatory and endoplasmic reticulum stress responses. Diabetologia. 2014;57(5):1067-77.

189. Malandrino MI, Fucho R, Weber M, Calderon-Dominguez M, Mir JF, Valcarcel L, Escoté X, Gómez-Serrano M, Peral B, Salvadó L. Enhanced fatty acid oxidation in adipocytes and macrophages reduces lipid-induced triglyceride accumulation and inflammation. American Journal of Physiology-Endocrinology and Metabolism. 2015;308(9):E756-E69.

190. Welham MJ, Bone H, Levings M, Learmonth L, Wang L-M, Leslie KB, Pierce JH, Schrader JW. Insulin receptor substrate-2 is the major 170-kDa protein phosphorylated on tyrosine in response to cytokines in murine lymphohemopoietic cells. Journal of Biological Chemistry. 1997;272(2):1377-81.

191. Kubota T, Inoue M, Kubota N, Takamoto I, Mineyama T, Iwayama K, Tokuyama K, Moroi M, Ueki K, Yamauchi T. Downregulation of macrophage Irs2 by hyperinsulinemia impairs IL-4-indeuced M2a-subtype macrophage activation in obesity. Nature communications. 2018;9(1):1-15.

192. Bar RS, Gorden P, Roth J, Kahn CR, De Meyts P. Fluctuations in the affinity and concentration of insulin receptors on circulating monocytes of obese patients: effects of starvation, refeeding, and dieting. The Journal of clinical investigation. 1976;58(5):1123-35.

193. Fung-Leung W-P. Phosphoinositide 3-kinase delta (PI3Kδ) in leukocyte signaling and function. Cellular signalling. 2011;23(4):603-8.

194. Fernández-Hernando C, Ackah E, Yu J, Suárez Y, Murata T, Iwakiri Y, Prendergast J, Miao RQ, Birnbaum MJ, Sessa WC. Loss of Akt1 leads to severe atherosclerosis and occlusive coronary artery disease. Cell metabolism. 2007;6(6):446-57.

195. Franke TF, Yang S-I, Chan TO, Datta K, Kazlauskas A, Morrison DK, Kaplan DR, Tsichlis PN. The protein kinase encoded by the Akt proto-oncogene is a target of the PDGF-activated phosphatidylinositol 3-kinase. Cell. 1995;81(5):727-36.

196. Iliopoulos D, Polytarchou C, Hatziapostolou M, Kottakis F, Maroulakou IG, Struhl K, Tsichlis PN. MicroRNAs differentially regulated by Akt isoforms control EMT and stem cell renewal in cancer cells. Science signaling. 2009;2(92):ra62-ra.

197. Arranz A, Doxaki C, Vergadi E, de la Torre YM, Vaporidi K, Lagoudaki ED, Ieronymaki E, Androulidaki A, Venihaki M, Margioris AN. Akt1 and Akt2 protein kinases

differentially contribute to macrophage polarization. Proceedings of the National Academy of Sciences. 2012;109(24):9517-22.

198. Lacy-Hulbert A, Moore KJ. Designer macrophages: oxidative metabolism fuels inflammation repair. Cell metabolism. 2006;4(1):7-8.

199. O'Neill LA, Kishton RJ, Rathmell J. A guide to immunometabolism for immunologists. Nature Reviews Immunology. 2016;16(9):553.

200. Kelly B, O'neill LA. Metabolic reprogramming in macrophages and dendritic cells in innate immunity. Cell research. 2015;25(7):771-84.

201. Kasmi KCE, Stenmark KR, editors. Contribution of metabolic reprogramming to macrophage plasticity and function. Seminars in immunology; 2015: Elsevier.

202. Law NC, White MF, Hunzicker-Dunn ME. G protein-coupled receptors (GPCRs) that signal via protein kinase A (PKA) cross-talk at insulin receptor substrate 1 (IRS1) to activate the phosphatidylinositol 3-kinase (PI3K)/AKT pathway. Journal of Biological Chemistry. 2016;291(53):27160-9.

203. O'Neill LA, Hardie DG. Metabolism of inflammation limited by AMPK and pseudo-starvation. Nature. 2013;493(7432):346-55. Epub 2013/01/18. doi: 10.1038/nature11862. PubMed PMID: 23325217.

204. Kelly B, O'Neill LA. Metabolic reprogramming in macrophages and dendritic cells in innate immunity. Cell research. 2015;25(7):771-84. doi: 10.1038/cr.2015.68. PubMed PMID: 26045163; PMCID: 4493277.

205. Rodríguez-Prados J-C, Través PG, Cuenca J, Rico D, Aragonés J, Martín-Sanz P, Cascante M, Boscá L. Substrate Fate in Activated Macrophages: A Comparison between

Innate, Classic, and Alternative Activation. The Journal of Immunology. 2010;185(1):605-14. doi: 10.4049/jimmunol.0901698.

206. Reczek CR, Chandel NS. ROS-dependent signal transduction. Current opinion in cell biology. 2015;33:8-13.

207. Toyama EQ, Herzig S, Courchet J, Lewis TL, Losón OC, Hellberg K, Young NP, Chen H, Polleux F, Chan DC. AMP-activated protein kinase mediates mitochondrial fission in response to energy stress. Science. 2016;351(6270):275-81.

208. Athéa Y, Viollet B, Mateo P, Rousseau D, Novotova M, Garnier A, Vaulont S, Wilding JR, Grynberg A, Veksler V. AMP-activated protein kinase α2 deficiency affects cardiac cardiolipin homeostasis and mitochondrial function. Diabetes. 2007;56(3):786-94.

209. Long YC, Cheng Z, Copps KD, White MF. Insulin receptor substrates Irs1 and Irs2 coordinate skeletal muscle growth and metabolism via the Akt and AMPK pathways. Molecular and cellular biology. 2011;31(3):430-41. doi: 10.1128/MCB.00983-10. PubMed PMID: 21135130; PMCID: 3028618.

210. Sadagurski M, Cheng Z, Rozzo A, Palazzolo I, Kelley GR, Dong X, Krainc D, White MF. IRS2 increases mitochondrial dysfunction and oxidative stress in a mouse model of Huntington disease. The Journal of clinical investigation. 2011;121(10):4070-81. doi: 10.1172/JCI46305. PubMed PMID: 21926467; PMCID: 3195462.

211. Bettencourt IA, Powell JD. Targeting metabolism as a novel therapeutic approach to autoimmunity, inflammation, and transplantation. The Journal of Immunology. 2017;198(3):999-1005.

212. Geeraerts X, Bolli E, Fendt S-M, Van Ginderachter JA. Macrophage metabolism as therapeutic target for cancer, atherosclerosis, and obesity. Frontiers in Immunology. 2017;8:289.

213. Frazao R, Lemko HMD, da Silva RP, Ratra DV, Lee CE, Williams KW, Zigman JM, Elias CF. Estradiol modulates Kiss1 neuronal response to ghrelin. American Journal of Physiology-Endocrinology and Metabolism. 2014;306(6):E606-E14.

214. Arkan MC, Hevener AL, Greten FR, Maeda S, Li Z-W, Long JM, Wynshaw-Boris A, Poli G, Olefsky J, Karin M. IKK-β links inflammation to obesity-induced insulin resistance. Nature medicine. 2005;11(2):191-8.

215. Weisberg SP, Hunter D, Huber R, Lemieux J, Slaymaker S, Vaddi K, Charo I, Leibel RL, Ferrante Jr AW. CCR2 modulates inflammatory and metabolic effects of high-fat feeding. The Journal of clinical investigation. 2006;116(1):115-24.

216. Bassaganya-Riera J, Misyak S, Guri AJ, Hontecillas R. PPAR γ is highly expressed in F4/80hi adipose tissue macrophages and dampens adipose-tissue inflammation. Cellular immunology. 2009;258(2):138-46.

217. Orr JS, Kennedy A, Anderson-Baucum EK, Webb CD, Fordahl SC, Erikson KM, Zhang Y, Etzerodt A, Moestrup SK, Hasty AH. Obesity alters adipose tissue macrophage iron content and tissue iron distribution. Diabetes. 2014;63(2):421-32.

218. Serbulea V, Upchurch CM, Schappe MS, Voigt P, DeWeese DE, Desai BN, Meher AK, Leitinger N. Macrophage phenotype and bioenergetics are controlled by oxidized phospholipids identified in lean and obese adipose tissue. Proc Natl Acad Sci U S A.

2018;115(27):E6254-E63. doi: 10.1073/pnas.1800544115. PubMed PMID: 29891687; PMCID: PMC6142199.